

NORM FASTENERS
AR-GE MERKEZİ YAYINLARI
R&D CENTER PUBLICATIONS



— 2022 —

VOLUME 8

NORM
FASTENERS

NORM FASTENERS

AR-GE MERKEZİ YAYINLARI

R&D CENTER PUBLICATIONS

Burada yer alan makale ve akademik yazıların tüm hakları yazarlara ve yayınların yapıldığı yayınevlerine ait olup, bu derlemeyi elinde bulunduranlara çoğaltma ve yayma hakkı tanınmaz. Bu hakların ihlali halinde Norm Fasteners'in ve yazarların yasal hakları saklıdır.

All rights to the articles and academic writings contained herein belong to the authors and the respective publisher, and those who hold this compilation do not have the right to reproduce and disseminate the content. In case of infringement of these rights, the legal rights of Norm Fasteners and the authors are reserved.



ÖN SÖZ 4-5

FATIGUE BEHAVIOR OF RE-TIGHTENED BOLTED JOINTS AFFECTED BY
VIBRATION INDUCED LOOSENING 8

BİLYALI DÖVME İŞLEMİ SONRASI TUNGSTEN KARBÜR-KOBALT (WC-CO)
SERTMETAL MALZEMELERİN YORULMA PERFORMANSININ İNCELENMESİ 14

INVESTIGATION OF FAILURE CRITERIA FOR TUNGSTEN CARBIDE-COBALT
HARD METALS 32

EXPERIMENTAL VALIDATION OF THE FORMULATION FOR MAXIMUM SOCKET
DEPTH ESTIMATION OF NON-REDUCED STRENGTH BOLTS 36

A MODEL TO CONSTRUCT AND PREDICT FLOW CURVE OF MATERIALS FROM
COMPRESSION TEST RESULTS WITH MACHINE LEARNING MODELS
USING PYTHON 48

OTOMOTIV ENDÜSTRİSİNDE KULLANILAN SAPLAMALARIN ÜRETİMİNDE
KULLANILAN KALIP SİSTEMLERİ: SEGMENTLİ KALIP KULLANIMI İLE
ÖMÜR ARTIŞI ELDE EDİLMESİ 60

SOĞUK DÖVME PROSESİNDE KULLANILAN BİR SIVAMA KALIBININ
SONLU ELEMANLAR YÖNTEMİ İLE İNCELENMESİ 64



SURFACE FINISHING OF CEMENTED TUNGSTEN CARBIDE USING ABRASIVE
FLOW MACHINING 68

HYBRID FAILURE CRITERIA APPLICATION FOR COLD FORGING DIES 78

FOR MORE SUSTAINABLE COLD FORGING PROCESS: USE OF SAND
BLASTING INSTEAD OF PICKLING AND RINSING 82

INDUSTRIAL WIRELESS TRACKING TOOLS OF COLD FORGING DIES
FOR INDUSTRY 4.0 SYSTEMS: RFID & QR CODE APPLICATIONS 86

APPLICATION OF COLD EXPANSION MECHANICAL SURFACE TREATMENT TO COLD
FORGING DIES AGAINST LOW CYCLE FATIGUE 96

COMPARATIVE WEAR PERFORMANCE OF TIN COATED AND SHOT PEENED
PIERCING PUNCHES USED IN NUT PRODUCTION BY COLD FORGING 100

NORM ONE WAY PATENTLİ ÜRÜNÜNDE AĞIRLIK AZALTIMI İÇİN MEKANİK
DAYANIM VE TORKLAMA ÇALIŞMALARININ GERÇEKLEŞTİRİLMESİ 104

ÖN SÖZ

Umut İnce

Norm Fasteners Ar-Ge ve Mühendislik Direktörü

Değerli İş Ortaklarımız;

Ar-Ge ve inovasyon kapsamında her yıl artan bir ivmeyle gerçekleştirdiği yatırımlarla sektörde sürdürülebilir bir gelişimi hedefleyen Norm Holding, "geleceğe değer" vizyonu doğrultusunda emin adımlarla ilerlemeye devam ederken sektörün talep ve ihtiyaçları doğrultusunda sizlerle ortak bir amaç çerçevesinde Ar-Ge çalışmalarını gerçekleştirmektedir.

Farklı disiplinlerde akademik geçmişe sahip, alanında uzman Ar-Ge ekibimizin gerçekleştirdiği çalışmalar ve güçlü iş birliklerimizin yanında her geçen gün artan bir motivasyon ve azim ile hedeflerimiz doğrultusunda kararlı bir şekilde ilerlemekteyiz. Müşterilerimizin ihtiyaç ve talepleri doğrultusunda katma değeri yüksek çözüm ve ürünler geliştirmekle birlikte ulusal ve uluslararası alanda gerçekleştirdiğimiz akademik çalışmalarla da teknolojik ilerlemelere katkıda bulunarak sektöre yön vermeyi ve birlikte güçlenerek ilerlemeyi bir sorumluluk kabul etmekteyiz. 2022 yılı içinde yaptığımız çalışmalardan ortaya çıkan makale ve bildirilerimizi bu kitapçıkta birleştirerek siz değerli iş ortaklarımızla paylaşmaktan gurur ve mutluluk duyuyoruz.

ÖN SÖZ

Dr. Muhammed Burak Toparlı

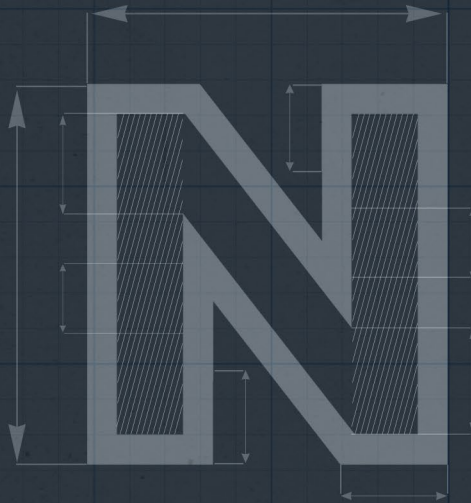
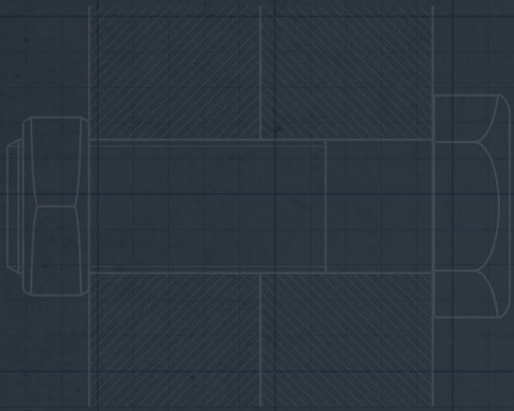
Norm Fasteners Ar-Ge Müdürü

Değerli İş Ortaklarımız;

Norm Fasteners Ar-Ge Merkezi olarak kurulduğumuz tarih olan 2011 yılından bu yana yürüttüğümüz projelerimiz ve gerçekleştirdiğimiz özgün çalışmalarımızın çıktıları olan makale ve bildirilerimiz, ulusal ve uluslararası saygın konferans, kongre, sempozyum ve dergilerde yayınlanmaktadır. Yayınlanan çalışmalarımız ile literatüre, sektöre ve teknolojik gelişmelere katkıda bulunmaktan her zaman gurur duyuyoruz.

Bu yıl 8. sayısını hazırladığımız "Ar-Ge Merkezi Yayınları" kitapçığımızı akademik ve sektörel işbirliğimiz olan yurt içi ve yurt dışındaki iş ortaklarımızla paylaşmaktayız. Bu kitapçık ile amacımız akademik ve sektörel gelişmelere verdiğimiz katkılar ortaya koyarken iş ortaklarımıza güncel çalışmalarımız ve çalışma alanlarımız hakkında bilgi vermektir. Özellikle otomotiv sanayinin içinde bulunduğu değişim ve bu kapsamda ağırlık azaltma faaliyetlerinin hem içten yanmalı motorlu araçlarda hem de hibrit ve elektrikli araçlarda giderek önem kazandığı bir gerçektir. Ağırlık azaltma, sürdürülebilirlik konuları başta olmak üzere sektör beklentilerini ve müşteri isteklerini karşılamaya yönelik birçok farklı konuda çalışmalar gerçekleştiren Norm Fasteners Ar-Ge Merkezi olarak yaptığımız yayınlar ile bu durumu desteklediğimizi göstermek bizim için çok önemlidir.

Bir gelenek haline getirdiğimiz ve diğer Ar-Ge ve Tasarım merkezlerine de örnek olduğumuz "Ar-Ge Merkezi Yayınları" kitapçığımızın bu sayısı ile 2022 yılında ortaya koyduğumuz akademik ve sektörel yayınlarımızı siz değerli iş ortaklarımız ile paylaşmaktan mutluluk duyuyoruz. Müşteri ve sektör odaklı inovatif projelerimize ve bu çalışmalarımızın çıktıları olan yayınlarımızı paylaşmaya aynı istek ve heyecanla devam edeceğiz.



FATIGUE BEHAVIOR OF RE-TIGHTENED BOLTED JOINTS AFFECTED BY VIBRATIONINDUCED LOOSENING

Baris TANRIKULU
Ramazan KARAKUZU
Sarper DOGAN
Sezgin YURTDAS



Virtual 20th International Colloquium on Mechanical Fatigue of Metals

FATIGUE BEHAVIOR OF RE-TIGHTENED BOLTED JOINTS AFFECTED BY VIBRATION-INDUCED LOOSENING

Baris Tanrikulu¹, Ramazan Karakuzu², Sarper DOĞAN³, Sezgin YURTDAS³

¹The Graduate School of Natural and Applied Science, Dokuz Eylül University, Izmir, Turkey

²Department of Mechanical Engineering, Dokuz Eylül University, Izmir, Turkey

³Norm Civata R&D Center, Norm Civata San ve Tic A.Ş. A.O.S.B. Izmir, Turkey

Abstract

Threaded fasteners are one of the most preferred joining methods today. Although there are many studies in this field, the number of researches on fatigue life as a result of the loosening behavior of fasteners is very limited. Within the scope of the study, the effects of preload loss due to transversal displacement for re-tightened bolted joints to their fatigue behaviors were investigated. The study was conducted by using M8x1.25 10.9 DIN 933 bolts and DIN 934 nuts with various preloads. Tightened bolts were subjected to repeated transversal displacement and clamp load values were monitored and recorded for each cycle. Bolts subjected to preload loss were re-tightened to their desired clamp load values and Junker vibration test was re-started. Increase on the tightening torque values after each usage was observed. This situation is caused by the friction coefficient change after re-using fasteners. Due to the increase in the friction coefficient, tightening torque values were increased as expected. Fastener subjected to repeated tightening failed during Junker vibration test due to fatigue. This phenomenon was mainly caused by high friction coefficient which prevent loosening and lead fasteners to take higher shear loads. A critical tightening-preload loss factor has been found for predicting early fatigue failure caused by loosening for re-tightened bolted joints.

Keywords: Fastener, Loosening, Fatigue, Re-tightening.

1. Introduction

Fasteners maintain their place as a basic component in many industries today. Although there are many types of threaded fasteners, in principle, they all work based on the same rule. Nowadays, many new studies are carried out to examine the behavior of fasteners, especially due to the increasing use of fasteners in vital applications. In a study conducted by Junker in 1969 [1], it was first discovered that bolts may lose their clamp loads under cyclic lateral loads. This study has formed the basis of vibration-induced relaxation studies today. In the following studies, it was revealed that cyclic loads acting perpendicular to the bolt axis caused micro-slippages in the bolt bearing surface and threaded region, and that there was a discrepancy in the clamp load over time. Within the scope of another study, the most effective parameters affecting the loosening mechanism were examined and it was determined that the most effective parameters were as clamp load, friction coefficient and lateral displacement values [2,3].

One of the most critical parameters in determining the service life of the fasteners has been the fatigue life. Although there are many different test and calculation methods in the industry, there are constant deviations in fatigue lives due to many variables affecting during assembly. Most basic reasons for fatigue-based damages encountered is that the insufficient clamp load values, which led to not obtain the desired number of lifetimes. Especially in the literature, studies have been started recently to examine the fatigue life of fasteners subjected to lateral displacement [4]. The obtained findings

shows that clamp load loss caused by vibrational loosening directly affects the fatigue behavior. As is known, fasteners are covered with special coatings in order to increase their corrosion resistance and to keep the friction coefficient value in a constant value. Although these coatings allow bolts to be used more than once, there are changes in the friction coefficient of the bolt after each use due to the wear. This situation reveals that even if the same bolt is tightened to the same torque value in the next time, it cannot show the same performance and there will be a change in the clamp load. In a study conducted for this purpose, it was revealed that the coefficient of friction obviously changes depending on the number of tightening [5].

Within the scope of the study, the fatigue life of the reused bolts exposed to lateral load, was investigated and a comparison was made. Findings of the study combines two main sections of the literature with a new perspective. Which is the effect of friction coefficient change under the combination of relaxation and fatigue.

2. Materials and Methods

Within the scope of the experimental studies, M8x1,25x 50 10.9 DIN 933 bolts and DIN 934 nuts, which are frequently used in the industry, were used. Since the behavior of the friction coefficients under repeated tightening will be examined, Delta Pro-tect KL100 VH301 GZ Zinc Flake coating system with 0.09-0.14 friction coefficient is preferred as the surface coating. In the experimental part of the study, the Junker vibration device given in Fig. 1 is used to obtain cyclic loosening values.



Fig. 1. Junker vibration test device.

3. Experimental Results

Six experiments were conducted for each combination and average of loosening curves were taken from the Junker vibration test device. Loosening rate values were obtained based on the slope of the clamp load-cycle graph for each combina-

tion. Clamp load cycle graphs for 12.1 kN and 17.1 kN were given in Fig.1 and Fig. 2. For 12.1 kN load set, fatigue failures of the bolts were observed at 8. re-tightening. On the other hand, for 17.1 kN bolts started to fail at fifth re-tightening. As expected, results re-reveals that higher initial clamp load values decrease fatigue life of the bolts under transverse loading as expected. Fracture surface of the bolt is given in Fig.3.

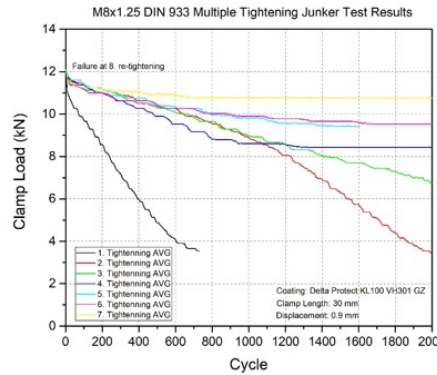


Fig. 2. Clamp load-Cycle graphs for 12.1 kN.

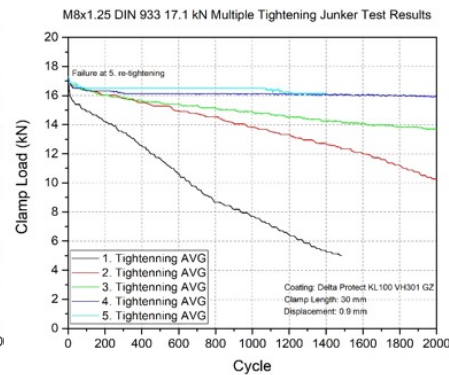


Fig. 3. Clamp load-Cycle graphs for 17.1 kN.

For bolts tested under 17.1 kN, it is clearly seen that, slowing on the loosening behavior causes to fail fasteners after repeated tightening. In the first three tightening operation, due to friction coefficient increase, bolt loosening rates decrease drastically. Total locking occurs after fourth tightening which causes extra stress on the radius region of the bolt head and cause failures. For bolts tested under 12.1 kN, same loosening rate decrease was figured out for the first three tightening.

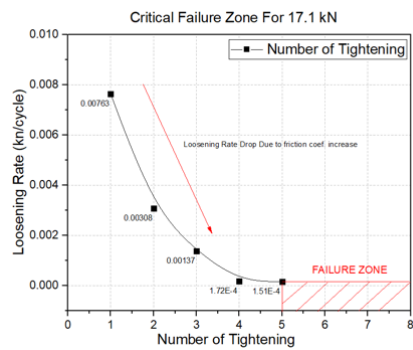


Fig. 4. Critical failure zone for 17.1 kN.

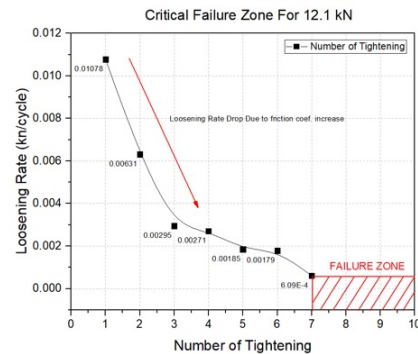


Fig. 5. Critical failure zone for 12.1 kN.

Critical failure zones were determined based on the number of tightening and loosening rates obtained from the experimental test. Both load cases show similar behavior with parallel to friction coefficient change with a repeated tightening.

4. Conclusion

Findings showed that lateral displacement which is causing loosening on bolt preload values are the main reason of the fatigue failures. Due to the increase in friction coefficient, which is mainly caused by the repeated usage, bolts start to gain resistance to loosening which is also in good agreement with the literature. Having an increased friction coefficient value with a combination of high lateral loads cause some locking phenomena which is reveal itself as a fatigue fracture due to the bending loads acting on under head radius. Findings also reveals that, loosening of the bolt prevents an early fatigue failure phenomenon in case of a high lateral displacement, but with the increase of the friction coefficient value, initial clamp load value and stress caused by bending loads, fatigue lives of bolts start to decrease drastically. A critical tightening-preload loss factor has been found for predicting early fatigue failure caused by loosening for re-tightened bolted joints with an enlarged experimental study. Ongoing experimental and simulation results which include an enlarged mapping shows that there is a critical equilibrium point for high lateral displacements with an increased fatigue life.

References

1. Junker, G., "New Criteria for Self-Loosening of Fasteners Under Vibration," SAE Technical Paper 690055, 1969,
2. Hess, D.P., Keifer, O.P., Moody, C.B., 2014. Tests on Loosening of Aviation Threaded Fasteners with Different Washer Configurations. J. Fail. Anal. Prev. <https://doi.org/10.1007/s11668-014-9873-8>
3. Sanclemente, J.A.A., Hess, D.P.P., 2007. Parametric study of threaded fastener loosening due to cyclic transverse loads. Eng. Fail. Anal. 14, 239-249. <https://doi.org/10.1016/j.engfailanal.2005.10.016>
4. Long Yang, Bing Yang, Guangwu Yang, Yang Xu, Shoune Xiao, Shilin Jiang, Jingsong Chen, Analysis of competitive failure life of bolt loosening and fatigue, Engineering Failure Analysis, Volume 129, 2021.
5. Liu Z, Zheng M, Yan X, Zhao Y, Cheng Q, Yang C, Changing behavior of friction coef-ficient for high strength bolts during repeated tightening, Tribology International (2020)

BILYALI DÖVME İŞLEMİ SONRASI TUNGSTEN KARBÜR-KOBALT (WC-CO) SERTMETAL MALZEMELERİN YORULMA PERFORMANSININ İNCELENMESİ

M. Burak TOPARLI



Journal of the Faculty of Engineering and Architecture of Gazi University 38:1 (2023) 269-281

BİLYALI DÖVME İŞLEMİ SONRASI TUNGSTEN KARBÜR-KOBALT (WC-CO) SERTMETAL MALZEMELERİN YORULMA PERFORMANSININ İNCELENMESİ

M. Burak Toparlı

NORM Cıvata Ar-Ge Merkezi, İ.A.O.S.B. Çiğli, İzmir, Türkiye

Öne Çıkanlar

- İmalat sanayinde kullanılan sertmetal malzemelerin yorulma performansı incelenmiştir.
- Yorulma ömründe iyileşme elde edebilmek için bilyalı dövme işlemi uygulanmıştır.
- Bilyalı dövme işlemi sonrası elde edilen sertlik artışı sayesinde malzemelerin yorulma performansında iyileşme elde edilmiştir.

Özet

Bu çalışmada, soğuk dövme kalıpları ve takım ucu gibi imalat sektörü açısından önemli alanlarda kullanılan tungsten karbür-kobalt (WC-Co) sertmetal malzemeler ele alınmıştır. İlgili metal-seramik kompozit malzemelerin yorulma ömrünün artırılması için özellikle havacılık ve otomotiv sanayinde kullanılan bilyalı dövme işlemi uygulanmıştır. Malzeme karakterizasyon testleri sonrası yorulma ömürleri elde edilmiştir. Yüzey pürüzlülük ölçümleri sonucunda, bilyalı dövme işlemi sonrası malzeme R_a ve R_z değerlerinde sırasıyla %113 ve %83'lük artışlar gözlenmiştir. Sertlik ölçümleri neticesinde, yüzeyde %13'lük bir artış olduğu ortaya çıkarılmıştır. Elde edilen derinlik profiline göre sertlik artışından etkilenen bölge derinliğinin yaklaşık 300 μm olduğu saptanmıştır. Yorulma testleri sonucunda bilyalı dövme işlemi sayesinde sertmetal numunelerin yorulma performansında iyileşme elde edilmiştir. Malzemedeki yorulma ömrü artışının bilyalı dövme sonucu elde edilen sertlik artışı sayesinde olduğu belirlenmiştir. Sertlik artışının plastik deformasyon sonucu gerinim sertleşmesi neticesinde olduğu ortaya konmuş, kobalt fazında herhangi bir kristal yapı değişikliği saptanmamıştır. Numunelerin kırılma yüzeyleri yorulma testleri sonrasında taramalı elektron mikroskobu ile incelenmiştir. Yorulma testi sonrasında gözlenen kırılmaların çoklu çatlak başlangıcı sonucu olduğu tespit edilmiştir. Tungsten karbür tanelerin hem bilyalı dövme hem de yorulma testi sonucunda kırıldığı gözlenmiştir. Kırılma esnasında hem tanelerarası hem de tane içi çatlak ilerleme mekanizmalarının kırılmaları neden olduğu ortaya konmuştur. Ayrıca, incelenen kırılma yüzeylerinde sünek malzemelerde görülen yorulma yivciklerine rastlanmamıştır.

Keywords: Sertmetal; metal seramik kompozit malzeme; bilyalı dövme; yorulma

1. Giriş (Introduction)

Literatürde sertmetaller (İng. hardmetals) sınıfına giren tungsten karbür-kobalt (WC-Co) metal-seramik kompozit malzemeler ile ilgili çalışmalar 20. yüzyılın başından itibaren yapılmaktadır [1]. Sert ve aşınmaya dirençli tungsten karbür parçacıkların daha sünek kobalt matrisi ile beraber toz şeklinde karıştırılıp sinterlenerek üretilmesi sonucu elde edilen sertmetaller farklı sektörlerde kullanılmaktadır [2,3]. İlk uygulamalarda yüksek aşınmaya maruz kalan ve malzeme sertliğinin önemli olduğu kesici takım uçlarında kullanılan sertmetaller, mikroyapı ve bileşenlerinin optimize edilmesiyle yorulmanın daha baskın olduğu alanlarda da kullanılmaya başlanmıştır [2,4,5]. Özellikle yüksek sertlik ve yorulma direnci

gereksinimlerinin kritik olduğu soğuk şekillendirme kalıplarında tungsten karbür-kobalt sertmetaller kullanılmaktadır. Ekstrüzyon, redüksiyon, kafa şişirme gibi soğuk şekillendirme operasyonlarında kullanılan kalıplarda uygulamaya göre farklı tungsten karbür-kobalt malzemeler tercih edilmektedir. Dolayısıyla, artan kullanım alanları sayesinde tungsten karbür-kobalt sertmetal malzemelerin imalat sektöründeki önemi artmaktadır. Ancak, yapılan literatür araştırmasına göre tungsten karbür - kobalt malzemeler ile ilgili çalışmaların sınırlı olduğu ve özellikle yorulma performansının artırılmasına yönelik çok fazla çalışmanın olmadığı tespit edilmiştir.

Tungsten karbür içeren sertmetal malzemelerde bağlayıcı seçimi nihai ürün performansını ciddi şekilde etkilemektedir. Nikel gibi farklı bağlayıcılar kullanılarak üretilen sertmetaller arasında kobalt en çok tercih edilen bağlayıcı malzemedir. Tungsten karbür parçacıkların matrisi içindeki ıslanabilirliğinin yüksek olması, düşük yüzey enerjisine sahip olmaları ve katı halde üstün mekanik yapışma sağlaması sayesinde, kobalt sertmetallerde bağlayıcı olarak kullanılmaktadır [6]. Belirtilen özellikler sertmetallerin boşluksuz olarak üretilmesi ve yapısal bütünlüğünün sağlanması için çok önemlidir. Boşluklu malzemelerde yük altında erken ve ani kırılmaların gözlenebileceği ve yorulma ömürlerinin düşük olacağı bilinmektedir.

Tüm mühendislik malzemeleri düşünüldüğünde en çok karşılaşılan hasar mekanizması olan yorulma, sertmetaller açısından da kritik öneme sahiptir [7,8]. Alüminyum alaşımları ve çeliklere göre sertmetallerde görülen yorulma davranışı malzeme yapısı gereği daha farklıdır. Sertmetallerin yorulma davranışını inceleyen çalışmaların özellikle son 20 yılda malzeme özelliklerinin iyileştirilmesi sayesinde yoğunlaştığı gözlenmektedir. Sertmetallerin yorulma performansının incelenmesi açısından S-N grafiklerinin deneysel olarak çıkarılması ve yorulma çatlak ilerlemesinin incelendiği çalışmalar öne çıkmaktadır [9,10]. Yapılan çalışmalarda incelenen diğer bir husus ise sertmetal üretiminde kullanılan bileşenlerin metalürjik ve mikroyapı özellikleri ve hasar mekanizmasına olan etkileridir [11,12]. Yapılan çalışmalarda kırılmaların sünek kobalt fazından başlayıp ilerlediğini gösteren çalışmalara rastlanmaktadır [1]. Çatlak başlangıç konumları incelendiğinde özellikle malzeme kusurları (boşluk, topaklanma vb.) veya tungsten karbür tanecik sınırlarının altı çizilmiştir [13]. Tungsten karbür toz parçacıklarının morfolojisinin ve büyüklüklerinin yorulma direnci açısından çok önemli olduğu belirtilmiştir [14]. Özellikle yorulma direncini artırmak için tungsten karbür malzemelerin tane büyüklüklerinin artırılması tavsiye edilmektedir [15]. Kobalt ile üretilen sertmetallerde dikkat edilmesi gereken bir diğer konu da kobaltın sıcaklık ve deformasyon ile kristal yapı değişikliği yaşamasıdır [5,16]. Hegzagonal sıkı paket yapısına sahip allotropu göz önünde bulundığında, kobalt malzemelerde içyapı ve kristal yapısına bağlı olarak kırılma bir kırılma davranışı gözlenebilmektedir.

Ülkemizde bilya püskürtme veya bilyalı dövme (İng. shot peening) olarak bilinen işlem özellikle havacılık ve otomotiv sanayinde tercih edilen ve başta alüminyum alaşımları ve çeliklere uygulanan lazerli dövme, ultrasonik darbe prosesi gibi mekanik yüzey işlemlerin başında gelmektedir [17,18]. Özellikle uygulandıkları malzemenin yorulma ömrünü artırmak için kullanılan bu prosenin, malzemelerin balistik performansını artırmaya yönelik uygulama alanları da bulunmaktadır [19]. Bu yöntem ile yüksek basınçlı hava ile çelik veya seramik malzemeden elde edilen bilyalar numune yüzeyine püskürtülmektedir [20]. Bilyaların malzeme yüzeyinde yol açtığı plastik deformasyon sonucu gerinim sertleşmesi sayesinde sertlik artışı elde edilebilmektedir [21]. Ayrıca, proses sonunda basma kalıntı gerilmeler işlenen malzeme yüzeyine yakın bölgede oluşmaktadır [22]. Ancak, püskürtülen bilyalar nedeniyle malzemede yüzey pürüzlülüğü artışı da gözlenmektedir. Literatürde yapılan çalışmalar incelendiğinde, malzemelerdeki sertlik artışı ve elde edilen bası kalıntı gerilmeler sonucu malzeme yorulma performansında artışlar elde edilebildiği ortaya konmuştur [23].

Soğuk dövme yöntemi gibi kalıp ile üretim yapılan tesislerde, kalıp ömrü hem maliyet hem de verimlilik açısından çok önemli bir konudur. Çalışma ömrü düşük kalıplarla yapılan üretimlerde kalıp sarf maliyetleri artmaktadır. Ayrıca, daha sık

kalıp değişikliği ihtiyacı ortaya çıktığı için duruşlar yaşanmakta ve proses verimliliğinde ciddi kayıplar gözlenmektedir. Bu nedenle, kalıp kullanılarak yapılan üretimlerde kalıp ömrünün artırılması çok önemli bir konudur. Bu çalışmada, özellikle cıvata, somun, perçin gibi bağlantı elemanı kalıplarında kullanılan ve %25 oranında kobalt içeren tungsten karbür-kobalt sertmetal malzemeler incelenmiştir. Soğuk şekillendirme kalıplarının yorulma direncinde iyileşme elde edebilmek için bilyalı dövme işlemi ele alınmıştır. Malzemelerin yorulma performansı ile beraber mikroyapı, sertlik, yüzey pürüzlülük ve kristal yapıları karşılaştırılmıştır. Yorulma deneyleri sonucu kırılan numuneler taramalı elektron mikroskobu yardımıyla incelenmiş ve kırılma karakteristikleri konusunda detaylı çalışmalar yapılmıştır.

2. Malzeme (Material)

Bu çalışmada tungsten karbür-kobalt metal seramik kompozit malzeme sınıfına giren sertmetaller kullanılmıştır. İlgili malzeme üretimi için tungsten karbür bileşenler toz halinde tedarik edilmektedir. Matriks malzeme olarak seçilen kobalt toz halinde kullanılmakta ve tungsten karbür parçacıkları ile karıştırılmaktadır. Karıştırma işlemi ile homojen dağılımları sağlanan malzemelerin ufalama sonrasında toz parçacık boyutları küçültülmekte ve preslenmeye hazır hale getirilmektedir. İstenen nihai ürün formu göz önünde bulundurularak presleme işlemi gerçekleştirilmekte ve sinterleme öncesi bu forma işlenmektedir. Yaklaşık 1300°C ve 100 bar basınç altında özel fırınlarda yapılan sinterleme işlemi ile ürün şekillendirme prosesi tamamlanmaktadır. Sinterleme sonrası, ürün formuna bağlı olarak talaşlı imalat ile ürün nihai forma getirilmektedir. Tungsten karbür ve kobalt ile üretimi yapılan sertmetallerde kontrol edilebilecek önemli iki parametre bulunmaktadır. Bunlar, iki fazın yüzdesel oranları ve tungsten karbür toz malzemenin tane boyutudur. İlgili sertmetal kullanım alanına göre ve beklenen performans kriterleri çerçevesinde bu iki parametre için optimum değerler belirlenmelidir. Malzemenin yüksek aşınmaya maruz kaldığı uygulamalarda sertlik değerini artırmak için kobalt oranının azaltılmasıyla beraber daha küçük tane büyüklüğüne sahip tungsten karbür tozlar kullanılmaktadır. Yorulma altında çalışan bileşenlerde ise kobalt oranı artırılarak daha büyük tane büyüklüğüne sahip karbür malzeme tercih edilmektedir.

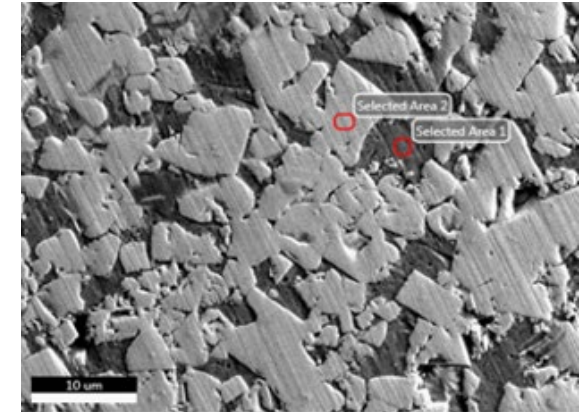
Bu çalışma kapsamında seçilecek malzemenin soğuk şekillendirme kalıplarında kullanılacak olmasından dolayı yüksek aşınma ve tokluk değerlerine sahip olması gerekmektedir. Bu nedenle %25 kobalt içeren ve büyük tungsten karbür tane yapısına sahip bir sertmetal seçilmiştir. Kullanılan malzemeye ait özellikler Tablo 1 ile verilmiştir.

Tablo 1. Bu çalışmada kullanılan WC-Co malzemesine ait elementel, fiziksel ve mekanik özellikler (Elemental, physical and mechanical properties of WC-Co material used in this study).

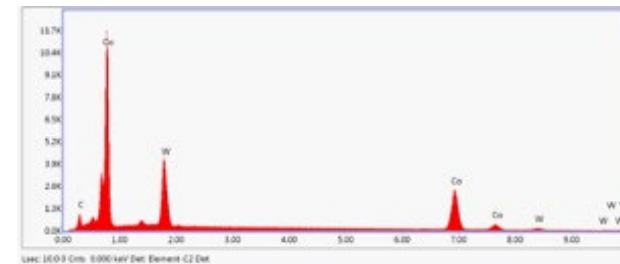
Malzeme	Co Oranı (%)	Yoğunluk (g/cm ³)	Tane Büyüklüğü	Elastisite Modülü (GPa)	Enine Kırılma Dayanımı (MPa)	Kırılma Tokluğu (MPa*m ^{1/2})
WC-Co Sertmetal	25	13.15	Ekstra kaba (>6 µm)	450	2700	27

Çalışmalarda kullanılan tungsten karbür-kobalt malzemesine ait taramalı elektrom mikroskobu ile elde edilmiş mikroyapı ve SEM EDX analiz sonuçları Şekil 1 ile verilmiştir. İlgili deneyler Carl Zeiss 300VP SEM kullanılarak gerçekleştirilmiştir. Mikroyapı görüntülerinde farklı şekil ve boyutlardaki açık gri tungsten karbür tanelerinin koyu gri kobalt matriks fazı içinde dağıldığı gözlenmiştir. İncelenen WC-Co numunelerde beklendiği gibi boyutları 6 µm'den büyük taneler olmasına rağmen daha küçük ve farklı morfolojide taneçiklere de rastlanmıştır. Kesit alımı sırasında taneçiklerin taşlandığı göz önünde bulundurulduğunda taneçiklerin bir kısmı bu nedenle küçük elde edilmiştir. Tungsten - karbon faz diyagramına

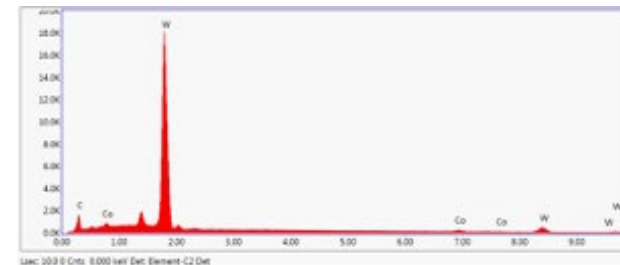
göre tungsten karbür içeren malzemelerde karbon oranının çok dar bir bandta olması gerekmektedir. Karbon miktarının stokiometrik oranın altında olması durumunda mikroyapı içerisinde dağınık şekilde η-fazı; stokiometrik oranın üstünde olması durumunda ise grafit oluşabilmektedir. Belirtilen iki durumda da malzeme tokluk değerlerinde düşüş olacaktır. Çalışma kapsamında incelenen numunelerde mikroyapı içerisinde η-fazına veya grafit rastlanmamıştır. Yapılan EDX analizlerinde, karbon, tungsten ve kobalt elementlerine ait pikler elde edilmiş olup farklı iki bölgeden yapılan ölçüm sonuçları Şekil 1 ile verilmiştir. Alan 1 kobalt fazından, Alan 2 ise tungsten karbür parçacıktan yapılan ölçümler olduğu için Alan 1'de elde edilen kobalt faz oranı %66,38, Alan 2 ölçümünde ise tungsten oranı %92,00 olarak elde edilmiştir. Alan 1 içerisinde elde edilen tungsten ve karbon pikleri X-ışınlarının kobalt içerisinde penetre ederek incelenen alanın altından ve çevredeki parçacıklardan gelmektedir. Tungsten ağır metal sınıfında bir element olduğundan X-ışınlarının penetresi çok daha sınırlıdır. Bu nedenle pikler yaklaşık %98 oranında tungsten ve karbondan elde edilmiştir.



(a)



(b)



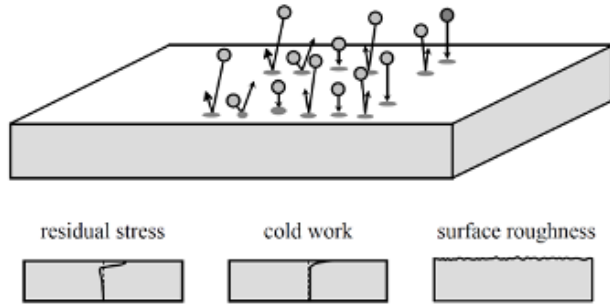
(c)

Şekil 1. WC-Co malzemesine ait taramalı elektron mikroskobu ile elde edilmiş (a) mikroyapı görseli. Mikroyapı görselinde belirtilen (b) Alan 1 ve (c) Alan 2'den elde edilen EDX sonuçları. ((a) Microstructure of WC-Co material obtained by scanning electron microscopy. EDX results of (b) Area 1 and (c) Area 2 shown in the microstructure image.)

Yorulma testlerinde kullanılacak yükleme koşulları ve numune geometrisi için uygun standartlar taranmıştır. Öncelikle, bu çalışmada kullanılan malzemelerin çok sert olmasından dolayı konvansiyonel yorulma testleri yerine yorulma eğmesinin tercih edildiği literatür araştırması sonucu ortaya konmuştur [24-26]. Uygulanacak yorulma testleri kapsamında ISO 3327:2009 numaralı "Sinterlenmiş karbür malzemelerin enine kırılma dayanımı" (İng. Hardmetals - Determination of transverse rupture strength [27]) standardına göre "B Tipi" numune geometrisi olarak belirlenmiş ve numune ölçüleri 20 mm, 6,5 mm ve 5,25 mm olacak şekilde üretilmiştir. İlgili numuneler sinterleme sonrasında taşlanarak yorulma testlerine hazır hale getirilmiştir.

3. Deneysel Metot (Experimental Method)

Sinterlenerek üretilen numuneler taşlama işleme sonrasında bilyalı dövme işlemine maruz bırakılmıştır. Bilyalı dövme işleminin malzeme yüzeyinde yarattığı etkiyi ve çalışma mekanizmasını gösteren şematik görsel Şekil 2 ile verilmiştir. Yüksek basınçlı hava ile bombardıman edilen bilyalar malzeme yüzeyinde plastik deformasyona neden olmakta ve sertlik artışı elde edilmektedir. Bu sayede malzemenin yüzeye yakın bölgelerde kırılmaya neden olabilecek çatlakların oluşması geciktirilmekte ve malzemenin yorulma direncinde artış elde edilmektedir. Bu çalışmada bilyalı dövme işlemi tam otomatik bir sistem kullanılarak gerçekleştirilmiştir. Bilyalı dövme işlemi numunelerin sadece bir yüzeyine uygulanmıştır.



Şekil 2. Bilyalı dövme işleminin şematik görüntüsü [17] (Schematic representation of shot peening process [17]).

Yorulma deneylerinde sinterlenerek üretilen ve sonrasında bilyalı dövme işlemine maruz bırakılan numunelerin karakterizasyon testleri gerçekleştirilmiştir. Numunelerin yüzey pürüzlülük ölçümleri Mitutoyo SurfTest SJ-400 kullanılarak R_a ve R_z olarak elde edilmiştir. Yüzey pürüzlülük ölçümleri üç kere tekrarlanarak bilyalı dövme öncesi ve sonrası yüzey dağılımının homojenliği de incelenmiştir.

Yüzey pürüzlülüğü testlerinin ardından makro ve mikro sertlik ölçümleri yapılmıştır. Makro sertlik ölçümleri BMS Digi-rock, mikro sertlik ölçümleri ise KB 30S cihazları kullanılarak gerçekleştirilmiştir. Makro sertlik testleri, herhangi bir yüzey hazırlığı olmadan yapılmıştır. Bu sayede, bilyalı dövme işleminden etkilenen yüzeye yakın bölgenin yüzey hazırlığı neticesinde bozulması engellenmiştir. İlave olarak, detaylı sertlik incelemesinin yapılabilmesi için mikro sertlik yöntemi ile yüzeyden ölçümler yapılmıştır. Ayrıca, numuneler kesilerek parlatılmış ve mikro sertlik cinsinden derinlik profilleri çıkarılmıştır.

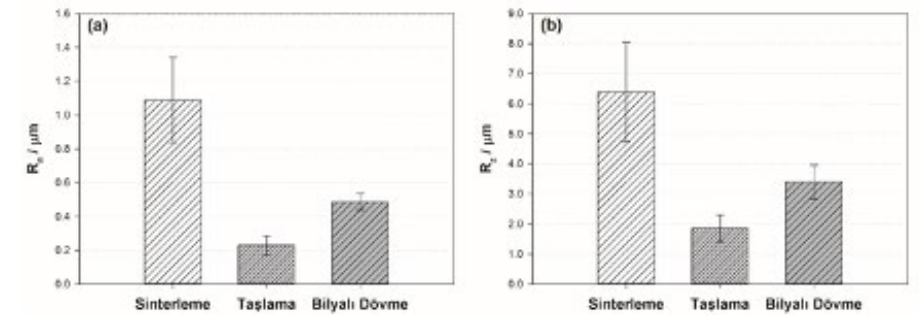
Bilyalı dövme işlemi sonrasında kobalt fazında herhangi bir kristal yapı değişikliği olup olmadığını ortaya çıkarmak için

X-ray ışınları kırınım yöntemi kullanılmıştır. Panalytical Empyrean XRD cihazı ile yapılan deneylerde anot olarak Cu K tercih edilmiştir. Tarama işlemi, kırınım açısı (2θ) 40° ile 70° derece arasında olacak şekilde ve 0.013° lik adımlarda yapılmış ve sayım değerleri kayıt altına alınmıştır. Deneylerde hem kobalt hem de tungsten karbür fazından kırınımlar elde edilmiştir. Test sonrası elde edilen ham veriler Pseudo-Voigt fit fonksiyonu kullanılarak işlenmiş ve elde edilen dorukların kırınım açıları elde edilmiştir.

Yorulma testleri yüksek frekanslı Zwick Roel 250 kN yorulma cihazı kullanılarak gerçekleştirilmiştir. Numune geometrisine uygun testlerin yapılabilmesi için özel çene ve aparatlar tasarlanarak üretilmiştir. Yorulma testlerinde ön statik yük $-7,6$ kN, dinamik yük ise $4,6$ kN olarak uygulanmıştır. Bilyalı dövme işleminin etkisini ortaya koymak için işlenmiş yüzeyler yükün uygulandığı yüzeyin karşısında kalacak şekilde numuneler yerleştirilmiştir. Bu sayede test esnasında bilyalı dövme ile işlenmiş yüzeyde çeki gerilmelerinin oluşması sağlanmış ve bilyalı dövme prosesinin etkisi incelenmiştir. Yorulma testleri, taşlanmış ve taşlama sonrası bilyalı dövme işlemi uygulanmış numuneler kullanılarak iki set halinde gerçekleştirilmiştir. Her set için 6 adet yorulma testi yapılmıştır.

4. Sonuçlar ve Tartışmalar (Results And Discussions)

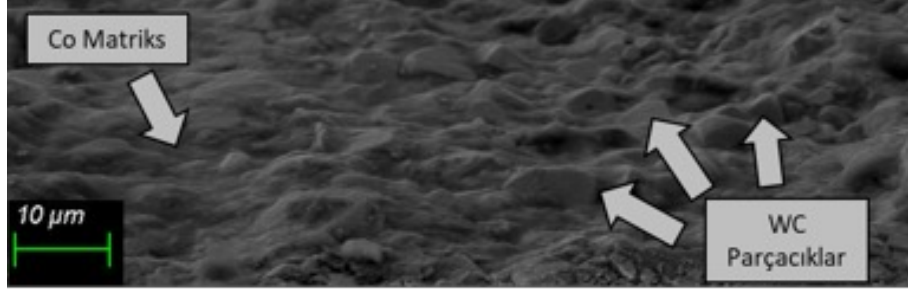
Sinterleme, taşlama ve bilyalı dövme işlemleri sonrasında elde edilen yüzey pürüzlülük sonuçları Şekil 3 ile verilmiştir. Sinterleme sonucu elde edilen yüksek yüzey pürüzlülük değerleri taşlama işlemi sayesinde R_a ve R_z için sırasıyla %79 ve %71 oranında azaltılarak bilyalı dövme işlemine hazır hale getirilmiştir. Bilyalı dövme işlemi ile yüksek basınçlı hava kullanılarak malzemeye yönlendirilen bilyaların yüzeye çarparak çukurlar oluşturduğu ve bu çukurların malzeme yüzey pürüzlülük değerlerinde artışa neden olduğu bilinmektedir. Bu çalışma kapsamında yapılan ölçümlerde, R_a ve R_z değerlerinde taşlama sonrası elde edilen yüzey ile karşılaştırıldığında sırasıyla %112 ve %83 artışın meydana geldiği tespit edilmiştir. Yorulma açısından bakıldığında yüzey pürüzlülük değerlerinin artması nedeniyle çatlak başlama bölgelerinde artış olabileceği ve malzemenin yorulma direncinde düşüşün yaşanabileceği literatürde sıkça tartışılmıştır [13]. Ancak, bilyalı dövme sonrası elde edilen sertlik artışı sayesinde, yüzey pürüzlülük değerlerindeki artışa rağmen yorulma değerlerinde iyileşme elde edilebilmektedir. Bu çalışmada işlenen malzemenin sertlik değerlerinin yüksek olması nedeniyle



Şekil 3. Sinterleme, taşlama ve bilyalı dövme işlemleri sonrası (a) R_a ve (b) R_z yüzey pürüzlülük değerleri ((a) R_a and (b) R_z surface roughness values after sintering, grinding and shot peening processes).

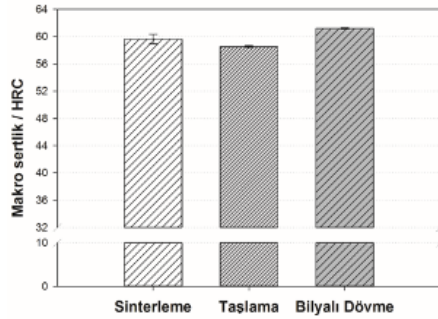
alüminyum veya çelik malzemelere nispeten yüzey pürüzlülük değerinde daha az artış meydana gelmiştir. Bilyalı dövme sonrası alüminyum Al6061-T651 malzeme yüzey pürüzlülük değerinde %780'e kadar artış elde edildiği çalışmalar göz

önünde bulunduğunda %112'lik artışın daha sınırlı olduğu ortaya konmuştur [19]. Yüzey pürüzlülük değerleri ile beraber ölçüm sonuçları sonrası elde edilen standart sapma değerleri de incelenmiştir. Taşlama sonrası standart sapma değerlerinde düşüş elde edilmiştir. Ayrıca, bilyalı dövme öncesi ve sonrasında elde edilen standart sapma değerleri birbirine yakın elde edilmiştir. Bu durum, bilyalı dövme işleminin homojen bir şekilde yapıldığını gösterir niteliktedir.



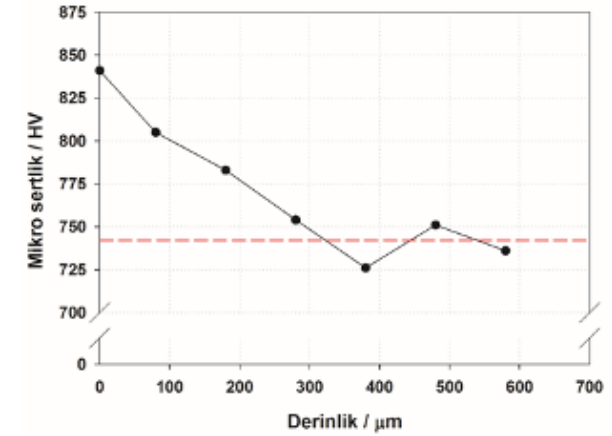
Şekil 4. Bilyalı dövme işlemi sonrası taramalı elektron mikroskobu ile elde edilen yüzey morfolojisi (Surface morphology after shot peening process obtained by scanning electron microscopy).

Bilyalı dövme işlemi sonrası taramalı elektron mikroskobu ile elde edilen yüzey morfolojisine ait görüntü Şekil 4 ile verilmiştir. Yüzeyde bilya bombardımanı sonrası oluşmuş çukurlar net bir şekilde görülmektedir. Ayrıca, yüzeye yakın yerlerde farklı büyüklükte tungsten karbür parçacıklarına rastlanmaktadır.



Şekil 5. Sinterleme, taşlama ve bilyalı dövme işlemleri sonrası makro sertlik (HRC) değerleri (Macro hardness (HRC) values after sintering, grinding and shot peening processes).

Bilyalı dövme işlemi öncesi ve sonrası HRC cinsinde elde edilen makro sertlik değerleri Şekil 5 ile verilmiştir. Sinterleme ve taşlama sonrası yapılan makro sertlik ölçümlerinde yaklaşık %2'lik bir fark ortaya çıkmış olup standart sapma değerleri göz önüne bulundurulduğunda taşlama sonrası ciddi bir sertlik değişimi olmadığı sonucuna varılmıştır. Bilyalı dövme sonrası numune yüzeyinden ölçülen makro sertlik artışı yaklaşık %5 olarak tespit edilmiştir. Herhangi bir yüzey işleme ihtiyaç olmadan ölçümlerin yapılabilmesine olanak sağladığı için öncelikle makro sertlik yöntemi tercih edilmiştir. Ancak, makro sertlik ile elde edilen sonuçların karşılaştırılması için mikro sertlik yöntemi ile ilave ölçümler yapılmıştır. HV10 cinsinden yapılan yüzey mikro sertlik ölçümlerinde sertlik değeri 841 HV olarak elde edilmiştir. Daha sonra, bilyalı dövme işleminden etkilenmiş bölgeyi belirleyebilmek için numunelerden bir tanesi kesilerek parlatılmış ve derinlik profili çıkarılmıştır. HV2 cinsinden elde edilen sertlik profili Şekil 6 ile verilmiştir. Derinlik profili göz önünde bulundurulduğunda



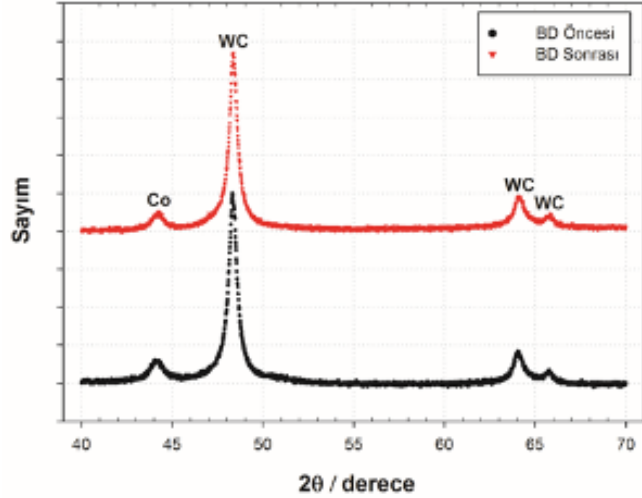
Şekil 6. Bilyalı dövme sonrası elde edilen mikro sertlik (HV) derinlik profili (Micro hardness (HV) depth profile obtained after shot peening).

sertlik değerlerinde kademeli bir azalma elde edilmiş ve yaklaşık 742 HV civarında sabitlenmiştir. Derinlik profili ile elde edilen dataların yüzeye ekstrapolasyon yapılması sonucu yüzeyde elde edilen sertlik değeri, yüzeyden HV10 mikro sertlik test sonucunda elde edilen ölçüm sonucu ile uyumlu olduğu gözlenmiştir. Bilyalı dövme sonrası malzeme yüzeyinde yaklaşık %13'lik bir mikro sertlik artışı olduğu ortaya çıkarılmıştır. Yüzeyde yaklaşık 841 HV olarak elde edilen mikro sertlik değeri yüzeyden yaklaşık 300 µm derinlikte 742 HV değerine ulaşmıştır.

Bilyalı dövme sonucu elde edilen sertlik artışı nedenlerinin ortaya çıkarılması için kobalt fazı detaylı incelenmiştir. Kobalt fazında oluşabilecek sertlik artışı iki ana mekanizma sonucu ortaya çıkmaktadır. Bunlardan ilki bilyalı dövme prosesi sonucu elde edilen plastik deformasyon ve gerinim sertleşmesi sonucu kobalt matriste sertlik artışı elde edilmesidir. Bir diğeri de farklı allotropları olan kobalt fazının yüzey merkezli kübik kristal yapısından mekanik deformasyon sonucu hegzagonal sıkı paket yapısına dönüşmesidir [24]. Kristal yapıda elde edilen bu değişim sonucu etkin sekme dizgesinde azalma elde edilerek dislokasyon hareketinde sınırlama ve plastik deformasyon olma limitinde yükselme sonucu sertlik artışı elde edilmektedir. Bilyalı dövme sonrası elde edilen yüzey pürüzlülük artışı malzeme yüzeyine yakın bölgede plastik deformasyon olduğunu ispatlamaktadır. Bu durum, gerinim sertleşmesinin bilyalı dövme sonrası sertlik artışına neden olduğunu göstermektedir.

Bilyalı dövme işlemi sonrası kobalt fazında olası kristal yapı değişikliğini ortaya çıkarmak için yapılan ve X-Işınları kırınım yöntemi kullanılarak elde edilen sayım-kırınım açısı sonuçları Şekil 7 ile verilmiştir. WC-Co sertmetaller, toz numunelerden sinterlenerek üretilmektedir. Proses öncesinde kobalt fazında yüzey merkezli kristal ve hegzagonal sıkı paket yapıları beraber gözlenirken karıştırma ve sinterleme sonrası çoğunlukla yüzey merkezli kristal yapının elde edildiği bilinmektedir [28]. Bu nedenle, kobalt fazında olası kristal yapı değişikliğini ortaya çıkarmak için hegzagonal sıkı paket yapısına ait dorukların varlığı ve/veya doruklardaki değişiklikler incelenmiştir. Öncelikle, bilyalı dövme uygulanmamış numune için kırınım açısı 40° ile 70° arasında olacak şekilde test gerçekleştirilmiştir. Sonuçlar incelendiğinde, kobaltın yüzey merkezli kristal yapısında görülen (111) düzlem ailesine ait doruk elde edilmiştir. Beklendiği gibi hegzagonal sıkı paket yapısına

ait herhangi bir doruk gözlenmemiştir. Bilyalı dövme sonrası X-ışınları kırınım testi tüm parametreler aynı olacak şekilde tekrarlanmıştır. Testler sonucunda, bilyalı dövme öncesi gözlenen benzer bir doruk yapısı elde edilmiş ancak bilyalı dövme işlemi sonrası doruklarda bir miktar kayma tespit edilmiştir [29]. Özellikle kırınım açısı yaklaşık 42° olduğunda hegzagonal sıkı paket yapısına sahip kobalttan güçlü bir doruk beklenmektedir [30]. Ancak, bilyalı dövme sonrası ele

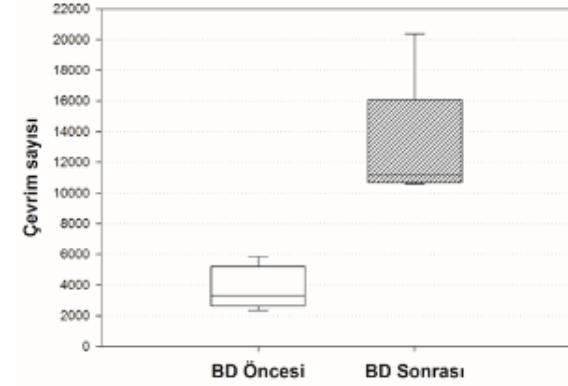


Şekil 7. WC-Co numunelere ait Bilyalı Dövme (BD) öncesi ve sonrası X-ışınları kırınım grafiği (X-ray diffraction pattern of WC-Co samples before and after shot peening).

edilen sonuçlarda (100) düzlem ailesine sahip ilgili doruğun gözlenmemesi numunelerde kayda değer bir hegzagonal sıkı paket yapısı veya değişimi olmadığını ortaya çıkarmıştır. Sonuç olarak bilyalı dövme işlemi sonrası elde edilen sertlik artışının gerininin sertleşmesi sonucu elde edildiği ortaya konmuştur.

Malzeme karakterizasyon testlerinin ardından bilyalı dövme ile işlenmiş ve işlenmemiş numuneler kullanılarak yorulma testleri gerçekleştirilmiştir. Yapılan deneylere göre elde edilen yorulma deney sonuçları Şekil 8 ile verilmiştir. Şekilde barlar içerisindeki çizgi medyan değerini, verilen barlar standart sapma ile belirlenmiş yorulma ömürlerini ve barların altında ve üstünde görülen çizgiler de testler sonucu elde edilen yorulma ömür aralığını göstermektedir. Öncelikle, yorulma testlerinde minimum-maksimum yorulma ömür aralığı yüksek elde edilmiştir. Bu durumun en önemli nedeni sertmetaller gibi çok sert malzemelerin yorulma testi ile çevrimli yüke maruz kalması durumunda yüzeydeki boşluk ve inklüzyon gibi malzeme kusurlarının çatlak başlangıç alanları gibi davranarak erken ve ani kırılmalara yol açmasıdır. Bu nedenle sertmetaller gibi sertlik değeri yüksek malzemelerin yorulma testleri sonuçlarında yüksek değer aralığı beklenebilir. Deneyler sonucu elde edilen minimum-maksimum yorulma ömür aralığı bilyalı dövme işlemi sonrasında daha fazla elde edilmiştir. Bu durum, bilyalı dövme sonrası artan yüzey pürüzlülük değerleri ve olası çatlak başlama alanlarının artması ile açıklanabilir. Ortalama yorulma değerleri göz önüne alındığında incelenen sertmetal numunelerde bilyalı dövme işlemi sonrası %248'lik iyileşme elde edilmiştir. Artan yüzey pürüzlülüğüne rağmen yorulma ömründeki artış sertlik miktarındaki iyileşmenin daha baskın olduğunu göstermektedir. Çatlakların yüzeyden başlayarak ilerlediği göz önünde bulundurulduğunda

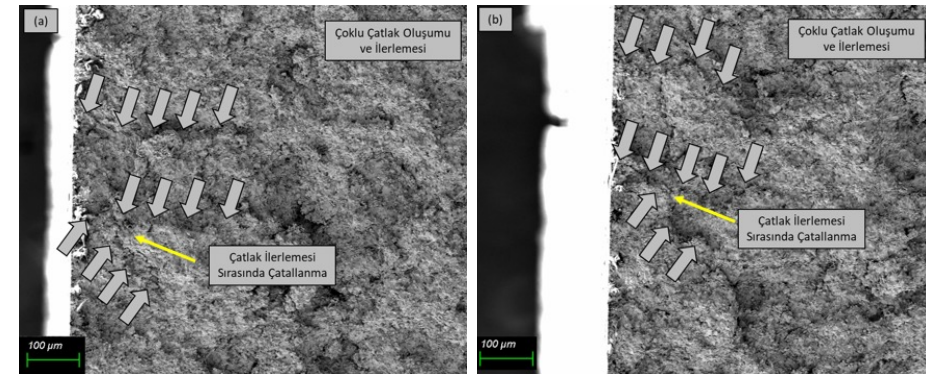
bilyalı dövme sonucu özellikle yüzeye yakın bölgede elde edilen sertlik artışının yorulma ömrünü artırdığı ortaya konmuştur. Özellikle daha az sünek olan ve çatlak ilerleme evresinin daha kısa olduğu malzemelerde yorulma ömrünün artırılması



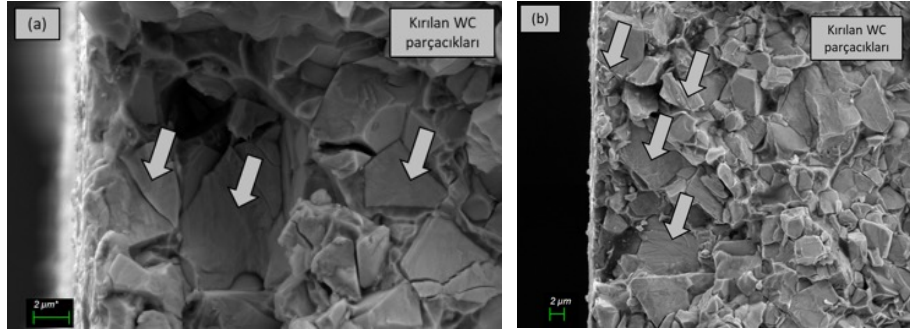
Şekil 8. Bilyalı Dövme (BD) öncesi ve sonrası numunelerin yorulma test sonuçları (Fatigue life results of samples before and after shot peening (SP)).

için özellikle çatlak başlamasının geciktirilmesi gerekmektedir. Yüzeye yakın bölgede elde edilen bilyalı dövme kaynaklı sertlik artışı sayesinde çatlak başlangıç evresi uzatılarak malzemenin yorulma ömründe artış elde edilmiştir.

Yorulma testlerinin ardından taramalı elektron mikroskobu ile detaylı mikroyapı incelemeleri gerçekleştirilmiştir. Bilyalı dövme yapılmamış ve yapılmış numunelerden yüzeye yakın yerden kesit olarak elde edilen kırılma yüzey görüntüsü Şekil 9 ile verilmiştir. Bilyalı dövme uygulanmış numelerde yapılan incelemelerde, yorulma çatlaklarının farklı noktalardan başladığı ve ilerlediği tespit edilmiştir. Çatlak ilerlemesi sırasında oluşan yüklem koşullarındaki değişim ve malzeme mik-



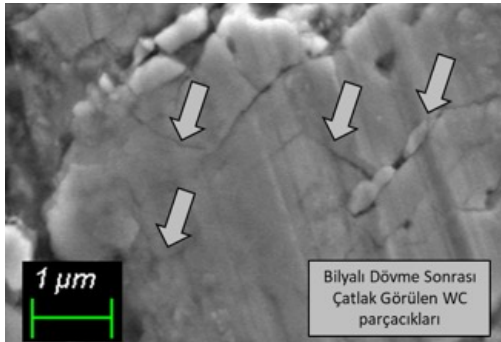
Şekil 9. (a) Bilyalı Dövme işlemi öncesi ve (b) Bilyalı Dövme işlemi sonrası yorulma çatlaklarını gösteren kırılma yüzey görüntüleri (Fracture surface images (a) before shot peening and (b) after shot peening process showing fatigue cracks).



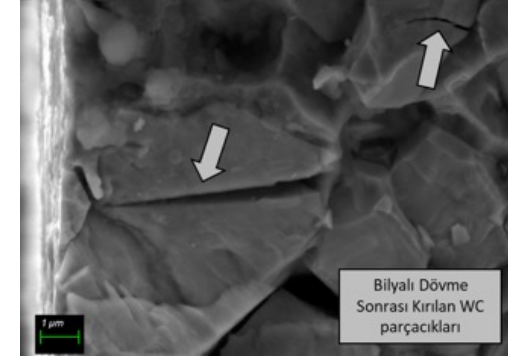
Şekil 10. (a) Bilyalı Dövme işlemi öncesi ve (b) Bilyalı Dövme işlemi sonrası yüzeye yakın kesitten elde edilen kırılma yüzey görüntüsü (Near-surface fracture surface images (a) before shot peening and (b) after shot peening process).

royayı değişkenliklerinden dolayı çatlak ilerlemesi sırasında çatallanmalar gözlenmiştir. Kırılma esnasında hem tane-lerarası hem de tane içi çatlak ilerleme mekanizmalarının kırılmaları neden olduğu saptanmıştır. Bunun yanında, incelenen numunelerde sünek malzemelerde gözlenen belirgin yorulma yivcilerine rastlanmamıştır. Bilyalı dövme uygulanmamış numunelerde de benzer çatlak oluşumları ve ilerleme mekanizmaları gözlenmiştir (Şekil 9).

Kırılma yüzeyindeki tungsten karbürler incelendiğinde bazı parçacıkların kırıldığı tespit edilmiştir. Yapılan detaylı incelemelerde farklı mekanizmalar sonucunda parçacıkların kırıldığı anlaşılmıştır. Öncelikle, bilyalı dövme işlemi uygulanmış ve uygulanmamış numunelerden elde edilen yüzeye yakın bölgelerde bazı parçacıkların yorulma neticesinde kırıldığı belirlenmiştir (Şekil 10). Ayrıca, yapılan incelemelerde bazı parçacıkların bilyalı dövme işlemi sonucunda kırıldığı ortaya çıkarılmıştır. Bu kapsamda, bilya dövme işlemi uygulanan alanlarda incelemeler yapılmış ve yüzeydeki bazı parçacıkların tekrarlı bilya bombardımanı neticesinde kırıldığı tespit edilmiştir. Şekil 11 ile verilen yüzeydeki parçacık görüntüsünde de görüldüğü gibi bilyalı dövme sonrası farklı yönlerde çatlaklar oluşmuştur. Bu durum, bilyalı dövme işlemi sırasında rastgele yüzeye çarpan bilyaların oluşturduğu yüklemeye koşulu neticesindedir. Kırılmaların yaşandığı kesitten yapılan incelemelerde yüzeye yakın bazı tungsten karbür parçacıklarının da kırıldığı anlaşılmıştır. Yüksek basınçlı bilyaların oluşturduğu bombardımana maruz kalan yüzeydeki parçacıklar, kendilerine gelen yükleri çevrelerindeki parçacıklara kobalt matrisi üzerinden veya direk temas yoluyla aktarmaktadır. Bu aktarım sırasında parçacık köşelerine denk gelen kısımlarda gerilme birikmesi sonucu kırılmaların oluştuğu tespit edilmiştir. Bu durum sonucu kırılan örnek parçacık görşeli



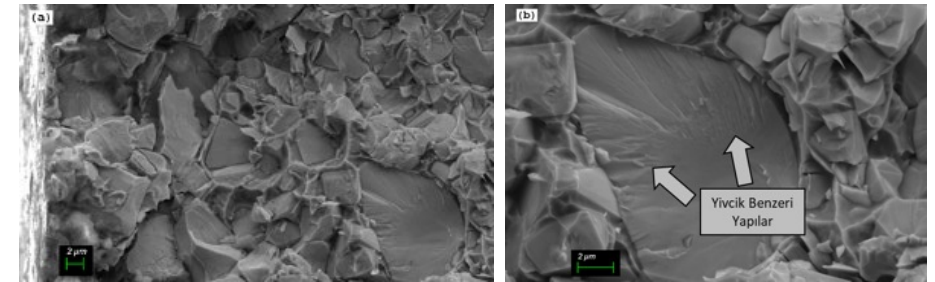
Şekil 11. Bilyalı Dövme uygulanan yüzeyde kırılan tungsten karbür parçacıkları. Görüntü Bilyalı Dövme yapılmış yüzeyden elde edilmiştir. (Fractured tungsten carbide particles after shot peening. Image was taken at the shot peened surface.)



Şekil 12. Bilyalı Dövme işlemi sonucu kırılan tungsten-karbür parçacıkları. Görüntü kırılma yüzeyinden elde edilmiştir. (Fractured tungsten carbide particles after shot peening. Image was taken at the fractured surface.)

Şekil 12 ile verilmiştir. Bu mekanizma sonucu kırılan parçacıklarda, kırılma morfolojisi, yüklemeye koşulları ve parçacık geometrisine bağlıdır. Dolayısıyla, farklı yönlerde benzer çatlak oluşumları malzeme içyapı incelemelerinde görülmüştür. Özellikle Şekil 12 ile verilen iki adet çatlak ve bu çatlakların başlama ve ilerleme yönleri bu durumu kanıtlar niteliktedir.

Çevrimli yüke maruz kalan numunelerde tane içi çatlak ilerlemesi sonucu tungsten-karbür parçacıklarının kırıldığı ortaya çıkarılmıştır (Şekil 13). Bilyalı dövme yapılmış ve yapılmamış yüzeylere yakın bölgelerde bu tipte kırılan parçacıklar gözlenmiştir. Bu durum, ilgili kırılmaların bilyalı dövme işlemi sonucunda oluşmadığını ortaya koymaktadır. Kırılan parçacıkların bazılarında yivcilerle benzer oluşumlara rastlanmıştır. Bu tür yivcik benzeri yapılar incelendiğinde kırılma ve farklı yönlerde ilerleme tespit edilmiştir. Bu durum, parçacıkların rastgele konumlanması ve farklı morfolojiye sahip olmaları nedeniyle çatlak ilerlemesi ile oluşan kompleks ve dinamik yüklemeye koşulu ve buna bağlı oluşan gerilme dağılımı sonucudur.



Şekil 13. (a) Tane içi çatlak ilerlemesi sonucu kırılan tungsten karbür parçacıkları ve (b) kırılan parçacık içerisindeki yivcik benzeri yapı ((a) Fractured tungsten carbide particles due to intergranular crack propagation and (b) striation-like features at the fractured particle).

Yapılan detaylı karakterizasyon testleri göz önünde bulundurulduğunda literatürde belirtildiği gibi bilyalı dövme sonrası yüzey pürüzlülüğü ve yüzeye yakın bir bölgede sertlik artışı elde edildiği ortaya konmuştur. X-ışınları kullanılarak yapılan

deneylerde kobalt fazında kayda değer kristal yapı değişikliğine rastlanmamıştır. Sonuç olarak, yorulma testlerinde elde edilen ömür iyileşmelerini sağlayan ana mekanizmanın gerinim sertleşmesi sonucu görülen sertlik artışı olduğu belirlenmiştir. Özellikle bilyalı dövme, lazerli dövme gibi mekanik yüzey işlemlerinde sertlik artışının olduğu literatürde belirtilmiştir [18,19]. Yorulma testleri sonucu oluşan kırılma yüzeyleri üzerine detaylı incelemeler gerçekleştirilmiştir. Taramalı elektron mikroskobu ile elde edilen görüntüler neticesinde, yorulma sonucu gözlenen kırılmalara neden olan çatlakların farklı konumlardan başladığı ve yükleme koşulu ile mikroyapı dağılımına göre çatlaklanarak ilerleyebildiği tespit edilmiştir. Çatlak ilerlemesi açısından yapılan analizlerde hem tanelerarası hem de tane içi çatlak ilerlemelerine rastlanmıştır. Ayrıca, tungsten karbür parçacıklarının hem bilyalı dövme sonrası hem de yorulma sonucu kırıldığı ortaya konmuştur.

5. Sonuçlar (Conclusions)

Bu çalışmada, kapsamında aşağıda sıralanan sonuçlar elde edilmiştir.

1. Tungsten karbür – kobalt tozlarından üretilen sertmetal malzemelerde bilyalı dövme işlemi sonrasında yüzey pürüzlülük değerlerinde artış elde edilmiştir. Ancak, ilgili artışın malzeme yorulma performansında iyileşme elde edilmesini engelleyecek boyutta olmadığı belirlenmiştir.
2. Bilyalı dövme işlemi sonrasında elde edilen numunelerde sertlik artışı olduğu ortaya konmuştur. Sertlik artışının kobalt malzemede yaşanan gerinim sertleşmesi sonucu elde edildiği yapılan deneysel çalışmalarla tespit edilmiştir. Kobalt fazında sertlik artışına neden olacak belirgin bir kristal yapı değişikliği gözlenmemiştir.
3. Bilyalı dövme işlemi sonrası incelenen malzemelerin yorulma ömürlerinde sertlik artışı neticesinde iyileşme elde edilmiştir. Ortalama ömürler göz önüne alındığında %248'lik bir yorulma ömür artışı tespit edilmiştir. Bilyalı dövme sonrasında yorulma ömür dağılımında artış gözlenmiştir.
4. Yapılan incelemelerde tungsten karbür parçacıklarının hem bilyalı dövme işlemi nedeniyle hem de kırılma esnasında farklı mekanizmalar sonucunda kırıldığı anlaşılmıştır. Kırılma yüzeyleri değerlendirildiğinde çoklu çatlak başlaması sonucunda tanelerarası ve tane içi çatlak ilerlemesi nedeniyle kırılmaların yaşandığı gözlenmiştir. İncelenen numunelerde sünek malzeme yorulma çatlak ilerlemesinde görülen yorulma yivcilerine rastlanmamış, kırılan tungsten parçacıklarda dinamik yükleme koşulları sonucunda farklı yönlerde benzer oluşumlar gözlenmiştir.

Teşekkür (Acknowledgements)

Bu çalışma, Norm Cıvata San. ve Tic. A.Ş. tarafından yürütülmüş olup Türkiye Bilimsel ve Teknolojik Araştırma Kurumu'nun (TÜBİTAK) 316082 numaralı TEYDEB1501 projesi kapsamında desteklenmiştir. Yazar, desteklerinden dolayı Umut İnce, Cenk Kılıçaslan, Barış Tanrıkulu, Sezgin Yurttaş, Prof. Dr. Mustafa Güden ve Buğra Karahan'a teşekkür eder.

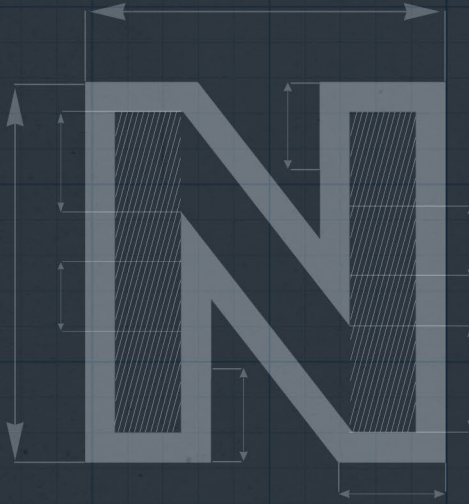
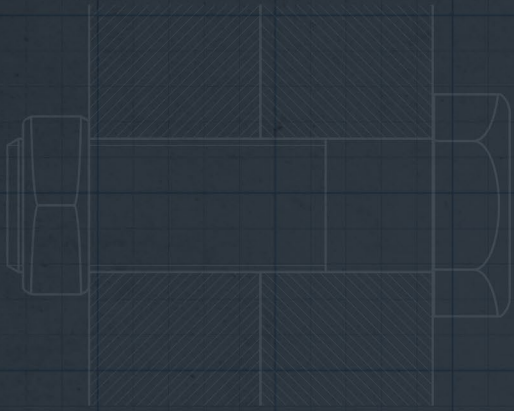
References

1. Jiang, K., Bezold, A., Broeckmann, C.: Numerical modeling of the progressive damage in the microstructure of WC-Co hardmetals under fatigue loading. *Procedia Structural Integrity* 23, 451-456 (2019). doi:https://doi.org/10.1016/j.prostr.2020.01.128
2. Yang, J., Odén, M., Johansson-Jöesaar, M.P., Llanes, L.: Grinding Effects on Surface Integrity and Mechanical Strength of WC-Co Cemented Carbides. *Procedia CIRP* 13, 257-263 (2014). doi:https://doi.org/10.1016/j.

- procir.2014.04.044
3. Yılmaz, O., Samet, K., Kocak, H., Karataş, Ç.: Toz enjeksiyon kalıplamada krom arayüzeyi kullanılarak montajlı parça imalatının araştırılması. *Gazi Üniversitesi Mühendislik Mimarlık Fakültesi Dergisi* 34(2), 621-634 (2019).
4. Yang, J., Roa, J.J., Schwind, M., Odén, M., Johansson-Jöesaar, M.P., Llanes, L.: Grinding-induced metallurgical alterations in the binder phase of WC-Co cemented carbides. *Materials Characterization* 134, 302-310 (2017). doi:https://doi.org/10.1016/j.matchar.2017.11.004
5. Yang, Q., Deng, D., Li, J., Chen, L., Guo, S., Liu, J., Chen, H.: Fabrication and mechanical properties of WC-10Co cemented carbides with plate-like WC grains. *Journal of Alloys and Compounds* 803, 860-865 (2019). doi:https://doi.org/10.1016/j.jallcom.2019.06.328
6. Tran, S.: Microstructure investigations of WC-Co cemented carbide containing Eta-phase and Cr. Student thesis, (2018)
7. Llanes, L., Torres, Y., Anglada, M.: On the fatigue crack growth behavior of WC-Co cemented carbides: kinetics description, microstructural effects and fatigue sensitivity. *Acta Materialia* 50(9), 2381-2393 (2002). doi:https://doi.org/10.1016/S1359-6454(02)00071-X
8. Stephens, R.I., Fatemi, A., Stephens, R.R., Fuchs, H.O.: *Metal Fatigue in Engineering*. John Wiley & Sons, (2001)
9. Tarragó, J.M., Coureaux, D., Torres, Y., Jiménez-Piqué, E., Schneider, L., Fair, J., Llanes, L.: Strength and reliability of WC-Co cemented carbides: Understanding microstructural effects on the basis of R-curve behavior and fractography. *International Journal of Refractory Metals and Hard Materials* 71, 221-226 (2018). doi:https://doi.org/10.1016/j.ijrmhm.2017.11.031
10. Torres, Y., Anglada, M., Llanes, L.: Fatigue mechanics of WC-Co cemented carbides. *International Journal of Refractory Metals and Hard Materials* 19(4), 341-348 (2001). doi:https://doi.org/10.1016/S0263-4368(01)00032-4
11. Garcia, J., Collado Ciprés, V., Blomqvist, A., Kaplan, B.: Cemented carbide microstructures: a review. *International Journal of Refractory Metals and Hard Materials* 80, 40-68 (2019). doi:https://doi.org/10.1016/j.ijrmhm.2018.12.004
12. Tarragó, J.M., Coureaux, D., Torres, Y., Casellas, D., Al-Dawery, I., Schneider, L., Llanes, L.: Microstructural effects on the R-curve behavior of WC-Co cemented carbides. *Materials & Design* 97, 492-501 (2016). doi:https://doi.org/10.1016/j.matdes.2016.02.115
13. Kanagarajan, D., Sivaraj, P., Seeman, M., Seetharaman, R.: Evaluation of the reliability on WC-40%Co composites through Weibull analysis. *Materials Today: Proceedings* 22, 519-524 (2020). doi:https://doi.org/10.1016/j.matpr.2019.08.124
14. Torres, Y., Tarrago, J.M., Coureaux, D., Tarrés, E., Roebuck, B., Chan, P., James, M., Liang, B., Tillman, M., Viswanadham, R.K., Mingard, K.P., Mestra, A., Llanes, L.: Fracture and fatigue of rock bit cemented carbides: Mechanics and mechanisms of crack growth resistance under monotonic and cyclic loading. *International Journal of Refractory Metals and Hard Materials* 45, 179-188 (2014). doi:https://doi.org/10.1016/j.ijrmhm.2014.04.010
15. Tanrıkulu, B., Karakuzu, R., Ince, U., Kılıncdemir, E.: Grain Size Effect on Fatigue Life of WC-Co40 Mainly Used in Cold Forging Tools. Paper presented at the THERMAM 2016 - International Conference on Thermophysical and Mechanical Properties of Advanced Materials, Izmir, Turkey, 1-3 September 2016
16. Benson, M.L., Liaw, P.K., Choo, H., Brown, D.W., Daymond, M.R., Klarstrom, D.L.: Strain-induced phase transformation in a cobalt-based superalloy during different loading modes. *Materials Science and Engineering: A* 528(18), 6051-6058 (2011). doi:https://doi.org/10.1016/j.msea.2011.03.096
17. Ruiz, A., Nagby, P.B.: SAW dispersion measurements for ultrasonic characterization of surface-treated metals. *Instrumentation Measure Metrologie* 3(3), 59-85 (2003).
18. Karahan, B., Ince, U.: Bilya Püskürtmenin (Shot Peening) Teknik-Teknolojideki Yolculuğu ve Soğuk Dövme Prosesine

- Adaptasyonu. Derin Ekim, 74-90 (2015).
19. Toparli, M.B.: Effect of Shot Peening on Ballistic Limit of Al6061-T651 Aluminium Alloy Plates. *Experimental Techniques* 44(1), 37-47 (2020). doi:10.1007/s40799-019-00335-x
 20. Al-Obaid, Y.F.: Shot peening mechanics: experimental and theoretical analysis. *Mechanics of Materials* 19(2), 251-260 (1995). doi:https://doi.org/10.1016/0167-6636(94)00036-G
 21. Gerin, B., Pessard, E., Morel, F., Verdu, C.: Influence of surface integrity on the fatigue behaviour of a hot-forged and shot-peened C70 steel component. *Materials Science and Engineering: A* 686(Supplement C), 121-133 (2017). doi:https://doi.org/10.1016/j.msea.2017.01.041
 22. Dölek, E., Orman, Ş., Karataş, Ç., Sarıtaş, S.: Bilyalı Dövme Parametrelerinin Ç1020 Çeliğinin Yorulma Dayanımına Etkisi ve Oluşan Kalıcı Gerilmenin Katman Kaldırma Yöntemi ile Araştırılması. *Gazi Üniversitesi Mühendislik Mimarlık Fakültesi Dergisi* 20(3), 289-295 (2005).
 23. Chang, S.-H., Lee, S.-C., Tang, T.-P.: Effect of Shot Peening Treatment on Forging Die Life. *MATERIALS TRANSACTIONS* 49(3), 619-623 (2008). doi:10.2320/matertrans.MER2007622
 24. Tarragó, J.M., Ferrari, C., Reig, B., Coureaux, D., Schneider, L., Llanes, L.: Mechanics and mechanisms of fatigue in a WC-Ni hardmetal and a comparative study with respect to WC-Co hardmetals. *International Journal of Fatigue* 70, 252-257 (2015). doi:https://doi.org/10.1016/j.ijfatigue.2014.09.011
 25. Tarragó, J.M., Roa, J.J., Valle, V., Marshall, J.M., Llanes, L.: Fracture and fatigue behavior of WC-Co and WC-CoNi cemented carbides. *International Journal of Refractory Metals and Hard Materials* 49, 184-191 (2015). doi:https://doi.org/10.1016/j.jrmhm.2014.07.027
 26. Klünsner, T., Morstein, M., Marsoner, S., Deller, M., Marklein, B.: Fatigue life equality of polished and electrical discharge machined WC-Co hard metal achieved solely by wet blasting. *International Journal of Refractory Metals and Hard Materials* 59, 61-66 (2016). doi:https://doi.org/10.1016/j.jrmhm.2016.05.001
 27. ISO: Hardmetals - Determination of transverse rupture strength. In. (2009)
 28. Tran, S.: Microstructure investigations of WC-Co cemented carbide containing γ -phase and Cr. Uppsala University (2018)
 29. Withers, P.J., Buschow, K.H.J., Robert, W.C., Merton, C.F., Bernard, I., Edward, J.K., Subhash, M., Patrick, V.: Residual Stresses: Measurement by Diffraction. In: *Encyclopedia of Materials: Science and Technology*. pp. 8158-8169. Elsevier, Oxford (2001)
 30. Meng, Q., Guo, S., Zhao, X., Veintemillas-Verdaguer, S.: Bulk metastable cobalt in fcc crystal structure. *Journal of Alloys and Compounds* 580, 187-190 (2013). doi:https://doi.org/10.1016/j.jallcom.2013.05.115





INVESTIGATION OF FAILURE CRITERIA FOR TUNGSTEN CARBIDE-COBALT HARD METALS

M. Burak TOPARLI
Sezgin YURTDAS
Sarper DOĞAN
İ. Burak ÖZHAN



Journal of the Faculty of Engineering and Architecture of Gazi University 38:1 (2023) 269-281

INVESTIGATION OF FAILURE CRITERIA FOR TUNGSTEN CARBIDE-COBALT HARD METALS

M. Burak Toparlı¹, Sezgin Yurtdaş¹, Sarper Doğan¹, İ. Burak Özhan²

¹Norm Fasteners San. ve Tic. A.Ş., A.O.S.B., İzmir, Turkey

²Norm Tooling San. ve Tic. A.Ş., A.O.S.B., İzmir, Turkey

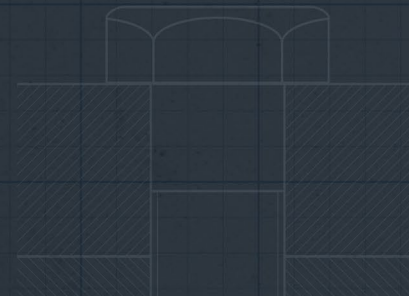
burak.toparli@normfasteners.com

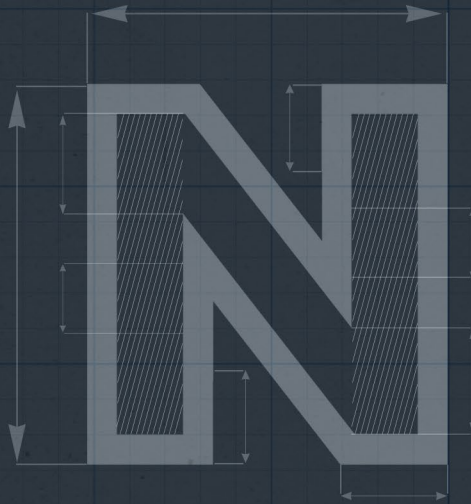
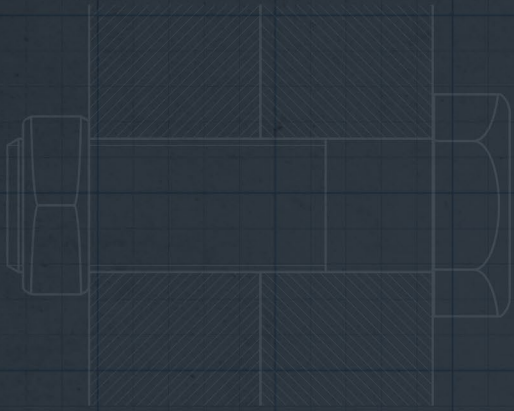
Öne Çıkanlar

- İmalat sanayinde kullanılan sertmetal malzemelerin yorulma performansı incelenmiştir.
- Yorulma ömründe iyileşme elde edebilmek için bilyalı dövme işlemi uygulanmıştır.
- Bilyalı dövme işlemi sonrası elde edilen sertlik artışı sayesinde malzemelerin yorulma performansında iyileşme elde edilmiştir.

Abstract

Predicting failure by a single universal failure theory covering all material types and loading conditions has not been demonstrated yet. Therefore, it is very crucial to choose a suitable failure criterion depending on material and application. In this study, various failure criteria were questioned for tungsten carbide cobalt (WC-Co) hard metals, used in cold forging dies. As known for WC-Co hard metals, the ratio of uniaxial tensile and compressive strengths of WC-Co materials is less than unity and the materials behavior under tensile loading is more close to brittle and defect-controlled. Considering the underlined nature of this type of materials, failure criteria such as Von Mises, Tresca, Coulomb-Mohr and Drucker-Prager were investigated to be employed for stress levels obtained by analytical or numerical methods. Von Mises (maximum distortion energy theory) and Tresca (maximum shear stress theory) failure criteria are widely employed particularly for ductile materials. Being independent of hydrostatic stresses, which is proven to be not contributing yielding for ductile materials and easy calculation for known stress state make these methods attractive. On the other hand, Coulomb-Mohr failure criterion accounts for hydrostatic stresses for failure and difference in yield strength of materials under tension and compression. Therefore, this criterion is preferred for brittle materials including rock and granular materials. However, being independent of the intermediate principal stress component and having sharp corners in yield surface are declared as the two disadvantages of this failure criterion. Drucker-Prager is one of the smooth alternatives of Coulomb-Mohr theory. Based on investigations carried out in this study, it was revealed that Coulomb-Mohr and Drucker-Prager failure criteria were more realistic compared to Von Mises and Tresca. However, due to nature of WC-Co materials, it is very challenging to obtain tensile properties, affecting the degree of approximation.





EXPERIMENTAL VALIDATION OF THE FORMULATION FOR MAXIMUM SOCKET DEPTH ESTIMATION OF NON-REDUCED STRENGTH BOLTS

Fatih KOCATÜRK
M. Burak TOPARLI
Barış TANRIKULU
Umut İNCE
Cenk KILIÇASLAAN



23 European Conference on Fracture - ECF23

EXPERIMENTAL VALIDATION OF THE FORMULATION FOR MAXIMUM SOCKET DEPTH ESTIMATION OF NON-REDUCED STRENGTH BOLTS

Fatih Kocatürk^a, M. Burak Toparlı^a, Barış Tanrıkulu^b, Umut İnce^a, Cenk Kılıçaslan^a

^aNorm Cıvata San. ve Tic. A.Ş., R&D Center, AOSB, Çiğli, İzmir, 35620, Turkey

^bGraduate School of Natural and Applied Sciences, Dokuz Eylül University, Buca, İzmir, 35390, Turkey

Abstract

The analytical formulation introduced for the estimation of the maximum depth of the socket of the bolts that have a shaft diameter smaller than the diameter of the socket was validated with experimental studies. The maximum socket depth of a chosen representative bolt calculated by the analytical formulation for weight reduction was verified experimentally. Bolts with varying socket depths were manufactured through cold forging method and bolt tension tests were carried out on quasi-static tension test machine. Results showed that experimental predictions were in good agreement with the results taken from developed analytical model. The critical depth of the socket calculated using the analytical formulation was 3.2% more secure compared to the experimental results. As a result, the validity of the analytical formulation to calculate the critical socket depths of bolts with smaller shaft diameter than socket diameter was confirmed by experimental studies.

Keywords: Failure criterion; Structural integrity; Mechanical testing; Experimental validation; Metal forming

1. Introduction

Fasteners are used in many sectors such as automotive, aerospace and defence industry to assemble two or more technical parts. The mechanical behaviour of fasteners or bolts should be examined in detail due to their usage areas. Bolts are produced in different sizes, shapes and grades that define their mechanical properties. Under assembly conditions, the factors to be taken into account when evaluating the strength of a threaded fastener were depicted in Bickford (1998) and various load types observed on threaded fasteners such as tensile, shear, torsional and combined were examined in detail.

In addition to loading types, there exist various technical properties of fasteners that have a strong influence on the failure and fatigue behaviours. The effect of using various socket depths on the failure types of fasteners were analysed in Tanrıkulu et al. (2018). Experimental studies were conducted with cold forged bolt specimens having different socket depths, and fatigue and torque-tension tests under different loading types were carried out in order to find out the effects of the critical socket depth in that study. Socket depth was shown to have a significant effect on fastener failure mechanism. As a continuation of the study by Tanrıkulu et al. (2018), M8x1.25x50 Fully Threaded bolts (FT) with grades of 10.9 and 8.8 were investigated to determine the effect of the socket depth on weight reduction in Tanrıkulu et al. (2019). Finite Element (FE) simulations and experimental fatigue and torque-tension tests were carried out for the bolts investigated to find the Maximum Socket Depth (MSD) that is not violating fastener specifications, i.e. the maximum reduction of weight. All tests were repeated for the bolts with grades of 10.9 and 8.8 obtained under different heat treatment conditions.

The effect of the washer on both fatigue and torque-tension performance was examined under assembly conditions. The critical socket depth values determined with numerical and experimental studies were also compared with the analytical model introduced by Thomala and Kloos (2007) to estimate the MSD.

Fatigue is one of the most common failure mechanisms for bolts. Fatigue occurs in bolt materials as the result of cyclic loading (Benac, 2007). A bolt fatigue failure follows three steps of damage: (1) crack initiates at a thread root, radius and/or material defect; (2) cyclic fatigue grows; and (3) finally, sudden failure of the remaining cross section of the bolt occurs. Since, fasteners are designed to fail from the region of thread, fatigue failures of bolts often occur at the first-engaged threads, which have the highest stress. The approach of estimating fatigue limits from stress concentration factors, calculated using thread load distributions obtained from analytical theories, was examined in Patterson (1990). As the eccentricity level increased during eccentric loading, it was observed that maximum stresses in helix of the thread root did not change significantly, but there was an increase in the length of helix exposed to high stresses in Burguete and Patterson (1995). In another study, linear finite element analysis was performed in Lehnhoff and Bunyard (2000) to determine the stress concentration factors for the threads and bolt head fillet in a bolted connection. 8, 12, 16, 20, 24 mm-diameter and grade of 10.9 metric bolts with standard M thread profile were worked on, and the threads were modelled at both minimum and maximum permissible depths. The fillet between the bolt shaft and the bolt head connection was modelled at its minimum radius and each bolt was loaded to its proof strength. Thread stress concentration factors were found to be highest in the first engaged thread and decreased in each consecutive threads moving towards the end of the bolt. The fatigue behaviour of bolts under axial load was examined by taking the fatigue limit of 50 MPa from the component point of view and there were very few results available to designers for limited lifetimes. This problem was addressed in terms of material point of view using a local approach in Fares et al. (2006). In fatigue tests, the stabilized local stress at the root of the first thread in contact with the nut was determined by using the finite element model of the bolt. The Dang Van multiaxial fatigue criterion was also employed to characterize bolt behaviour with these numerical results. Finally, an analytical model to estimate lifetime for failure risk level using statistical Gauss method was introduced and local stress state from nominal loading data was determined. It was claimed that the fatigue strength of mechanical structures was a non-local phenomenon, and the spatial distribution of stresses affected not only the local value of stresses, but also the fatigue behaviour. Therefore, changing fatigue behaviour due to high stress concentration and stress gradients were investigated using stress gradient approach in Novoselac et al. (2014b). The effect of stress gradients on high cycle fatigue was estimated on the M10 bolt by IABG (Hück, M., Thrainner, L., Schütz, 1983), FemFat (ECS Steyr, 2007; Eichlseder, 1989), Stieler (GDR Standard, 1983) and FKM-Guideline (Forschungskuratorium Maschinenbau (FKM), 2003) methods.

The behaviour of threaded fasteners exposed to combined tension and shear loading has attracted attention of many researchers. This behaviour of steel fasteners was analysed experimentally and numerically at high loading rates by Fransplass et al. (2015). The experimental tests were performed with three different angles: 0°, 45° and 90° wherein 0° corresponds to loading along the axis of the fasteners. A three dimensional finite element model was constructed to simulate the strength and behaviour characteristics of the threaded steel fasteners. The ultimate load of the threaded steel fasteners with reasonable accuracy was represented by the proposed finite element model and the loading angles not covered in the experimental study were used to simulate tests. The behaviour of threaded fasteners at high strain rates was studied experimentally in Fransplass et al. (2011). A special fixture was used to satisfy uniform test conditions, and to control the failure location occurred by thread shearing during the tests. Approximately the same trend of an increased strength with increasing strain-rate was observed as a result of the material tests and the threaded assembly tests. It was also observed that the grip length, the length of the thread engagement, and the strainrate has an influence on the failure mode.

Bolt-nut assemblies are extensively investigated in terms of the failure modes in the literature. Bolt-nut assemblies under tension have three different failure modes according to the fault location, such as bolt fracture, bolt thread failure and nut thread failure. The probability of thread failure could be increased if partially threaded bolts are used instead of fully threaded bolts in the connections Grimsmo et al. (2016). Tensioned bolt-nut assemblies are not expected to fail from thread region since thread failure is a less ductile failure than bolt fracture (threaded shaft fracture). Therefore, it is crucial to find the causes of the failure of the thread and the influence of the threaded bolt shaft length within the grip was examined in Grimsmo et al. (2016).

The numerical simulations based on 3D finite elements model was used to predict the global behaviour of a bolted joint under tension-shear loading (substrates, bolt, nut and washer) in Dang Hoang et al. (2013). A decoupled model based on energy model of Cockroft and Latham was used to improve the elasto-plastic model and it was improved model described the different phases occurring during the global mechanical behaviour of a bolted joint correctly (elastic phase, slippage, elastic phase of the structure, plasticization and crack initiation, damage). The fatigue damage analysis of M10 bolted joint made of heat-treatable 42CrMo4 steel with grade 10.9 was carried out in Novoselac et al. (2014a) for 0%, 50%, 70%, 90% preload forces of the bolt yield strength force and eccentric forces with variable amplitudes for high reliability. The dispersion range was used to define the cyclical scatter band of the material with the Gaussian normal distribution, and the multi-axial stress field in the thread root was obtained by utilising the multi-axial fatigue stress criterion. Fatigue damage and the location of the fatigue fracture plane were estimated by using the approach of critical plane. The bolt fatigue life is normally calculated under normal loads, but multiaxial loads occur on bolts during the assembly and service. A new method of calculating the fatigue damage of bolts was introduced by improving the method of Schneider in Sorg et al. (2017). The effect of nut geometry, curved spring washer and Teflon tape sealing material on fatigue life of M12 and M16 ISO bolts were analysed in Majzoobi et al. (2005). In this study, numerical simulation of bolt and nut connections and axial and bending stress distribution in threads are examined by using finite element method. As a result of the experimental studies, the highest fatigue life was obtained for a slotted tapered nut. It was also observed that the use of spring washers increases the fatigue life provided that the correct tightening torque was applied and the use of Teflon tape as a filler between bolt and nut threads increased the fatigue life significantly.

High-strength bolts of grade 8.8 were investigated in terms of mechanical performance under tensile load by carrying out experimental studies in Hu et al. (2016). As a result of tests, two different structural bolt failures were observed: thread stripping, and necking of threaded bolt shaft. In this study, it was observed that the type of failure occurring in the form of shear on the thread originates from different tolerance classes defined for the coating process and the use of a nut having one higher grade than the bolt grade increased the probability of neck failure. Several experimental analyses were conducted in Hongfei et al. (2019) to investigate the fracture formation of a 42CrMo steel-based bolt including a metallographic test, a test of mechanical properties, and an energy spectrum analysis. A large number of structural defects was observed such as sulphur inclusions, band and carbon depletion occurred on the centre of the fracture and in the bolt matrix. Fatigue strength of the materials were affected due to such defects and fatigue failure was observed on the bolts. Finite element analysis was examined in two main categories in Hedayat et al. (2017) to ascertain convenient failure criteria and predict bolt fracture in the case of shear assuming no threads in shear plane: i) Stress/strain analysis on critical elements of the bolt axis, ii) Description of the initiation and formation of the crack.

An optimization study to investigate the tensile status of bolts and nuts was performed in Pedersen (2013). The fillet under the head, the thread beginning or the thread root was the region that the maximum tension was observed in the bolt, and a form optimization was applied to minimize the concentration of stresses. To this end, the under-head fillet was first optimized and a stress reduction of 25.3% was achieved. Then, the optimized under-head fillet design was

applied to the thread in conjunction with a nut design that distributed the load more evenly along the connected thread, achieving a 15.8% stress reduction. Finally, the fillet was optimized in the transition region of the shaft and the thread and a reduction of stress of 34% was achieved. These design improvements, which result in reduced stress on the bolt, were also found to reduce hardness. Fasteners are expected to fracture at the threaded region under assembly loads. The ISO 898-1 (2004) standard prescribes the Ultimate Tensile Strengths (UTS) for bolts that the fracture in the region of the thread was expected. The structural integrity of bolts was affected mostly by the internal socket depth of bolt head, as the fracture region of bolts can move from threaded region to under-head region depending on the depth of socket. However, some specially designed bolts are required to fracture in the under-head region, and these types of bolts must meet the minimum UTS under tension given in the ISO 898-1 (2004) standard.

The Fracture Cone (FC) formed in the head region was investigated in Thomala and Kloos (2007) in terms of the failure mechanisms of bolts having greater SHaft Diameter (SHD) than the SOcket Diameter (SOD). To estimate the residual floor thickness, y_{min} , representing the height between the end of the socket and under-head, an analytical formulation was introduced for the bolts with greater SHD than the SOD. The equation given in Eq. (1) was derived by Thomala and Kloos (2007) to estimate the MSD for bolts that have a SHD greater than the SOD, and is referenced in VDI 2230 standard:

$$y_{min} = \frac{\sqrt{16A_s^2 - \pi^2(d_{sch}^2 - d_m^2)^2}}{2x^* \cdot \pi \cdot (d_{sch} + d_m)} \quad (1)$$

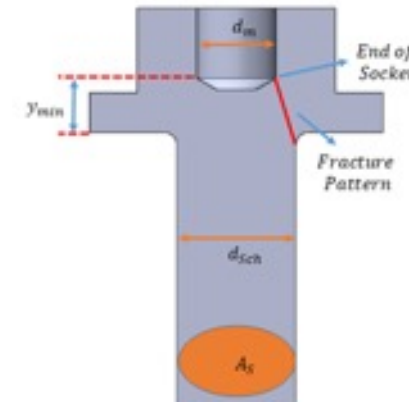


Fig. 1. Cross-section view of the bolt with a SHD larger than the SOD (Kocatürk et al., 2020).

where A_s is the nominal cross-section area of the shaft, d_{sch} is the SHD, d_m is the average SOD, $x^* = \tau_b / R_m$ is the strength ratio where τ_b is the torsional strength and R_m is the tensile strength (see Fig. 1).

Bolts with a SHD less than the SOD are also widely used in industry over the type of bolt investigated in Eq. (1). In the authors' previous study (Kocatürk et al., 2020), an analytical formulation was introduced to estimate the MSD for bolts with a SHD less than the SOD. The developed analytical formulation was used to calculate the MSD for a representative bolt that satisfies the minimum UTS, the analytical results were validated with numerical simulations. To carry out the numerical simulations, Simufact.forming finite element analysis software was used. The estimated maximum depth of

the socket with the developed analytical formulation was compatible with the numerical results. Within the scope of this study, a bolt with internal socket form was chosen and specimens with various values of socket depth were produced by the cold forging method. Then, the analytical model developed in Kocatürk et al. (2020) was validated by tensile tests performed using the produced bolt specimens.

2. Sample specification

In this study, a representative sample of M8 bolts with a SHD less than the SOD was chosen. The selected bolts were produced by cold forging with various socket depth values. After forming, heat-treatment was applied to the bolts to achieve the mechanical properties for 8.8 grade defined in ISO 898-1 (2004). The specimens were produced by using 23MnB4 material which is widely used low alloyed steel in cold forging. One of the bolts and its cross-sectional view was given in Fig. 2.

3. Experimental validation studies of analytical formulation for maximum socket depth estimation

The residual floor thickness between the end of the socket and the bottom of the head, y_{min} , can be estimated by using Eq. (2) developed in Kocatürk et al. (2020).

$$y_{min} = \frac{-\frac{1}{\pi} \cos \alpha^4 (\pi \cdot f^2 - 16 \cdot A_s \cdot \sqrt{\frac{1 - \cos \alpha^2}{x^2 \cdot \cos \alpha^2 - \cos^2 \alpha + 1}} + \pi \cdot t^2 + 2 \cdot \pi \cdot t \cdot f) - \cos \alpha^2 \cdot f + 2 \cdot \cos \alpha^4 \cdot f + \cos \alpha^2 \cdot t}{4 \cdot \cos \alpha^3 \cdot \sin \alpha} - R \quad (2)$$

where α is the angle between horizontal x axis and the line formed between end of the socket and tip of the socket, $t = d_{Sch} + d_{mf}$, $f = d_{Sch} - d_m$ are the parameters to simplify Eq. (2), and R is the radius of the head. The MSD, s , can be obtained by subtracting the residual floor thickness, y_{min} , from the head height value, k , as given in Eq. (3). The residual floor thickness, socket depth and head height were presented in Fig. 3.

$$s = k - y_{min} \quad (3)$$

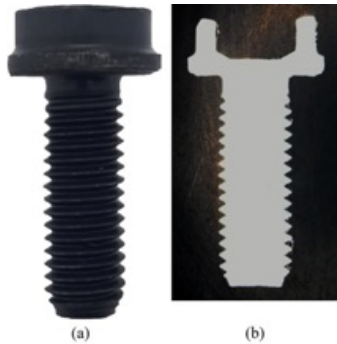


Fig. 2. (a) Bolt specimen produced by cold forging and (b) cross-section view.

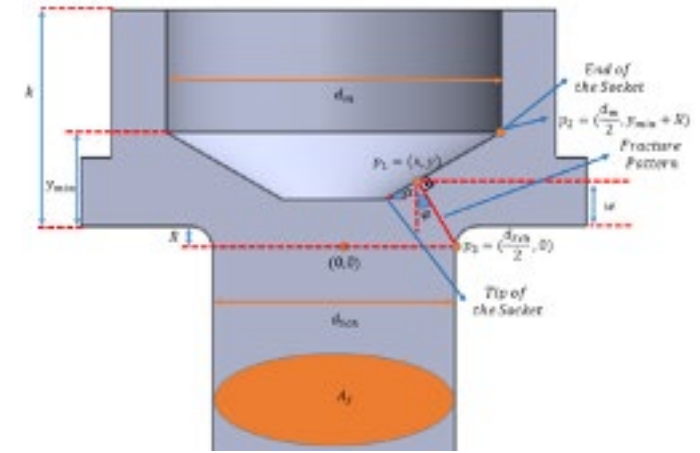


Fig. 3. Cross-section view of the bolt with a SHD smaller than the SOD (Kocatürk et al., 2020).

Experimental tension tests were carried out to validate the analytical model given in Eq. (2). In experiments, bolt specimens were subjected to tension until their total failure by fracture. Tensile tests were performed on a Zwick Roel tension-compression testing machine with capacity of 300 kN. The FC height, w , formed in the broken specimens as a result of tensile tests, is shown in Fig. 4. The w values of the fractured specimens were measured using the profile projection device. The average of the three different w values obtained by turning each sample 120° was determined as the w value for a specimen. Dimensional measurements were performed to determine the y value precisely before each specimen was tested. In order to determine the socket depth at the measurement stage, socket depth values were measured by using the comparator for N10 head socket form. Then, bolt head height, k , is measured with the caliper, and y values were determined by subtracting the socket depth value, s , from the head height value.



Fig. 4. Specimen that fractured after tensile tests.

4. Results and discussion

According to Eq. (3), y_{min} value for the selected bolt specimen was estimated as 2.82 mm. y-axis value of p_1 , y, that is shown in Fig. 3 was calculated as 2.33 mm and w is evaluated by subtracting the half of radius R from the y value as $w = y - R/2 = 2.33 - (0.63/2) = 2.02$ mm. The half of the radius value was subtracted from y value, since the specimens fractured from the middle of the radius in experimental studies.

The analytical formulation was validated by conducting numerical analysis for different socket depth values in Kocatürk et al. (2020). A detailed statistical study was performed by recording 10 effective stress measurements (Von-Mises) from two regions on the bolts whose y-values range between 2.10 and 3.45 mm: i) under-head, ii) thread regions. Higher stress values were observed in the thread region for y-values of 3.10 mm and above. Also, higher stress values were observed in the under-head region compared to the thread region for y-values values less than 2.45 mm. As a result, the value of y_{min} was determined as 2.78 mm in Kocatürk et al. (2020) considering numerical analysis.

Table 1. Tensile test results for M8x1.25 8.8 grade bolts.

Test samples	y (mm)	w (mm)	Fracture Load (kN)
1	2.21	1.68	25.84
2	2.21	1.67	25.69
3	2.26	1.56	25.65
4	2.26	1.62	25.77
5	2.30	1.60	25.41
6	2.30	1.67	25.75
7	2.35	1.58	25.86
8	2.62	1.97	27.34
9	2.62	1.82	26.93
10	2.70	1.96	30.05
11	2.74	1.77	30.14
12	2.77	2.06	30.21
13	2.77	1.95	30.09
14	2.82	1.94	30.09
15	2.86	2.01	30.12
16	2.86	1.96	29.42

The experimental tensile test results of bolts with different socket depths were introduced in Table 1. As described, each socket depth of the bolts was measured before and after the actual tensile test to determine the exact y and w values, as described in Section 3. During tensile tests, load was applied until bolts were fractured and the final fracture load was recorded. The y values with respect to fracture load was plotted in Fig. 5. In Eq. (4), total stress occurring on the FC

formed in head and the tensile stress acting on thread are compared to find the minimum residual floor thickness that results failure in thread region. In order to obtain the minimum y value, i.e. y_{min} , $(R_m \cdot A_s)$ value was used. The $(R_m \cdot A_s)$ value for the bolts used in this study was obtained from ISO 898-1 (2004) standard, given as the minimum ultimate tensile load. According to ISO 898-1 (2004), the $(R_m \cdot A_s)$, i.e. the minimum ultimate tensile load for M8x1.25 for 8.8 grade was 29.2 kN. Therefore, the y_{min} value was obtained as the y value satisfying the fracture load of 29.2 kN. Based on the experimental fracture loads given in Fig. 5, the y_{min} value was obtained as 2.73 mm.

$$R_{mred} \cdot A_{Sch} > R_m \cdot A_s \quad (4)$$

where R_{mred} is the compound of tensile stress and shear stress acting on the head, A_{Sch} is the surface area of the FC.

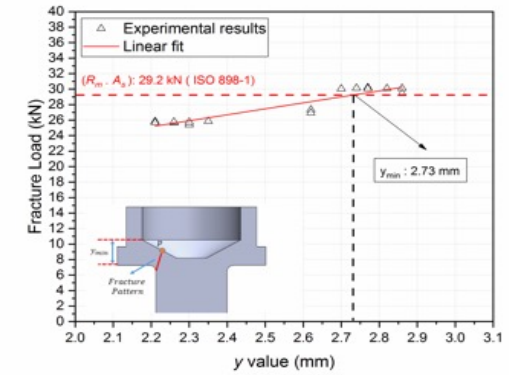


Fig. 5. Experimental fracture load obtained for different y values. The critical y value, i.e. y_{min} was obtained as 2.73 mm.

The analytical formulation proposed in Kocatürk et al. (2020) estimated y_{min} value of the chosen bolt specimen as 2.82, and the numerical studies were determined y_{min} value as 2.78 mm. In this study, the experimental studies revealed the value of y_{min} as 2.73 mm. Taking into account the three methods, the analytical model estimation for the MSD was on the safe side, that is, the value of the MSD estimated by the analytical formulation was greater compared to the numerical model and the experimental results (Table 2). The difference between the analytical and experimental results was 3.2%. Therefore, the analytical and experimental results were found to be in good agreement.

Table 2. Obtained y_{min} values from analytical model, numerical model and experiments.

	y_{min} (mm)	% difference
Analytical model	2.82	-
Numerical model	2.78	1.4
Experiments	2.73	3.2

In addition to y_{min} value, the w values from analytical model and experimental studies were also compared. Since the w values were obtained experimentally after the tested bolts were fractured, the w values would ensure the FC specified during the analytical model was correct. The w values with respect to fracture load was presented in Fig. 6. The critical w value was obtained as 1.94 mm, which was 4.0% safer compared to 2.02 mm of analytical model result. Therefore, the FC specified during the derivation of the analytical model was correct.

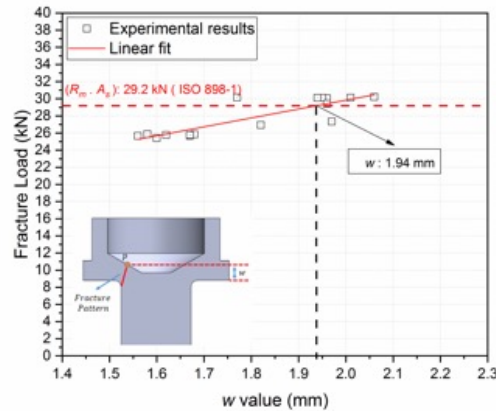




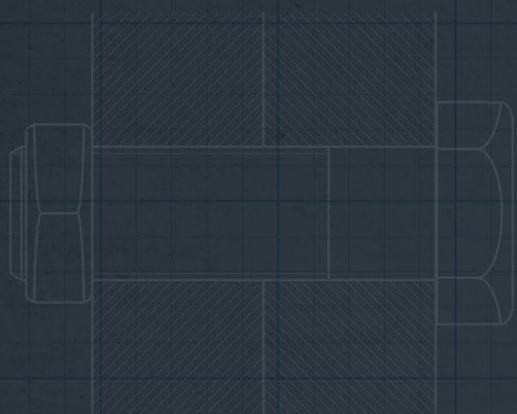
Fig. 6. Experimental fracture load obtained for different w values. The critical w value was obtained as 1.94 mm.

5. Conclusions

In this study, the analytical formulation, that estimates the MSD for bolts with a SHD less than the SOD, was validated by conducting experimental studies. The residual floor thickness, y_{min} , estimated by the analytical formulation was 3.2% more secure compared to the experimental studies that revealed the y_{min} value as 2.73 mm. Therefore, it was validated that the developed analytical formulation would be used to estimate the MSD for bolts with a SHD less than the SOD. As a result, the MSD of the investigated bolt type that satisfies the minimum UTS defined in ISO 898-1 (2004) and provides the maximum weight reduction can be estimated using the experimentally validated analytical formulation.

References

- Benac, D.J., 2007. Technical Brief: Avoiding Bolt Failures. *Journal of Failure Analysis and Prevention* 7, 79–80.
- Bickford, J., 1998. *Handbook of Bolts and Bolted Joints*, 1st ed, Handbook of Bolts and Bolted Joints. CRC Press, Boca Raton.
- Burguete, R.L., Patterson, E.A., 1995. The Effect Of Eccentric Loading On The Stress Distribution In Thread Roots. *Fatigue & Fracture of Engineering Materials & Structures* 18, 1333–1341.
- Dang Hoang, T., Herbelot, C., Imad, A., Benseddig, N., 2013. Numerical modelling for prediction of ductile fracture of bolted structure under tension shear loading. *Finite Elements in Analysis and Design* 67, 56–65.
- ECS Steyr, 2007. *FemFat 4.7: Theory Manual*. St. Valentin.
- Eichseder, W., 1989. *Rechnerische Lebensdaueranalyse von Nutzfahrzeugkomponenten mit der FE methode*. TU Graz.
- Fares, Y., Chaussumier, M., Daidie, A., Guillot, J., 2006. Determining the life cycle of bolts using a local approach and the Dang Van criterion. *Fatigue & Fracture of Engineering Materials & Structures* 29, 588–596.
- Forschungskuratorium Maschinenbau (FKM), 2003. *Analytical strength assessment of components in mechanical engineering*, 5th Ed.
- Fransplass, H., Langseth, M., Hopperstad, O.S., 2015. Experimental and numerical study of threaded steel fasteners under combined tension and shear at elevated loading rates. *International Journal of Impact Engineering* 76, 118–125.
- Fransplass, H., Langseth, M., Hopperstad, O.S., 2011. Tensile behaviour of threaded steel fasteners at elevated rates of strain. *International Journal of Mechanical Sciences* 53, 946–957.
- GDR Standard, 1983. *TGL 19340: Dauerfestigkeit der Maschinenbauteile*. Berlin: GDR State Publisher.
- Grimsmo, E.L., Aalberg, A., Langseth, M., Clausen, A.H., 2016. Failure modes of bolt and nut assemblies under tensile loading. *Journal of Constructional Steel Research* 126, 15–25.
- Hedayat, A.A., Afzadi, E.A., Iranpour, A., 2017. Prediction of the Bolt Fracture in Shear Using Finite Element Method. *Structures* 12, 188–210.
- Hongfei, G., Yan, J., Zhang, R., He, Z., Zhao, Z., Qu, T., Wan, M., Liu, J., Li, C., 2019. Failure Analysis on 42CrMo Steel Bolt Fracture. *Advances in Materials Science and Engineering* 2019, 1–8.
- Hu, Y., Shen, L., Nie, S., Yang, B., Sha, W., 2016. FE simulation and experimental tests of high-strength structural bolts under tension. *Journal of Constructional Steel Research* 126, 174–186.
- Hück, M., Thrainer, L., Schütz, W., 1983. *Berechnung von Wöhlerlinien für Bauteile aus Stahl, Stahlguss und Grauguss – Synthetische Wöhlerlinien – Verein deutscher Eisenhüttenleute*, Report no. ABF 11. Düsseldorf.
- ISO 898-1, 2004. *Mechanical Properties of Fasteners Made of Carbon Steel and Alloy Steel*.
- Kocatürk, F., Toparli, M.B., Tannkulu, B., İnce, U., Kılıçaslan, C., 2020. A new analytical model to estimate maximum internal socket depth of non-reduced strength bolts. *Procedia Structural Integrity* 28, 1276–1285.
- Lehnhoff, T.F., Bunyard, B.A., 2000. Bolt Thread and Head Fillet Stress Concentration Factors. *Journal of Pressure Vessel Technology* 122, 180–185.
- Majzoobi, G.H., Farrahi, G.H., Hardy, S.J., Pipelzadeh, M.K., Habibi, N., 2005. Experimental results and finite-element predictions of the effect of nut geometry, washer and Teflon tape on the fatigue life of bolts. *Fatigue & Fracture of Engineering Materials & Structures* 28, 557–564.
- Novoselac, S., Kozak, D., Ergić, T., Damjanović, D., 2014a. Fatigue damage assessment of bolted joint under different preload. *Structural Integrity and Life* 14, 93–109.
- Novoselac, S., Kozak, D., Ergić, T., Šimić, I., 2014b. Influence of stress gradients on bolted joint fatigue behaviour under different preloads and cyclic loads ratio. *Structural Integrity and Life* 14, 3–16.
- Patterson, E.A., 1990. A Comparative Study Of Methods For Estimating Bolt Fatigue Limits. *Fatigue & Fracture of Engineering Materials & Structures* 13, 59–81.
- Pedersen, N.L., 2013. Overall bolt stress optimization. *Journal of Strain Analysis for Engineering Design* 48, 155–165.
- Sorg, A., Utzinger, J., Seufert, B., Oechsner, M., 2017. Fatigue life estimation of screws under multiaxial loading using a local approach. *International Journal of Fatigue* 104, 43–51.
- Tanrikulu, B., Toparli, M.B., Kılıncdemir, E., Yurttaş, S., İnce, U., 2019. Determination of the critical socket depths of 10.9 and 8.8 grade M8 bolts with hexagonal socket form. *Engineering Failure Analysis* 104, 568–577.
- Tanrikulu, B., Toparli, M.B., Kılıncdemir, E., Yurttaş, S., İnce, U., 2018. Effect of socket depth on failure type of fasteners. *Procedia Structural Integrity* 13, 1840–1844.
- Thomala, W., Kloos, K.-H. (Eds.), 2007. *Tragfähigkeit von Schraubenverbindungen bei mechanischer Beanspruchung*, in: *Schraubenverbindungen*. Springer Berlin Heidelberg, Berlin, Heidelberg, pp. 135–208.



A MODEL TO CONSTRUCT AND PREDICT FLOW CURVE OF MATERIALS FROM COMPRESSION TEST RESULTS WITH MACHINE LEARNING MODELS USING PYTHON

Tolga AYDIN
Fatih KOCATÜRK
Doğuş ZEREN



Key Engineering Materials ISSN: 1662-9795, Vol. 926, pp 2022-2030
 © 2022 The Author(s). Published by Trans Tech Publications Ltd, Switzerland.

A MODEL TO CONSTRUCT AND PREDICT FLOW CURVE OF MATERIALS FROM COMPRESSION TEST RESULTS WITH MACHINE LEARNING MODELS USING PYTHON

Tolga AYDIN^{1,a,*}, Fatih KOCATÜRK^{1,b}, Doğuş ZEREN^{1,c}

¹R&D Center, Norm Cıvata San. ve Tic. A.Ş., AOSB, İzmir, Turkey

^atolga.aydin@norm-fasteners.com.tr, ^bfatih.kocaturk@norm-fasteners.com.tr, ^cdogus.zeren@norm-fasteners.com.tr

Abstract

In order to obtain flow curves from compression test results of a cold forging material and predict flow curves of the material at intermediate temperature and strain rate values, a model was developed using Python programming language in this study. The model consists of two parts: Flow curve determination and flow curve prediction. The compression test data including force-stroke values was processed to determine the flow curves in the first part, and the flow curve data constructed for certain temperature and strain rate values of the material was used as input for the machine learning algorithms to predict flow curve at desired intermediate temperature and strain rate values in the second part. Moreover, Ludwik material model parameters were estimated by using curve fitting methods in order to define the material model into the simulation software. Machine learning algorithms and various regression models in Python libraries were tested to predict the flow curves. The performances of different machine learning and regression models were compared with respect to the mean squared error and coefficient of determination performance measures. Support vector regression, k-Nearest Neighbour (kNN) and artificial neural network models were used to predict flow curves of cold forging materials and kNN regression model was able to find predictions with the lowest error rate. As a result, a model that can process the compression test data to predict flow curves at intermediate temperature or strain rate values was developed.

Keywords: Metal forming, Flow curve prediction, Machine learning, ANN, Python.

1. Introduction

Metal forming is widely used to produce cold forged fasteners for automotive, construction and machinery industries. Numerical simulations in metal forming are preferred to predict material flow, crack evolution, forging load, and die life. In order to be able to simulate the forming process, material characteristics must be integrated into the simulation program. One of the most preferred methods of this integration is to incorporate Ludwik parameters of the material. The mathematical formulation of Ludwik model was given in Eq. 1 in which σ is the true stress, σ_0 is the yield stress, K is the strength coefficient, ϵ is the true plastic strain and n is the strain hardening exponent. Introducing robust material models of various temperatures and strain rates for a material increases the accuracy of the forming simulation. For this reason, compression tests were carried out on the raw materials used in production at different deformation rates and temperatures in order to obtain more realistic simulation results. In this study, a model was developed that processes the compression test data and converts them into Ludwik material model coefficients that can be integrated into simulation software. This model also predicts the coefficients at untested temperature and strain rate points using predictive machine learning libraries of Python.

$$\sigma = \sigma_0 + K\epsilon^n. \quad (1)$$

Machine learning algorithms, especially Artificial Neural Network (ANN), are frequently used in the field of materials science to predict flow curves. The number of studies on cold forging applications and material flow curve estimations has increased recently. One of the first studies published in these area was by Osakada and Yang (1991) [1]. In the study, ANN was used to solve the problems on the expert system and to optimize the final shape of the cold forged product. Also, the number of forging stages was redesigned according to the results of neural network and the difference was taken into account by Finite Element Method (FEM) simulation. Mandal et al. (2008) [2] predicted the behaviour of 304L stainless steel against torsion using ANN. An ANN model based on flow curve estimation for Al-Mg alloys was created by Toros and Ozturk (2011) [3]. It was aimed to calculate flow curves at temperatures between 25°C and 300°C. The estimated values were compared with the experimental results. Bingöl and Misiolek (2015) [4] conducted compression tests at temperatures of 200-400°C and strain rate of 0.01-15 s⁻¹. Then, true stress and true strain values at certain temperature and strain rate points were estimated by using ANN and Gene Expressing Programming (GEP) models and compared with the experimental results. Both models were found to be successful, however ANN model was slightly more accurate than GEP model. Flow curves of ZAM100 magnesium alloy sheets were estimated by Mehtedi et al. (2019) [5] for use in hot forging applications. Within the scope of the study, a multivariable model was created using ANN. Results were tested by using cross validation and estimating the flow curves that are not included in the datasets. Machine learning algorithms were applied to phenomenological flow curve estimation by Stendal et al. (2019) [6]. In the study, flow curve estimation was made using a previously developed phenomenological model and machine learning separately and together. The obtained data were compared among the methods. Similar studies have been carried out not only for metals but also for polymers. Tensile stress of TPE Hytrel material mapped for different strain and temperature values by Rodriguez et al. (2019) [7] using ANN. Mahalle et al. (2019) [8] investigated work hardening behaviour for Inconel 718 alloys using ANN model that was created according to tensile tests. Kabliman et al. (2019) [9] preferred machine learning and estimated stress-strain curves for aluminium alloys using symbolic regression. Lastly, Kocatürk et al. (2021) [10] obtained flow curves at different temperature and strain rate values for the medium carbon steel alloy frequently used in fastener production. Flow curves were predicted using ANN for intermediate temperature and intermediate strain rate values with experimentally obtained flow curves.

As a result, it was revealed that the ANN model is successful in estimating material flow curves with respect to the studies in the literature, but regression-based machine learning models were not used to predict flow curves. In this study, firstly, the method of obtaining the material flow curves, which will form the inputs of the machine learning models, by processing from the experimental compression test data was automated, and then machine learning models were proposed to predict the flow curves at intermediate temperature and strain rate values without experimental results.

Constructing Flow Curve of Materials from Compression Test Results

Introducing material data is mandatory in order to perform the necessary numerical simulations and analyses. For this reason, experimental compression tests results must be processed to get the flow curves of the materials. Experimental results are usually processed manually in statistical programs which leads to great loss of time.

Within the scope of this study, a model was developed that converts the Force-Stroke data obtained from the experimental compression test to the flow curve data of material by using the necessary formulations on Python. Curve fitting operation was applied to the flow curve by using the `curve_fit` function of Scipy.Optimize library on Python. The obtained coef-

ficients of the Ludwik material model can be defined into the analysis program. In addition, the model can perform these operations by taking the average of multiple compression tests conducted to reduce the error rate in the test results.

Materials and Experimental Setup

The operability of the developed program was tested using compression tests of a Stainless Steel (SS) and a Medium Carbon Alloyed Steel (MCAS) material. Compression tests were carried out at different temperatures and strain rates in accordance with the ASTM E9 standard [11]. Compression tests were carried out with ZWICK universal tensile/compression test device for the temperature values of 25-100-200 °C and strain rates of 0.001 and 0.275 s⁻¹. The friction condition affecting the material flow was minimized by using MoS₂ based lubricant for machine compression tables before each compression test. In general, it is expected that the true stress values decreased as the temperature increased, and the true stress values increased as the strain rate increased. In other words, increasing the strain rate generally increases the work hardening rate at smaller strains, which may contribute to a wider initial strain distribution in compression. However, the work hardening rate decreases with increasing strain rate due to adiabatic heating at larger strains. Experimental flow curves for MCAS material at different strain rates for 100 °C was given in Fig. 1. Yield strength values were increased as the strain rate increased for 100 °C. Experimental flow curves for MCAS material at different temperatures for strain rate 0.001 s⁻¹ was depicted in Fig. 2. One can observe that true stress values were decreased as the temperature increased for strain rate 0.001 s⁻¹.

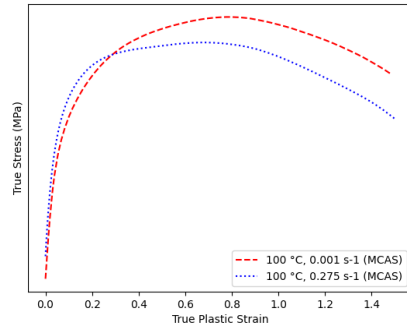


Fig. 1. Experimental flow curves for MCAS material at different strain rates for 100 °C.

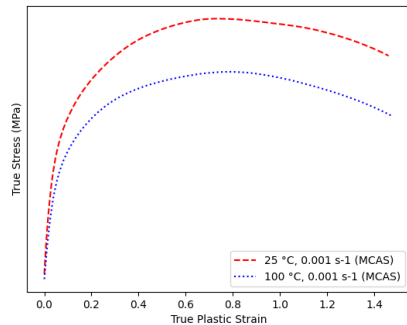


Fig. 2. Experimental flow curves for MCAS material at different temperatures for strain rate 0.001 s⁻¹.

Flow Curve Construction Model

In order to convert manual flow curve construction method into a model, experimental data must be subjected to certain intermediate regulations in order to apply necessary formulations. These steps are removal of faulty data at the beginning of the test, determination of the proportional limit point, translation of the data, determination of the slope of the elastic region and the determination of the yield point. The respective engineering stress value was calculated by using the line equation of the elastic region for each experimental engineering strain value starting from the smallest one and compared to the corresponding experimental stress value. These process was iterated until the difference between the experimental stress value and calculated stress value becomes negative. The last calculated engineering strain was determined as the respective strain value of the yield point searched for.

After finding the yield point, the model constructs the flow curve of the material. The obtained flow curve can be curve fitted according to Ludwik material model and the coefficients can be obtained (Fig. 3).

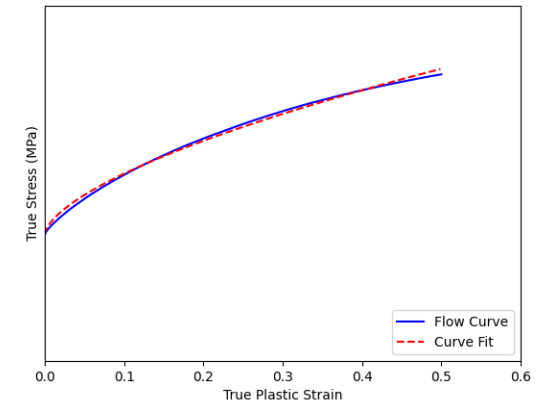


Fig. 3. Flow curve fitting for SS material at 100 °C and 0.001 s⁻¹ strain rate.

Machine Learning Methods to Predict Flow Curve

It was aimed to predict flow curves for the intermediate temperature and strain rate values with the flow curves created from the force-stroke data by using the developed flow curve construction model. Temperature, strain rate and plastic strain parameters were used as independent variables or input variables to predict true stress dependent variable or output variable in this study. Machine learning applications such as k-nearest neighbour (kNN), support vector regression (SVR) and ANN models were chosen to predict flow curves, since ANN is known to be successful to predict continuous target variable [8] and regression models are generally used in numerical estimations. The predictive performances of classification, regression and neural network models was analysed in this study.

SVR was developed by Drucker et al. (1997) [12] and the aim was to determine the line or curve so that the maximum point in the range of a margin can be taken with the lowest error rate. Compared to other traditional learning methods, this method performs much better in solving nonlinear problems. SVR model has different kernel functions to optimize

the equational structure of the flow curve. They are specified as linear, polynomial and radial basis function (RBF). The mathematical formulations of linear, polynomial and RBF were presented in Eq. 2, 3 and 4, respectively. In these equations, x and y represent the vector of independent and dependent variables, respectively. SVR function included in the regression part of support vector machines api of scikit-learn library was tested for these kernel functions on Python. Mean squared error rates (MSE) and determination coefficients (R²) were reported to obtain the optimum function within the scope of the study.

$$k(x, y) = x^T y. \quad (2)$$

$$k(x, y) = (x^T \cdot y + 1)^p. \quad (3)$$

$$k(x, y) = \exp(-\gamma \|x - y\|^2). \quad (4)$$

The kNN algorithm, which is one of the supervised learning methods, is a versatile algorithm that can be used both in classification and regression. In this study, KNeighborsRegressor function of scikit-learn library was used. A simple implementation of kNN regression is to calculate the average of the numerical target of the k nearest neighbours by selecting "uniform" option in weights function of KNeighborsRegressor. Another approach uses an inverse distance weighted average of the k nearest neighbors with "distance" option. Both approaches have been tested and errors rates were compared in this study.

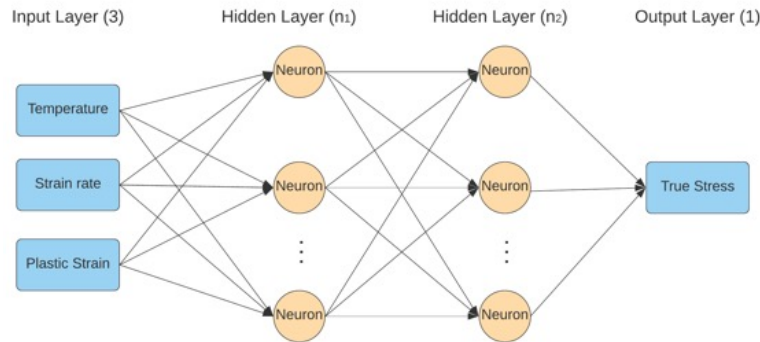


Fig. 4. Schema of an ANN model with two hidden layers.

In general, ANN is a feed forward Multi Layer Perceptron (MLP) application consisting of input, hidden and output layers. Activation functions are used to switch between layers, and back propagation method is used to optimize the weight parameters connecting the layers and neurons in the hidden layers, aiming to reduce the error rate between the estimated value and the actual value of the output parameter. In this study, two different ANN models consisting of one and two hidden layers are proposed by using the MLPRegressor function in the scikit-learn library. For both ANN models, 3 input parameters as temperature, strain rate and plastic strain were used and true stress value was determined as output parameter. The "lbfgs" algorithm, which is considered to perform well in small data sets, was used as the solution algorithm, and the hyperbolic tangent function, $f(x) = \tanh(x)$, was determined as the activation function. In order to determine the number of neurons used in the hidden layers and to determine the "random_state" parameter, which significantly affects the ANN performance, an optimization study was carried out to obtain the predictions with the lowest error. Parameter

optimization of the ANN models was carried out for both materials (MCAS, SS) investigated in this study. For the model consisting of two hidden layers, the number of neurons in both layers was optimized with respect to the R² value for all integer values between 1-40 and the "random_state" parameter for integer values between 0-9. For the ANN model with single hidden layer, the number of neurons was optimized according to the R² value for all integer values between 0-150 and the "random_state" parameter for integer values between 0-9. The parameter setting results of ANN models with single and two hidden layers were presented in Table 1 for both materials. In Fig. 4, schema of the ANN model with two hidden layers was depicted in which n_1 is the number of neurons in the first hidden layer and n_2 is the number of neurons in the second hidden layer. This ANN model was represented shortly as $(3, n_1, n_2, 1)$. Accordingly, for MCAS material, the ANN model with a single hidden layer obtained the highest R² value with 136 neurons and random_state=6, i.e. $(3, 136, 1)$, the ANN model with two hidden layers had 32 neurons in the first layer, 23 neurons in the second layer and random_state=6, i.e. $(3, 32, 23, 1)$. For SS material, the ANN model with a single hidden layer obtained the highest R² value with 82 neurons and random_state=9, i.e. $(3, 82, 1)$, the ANN model with two hidden layers had 32 neurons in the first layer, 37 neurons in the second layer and random_state=0, i.e. $(3, 32, 37, 1)$.

Result and Discussion

In order to verify the generalization capability of the developed machine learning algorithms, 20% of the data obtained by the experimental compression tests was determined as test data and remaining data was determined as training data by using "train_test_split" function of scikit-learn library. In order to measure the performance of the developed machine learning algorithms; the determination coefficient, R², and MSE were utilized. As can be seen in Table 1, SVR with the kernel RBF and the kNN algorithm with both weight can predict the test dataset at lowest error rates and above 0.99 R² values for both material types. The prediction performances of ANN models with single and two hidden layers were presented in Table 2 for both materials. The test data for both ANN models were estimated very close to each other with high R² values for both material types. When the obtained MSE values were considered, the ANN model with two hidden layers was able to predict the test data with less error rate for both material types. Therefore, while estimating the flow curve for the intermediate temperature and strain rate values, the ANN model with two hidden layers was used with the best neuron and "random_state" parameter values found for the material types. Flow curve estimation was performed for intermediate temperature and strain rate values by using the SVR model with the RBF kernel function and the kNN model with the "uniform" weight option.

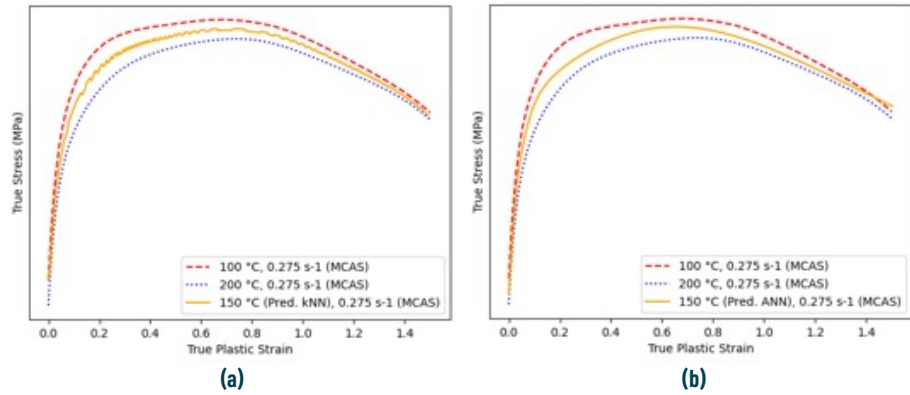
Table 1. Performance of kNN and SVR algorithms on 20% test data.

		SS		MCAS	
SVR	Kernel	MSE	R ²	MSE	R ²
	RBF	110.200	0.996	101778.000	0.987
	Linear	7557229.000	0.731	3950.650	0.486
	Polynomial	13563.120	0.517	5431.950	0.294
		SS		MCAS	
kNN	Weight	MSE	R ²	MSE	R ²
	uniform	0.016	0.999	0.012	0.999
	distance	0.012	0.999	0.008	0.999

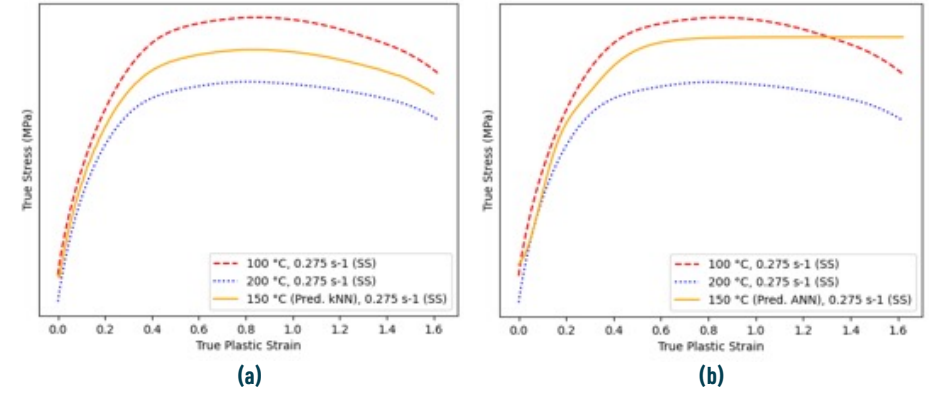
Table 2. Performances of ANN models on 20% test data.

Model	SS		MCAS	
	MSE	R ²	MSE	R ²
ANN with 1 Hidden Layer	52766.013	1.000	14777.749	0.999
ANN with 2 Hidden Layers	47995.138	0.999	14724.192	0.997

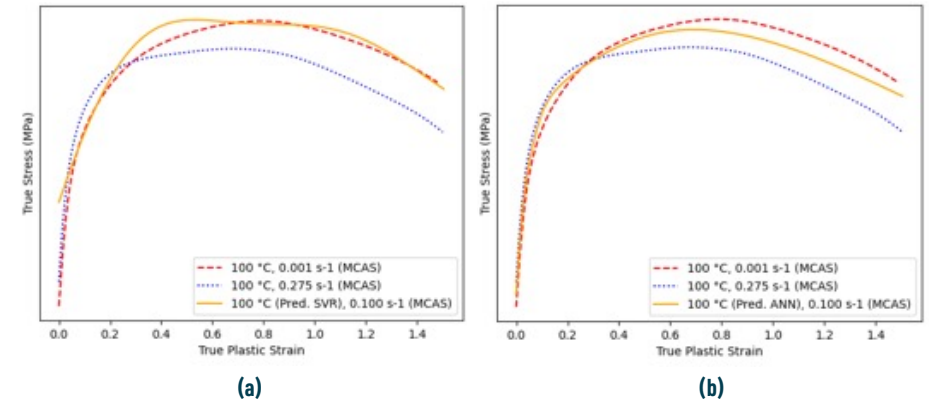
Within the scope of the study, compression tests were performed for 3 different temperature values (25, 100, 200 °C) and 2 different strain rate values (0.001, 0.275 s⁻¹) and the models with optimum parameter settings were trained by using all experimental data in order to predict the flow curves at intermediate temperature and strain rate values.

**Fig. 5.** Flow curve prediction at for MCAS material at 150 °C and strain rate 0.275 s⁻¹ with the (a) kNN, (b) ANN models.

In Fig. 5(a), the prediction results of the kNN model for the MCAS material at a strain rate of 0.275 s⁻¹ and at 150 °C were compared with the experimental flow curves of the MCAS at a strain rate of 0.275 s⁻¹ at 100 and 200 °C. The flow curve estimated by the kNN model was obtained between the two experimental curves as expected, that is, the true stress values obtained at 150 °C were found between the true stress values obtained at 100 and 200 °C. The same consistent results were also observed for the ANN model in Fig. 5(b). In the flow curve predicted with kNN, oscillation in the data was observed due to the number of neighbours k used in the model. The oscillation can be eliminated by increasing the training data size and the number of neighbours in correlation.

**Fig. 6.** Flow curve prediction for SS material at 150 °C and strain rate 0.275 s⁻¹ with the (a) kNN, (b) ANN models.

In Fig. 6(a), the estimation results of the kNN model at 0.275 s⁻¹ strain rate and 150 °C for SS material were compared with the experimental flow curves performed for SS material at 0.275 s⁻¹ strain rate and at 100 and 200 °C. The flow curve predicted by the kNN model was between the experimental true stress values obtained at 100 and 200 °C. In Fig. 6(b), the estimation results of the ANN model for SS material were compared with the experimental flow curves performed for SS material at 0.275 s⁻¹ strain rate and at 100 and 200 °C. The flow curve predicted by the ANN model was obtained between the two experimental curves as expected, that is, the true stress values obtained at 150 °C were found between the true stress values obtained at 100 and 200 °C. Due to the smaller data size at high strain rates, the ANN model showed a lower performance in prediction than the kNN model. Since the kNN model calculates the average of the points within the determined neighbourhood, it obtained more accurate results at high strain rate values.

**Fig. 7.** Flow curve prediction for MCAS material at 100 °C and strain rate 0.100 s⁻¹ with the (a) SVR, (b) ANN models.

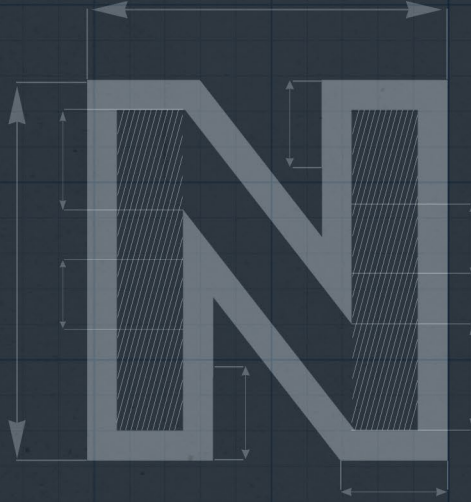
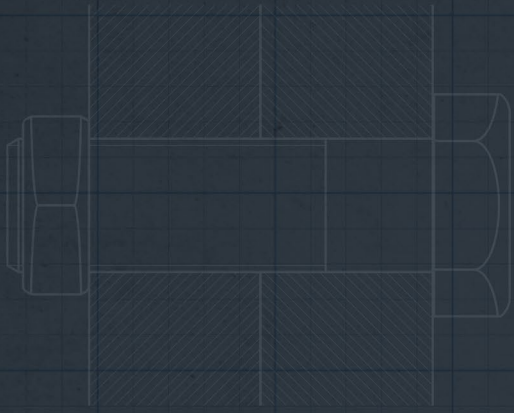
In Fig. 7(a), the prediction results of the SVR model for the MCAS material at a strain rate of 0.100 s^{-1} and at 100°C were compared with the experimental flow curves of the MCAS at strain rates of 0.001 and 0.275 s^{-1} at 100°C . The flow curve estimated by the SVR model was obtained close to the experimental flow curve of 0.001 s^{-1} strain rate. The flow curve prediction of SVR for the intermediate strain rate values gives more inconsistent results than the predicted flow curves for the intermediate temperature values. It is assumed that this consistency is due to the fact that the number of strain rate levels is less than the number of temperature levels in the experimental training data. In Fig. 7(b), the estimation results of the ANN model were compared with the experimental flow curves performed for MCAS material at the same conditions. The flow curve predicted by the ANN model was obtained between the two experimental curves as expected and more harmonious results were found than the SVR model.

Conclusion

In this study, a model was developed that converts the force-stroke data obtained from the experimental compression tests to true stress-plastic strain flow curve using the necessary formulations on Python programming language. Then, experimentally obtained flow curves at different temperatures and strain rates were used to train the proposed machine learning models to make flow curve estimation at intermediate temperature and strain values. Parameter optimization of these models was carried out using 20% of the experimental data as test data and the remainder as training data. Then, the estimation performances of the three models with optimum parameters were compared at intermediate temperature and strain rate values. According to the results, kNN and ANN models obtained similar and favourable results for flow curve estimation at intermediate temperature value, while ANN model with two hidden layers predicted the flow curve more reasonable at intermediate strain rate value. As a result, a model that can process the compression test data to predict flow curves at intermediate temperature or strain rate values was developed.

References

1. K. Osakada, G. Yang, Application of Neural Networks to an Expert System for Cold Forging, *Int. J. Mach. Tools Manuf.* Vol. 31 (1991) Issue 4.
2. S. Mandal, P.v. Sivaprasad, S. Venugopal, K. P. N. Murthy, Artificial neural network modeling to evaluate and predict the deformation behavior of stainless steel type AISI 304L during hot torsion, *Applied Soft Computing Journal*, 9(1) (2009) 237–244.
3. S. Toros, F. Ozturk, Flow curve prediction of Al-Mg alloys under warm forming conditions at various strain rates by ANN, *Applied Soft Computing Journal*, 11(2) (2011) 1891–1898.
4. S. Bingöl, W. Misiölek, Prediction of the true stress of ZE20 magnesium alloy at different temperatures and strain rates, *Strojniski Vestnik/Journal of Mechanical Engineering*, 61(10) (2015) 610–617.
5. M. el Mehtedi, A. Forcellese, L. Greco, M. Pieralisi, M. Simoncini, Flow curve prediction of ZAM100 magnesium alloy sheets using artificial neural network-based models, *Procedia CIRP* 79 (2019) 661–666.
6. J. A. Stendal, M. Bambach, M. Eisentraut, I. Sizova, S. Weiß, Applying machine learning to the phenomenological flow stress modeling of TNM-B1, *Metals* 9(2) (2019).
7. A. E. Rodríguez-Sánchez, E. Ledesma-Orozco, S. Ledesma, A. Vidal-Lesso, Application of artificial neural networks to map the mechanical response of a thermoplastic elastomer, *Materials Research Express* 6 (2019).
8. G. Mahalle, O. Salunke, N. Kotkunde, A. K. Gupta, S. K. Singh, Neural network modeling for anisotropic mechanical properties and work hardening behavior of Inconel 718 alloy at elevated temperatures, *Journal of Materials Research and Technology* 8(2) (2019) 2130–2140.
9. E. Kablman, A. H. Kolody, M. Kommenda, G. Kronberger, Prediction of stress-strain curves for aluminium alloys using symbolic regression, *AIP Conference Proceedings* 2113 (2019).
10. F. Kocatürk, M. B. Toparli, B. Tanrikulu, S. Yurttaş, D. Zeren, C. Kılıçaslan, Flow curve prediction of cold forging steel by artificial neural network model, 24th International Conference on Material Forming (2021).
11. ASTM E9-19, Standard Test Methods of Compression Testing of Metallic Materials at Room Temperature, ASTM International, West Conshohocken, PA (2019).
12. H. Drucker, C. J. C. Surges, L. Kaufman, A. Smola, V. Vapnik, Support vector regression machines, *Advances in Neural Information Processing Systems* (1997).



OTOMOTİV ENDÜSTRİSİNDE KULLANILAN SAPLAMALARIN ÜRETİMİNDE KULLANILAN KALIP SİSTEMLERİ: SEGMENTLİ KALIP KULLANIMI İLE ÖMÜR ARTIŞI ELDE EDİLMESİ

Sarper DOĞAN

M. Burak TOPARLI

Sezgin YURTDAS

Tayfur YAVUZBARUT



5. International Conference on Materials Science, Mechanical and Automotive Engineerings and Technology (IMSMATEC'22)

OTOMOTİV ENDÜSTRİSİNDE KULLANILAN SAPLAMALARIN ÜRETİMİNDE KULLANILAN KALIP SİSTEMLERİ: SEGMENTLİ KALIP KULLANIMI İLE ÖMÜR ARTIŞI ELDE EDİLMESİ

Sarper DOĞAN - M. Burak TOPARLI - Sezgin YURTDAS - Tayfur YAVUZBARUT

Bu çalışmada, otomotiv endüstrisi başta olmak üzere farklı alanlarda kullanılan saplama türü bağlantı elemanları üretiminde kullanılan kalıp sistemi ele alınmıştır. Saplamalar uygulama alanlarına bağlı olarak farklı formlarda üretilebilmektedir. Yatay preslerde çoklu istasyon tasarımı ile üretimi yapılan flanşlı altıköşe saplamaların şekillenmesi sırasında özellikle plastik deformasyon kaynaklı gerinim sertleşmesi nedeniyle son istasyonlarda kalıplara gelen yükler artmaktadır. Ayrıca, altıköşe ve flanş gibi unsurları oluşturan kalıplar yüksek gerilmelere maruz kalmaktadır. Bu tip faktörler göz önüne alındığında özellikle son istasyonlarda kompleks formları oluşturan kalıplarda erken çevrimde hasar görülebilmektedir. Bu çalışma kapsamında flanşlı M14 altıköşe kafa formuna sahip bir saplama türü üretiminde kafa formunun oluşturulmasında kullanılan kalıplar incelenmiştir. Öncelikle, üretimden alınan hasarlı kalıplar incelenmiş ve etkin hasar mekanizmaları ortaya çıkarılmıştır. Daha sonra sonlu elemanlar analizi ile mevcut durum modellenmiş ve karşılaştırma yapılmıştır. Kalıp ömürlerini artırmak için alternatif kalıp tasarımları gerçekleştirilmiş ve revize tasarımların maruz kaldığı gerilme seviyeleri sonlu elemanlar yöntemi ile belirlenmiştir. Yapılan çalışmalar kapsamında gerilme birikmesi yaşanan bölgelerdeki hasar ihtimalini azaltmak için segmentli kalıp sistemine geçilmiş ve gerilme miktarlarında ciddi azalmalar elde edilmiştir. Ayrıca, soğuk şekillendirme kalıplarında kullanılan malzemeler ve kalıp sıkı geçme oranları belirlenmiştir. Nihai revize kalıp sistemine göre kalıp üretimleri yapılmış ve seri üretim koşullarında denenmiştir. Elde edilen sonuçlara göre, kalıp ömründe yaklaşık 3 katlık bir artış sağlanmıştır. Sonuç olarak segmentli kalıp tasarımı sayesinde gerilme birikmeleri önlenerek kalıp ömründe iyileşme sağlanmıştır.



SOĞUK DÖVME PROSESİNDE KULLANILAN BİR SIVAMA KALIBININ SONLU ELEMANLAR YÖNTEMİ İLE İNCELENMESİ

Sarper DOĞAN
Cenk KILIÇASLAN
Sezgin YURTDAS
M. Burak TOPARLI

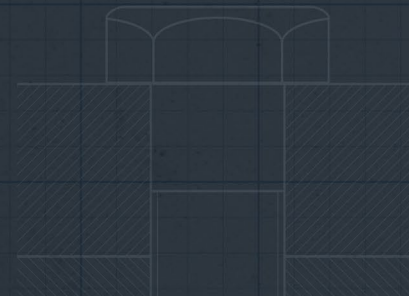
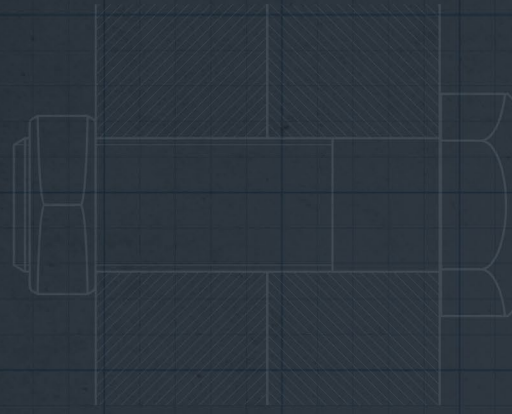


The 4th International Conference of Materials and Engineering Technology (TICMET'22)

SOĞUK DÖVME PROSESİNDE KULLANILAN BİR SIVAMA KALIBININ SONLU ELEMANLAR YÖNTEMİ İLE İNCELENMESİ

Sarper DOĞAN - Cenk KILIÇASLAN - Sezgin YURTDaş - M. Burak TOPARLI

Sivama operasyonu; soğuk dövme yöntemi ile üretilen ürünlerde tercih edilen bir şekillendirme metodudur. Sivama işlemi, önceki istasyonlarda silindirik ve daha büyük çapa şişirilen veya bu şekilde elde edilen iş parçasının, çapından küçük ve genelde eksenel simetrik olmayan bir forma dolmaya zorlanması/ilerletilmesi ile gerçekleştirilmektedir. Bağlantı elemanı üretimi düşünüldüğünde; sivama işlemi, genelde kafa altında bulunan formların oluşturulmasında (kare, altı köşe vb.) kullanılmaktadır. Sivama işlemi kalıp açısından düşünüldüğünde zorlayıcı bir operasyondur. Özellikle malzeme akışı kaynaklı aşınma ve şekillenme işlemi sırasında oluşan yüklem koşulları nedeniyle kalıbın ince cidarlarında veya gerilme birikmesi olabilecek yerlerinde mikro çatlak oluşumu gözlenebilmektedir. Sonuç olarak, kalıplar hasara uğramakta ve kullanılamaz hale gelmektedir. Bu çalışmada, M14X115 özel bir civatanın kafa altında bulunan ve rondela montajında kullanılan altı köşe kademe formunun sivama operasyonu detaylı olarak incelenmiştir. Kalıp performansının artırılması için öncelikle mevcut durumda kullanılan kalıplar; hem sonlu elemanlar yöntemi ile modellenmiş hem de üretim ortamında performansı takip edilmiştir. Kırılan kalıplar üzerinde yapılan baskın hasar mekanizması incelemeleri ve simülasyon sonuçları eşleştirilerek kalıp ömrünün artırılması için yapılması gereken tasarım revizyonları ve olası kalıp malzemesi değişiklikleri belirlenmiştir. Sonlu elemanlar yöntemi ile alternatif kalıp revizyonları incelenmiş ve nihai kalıp tasarımı ortaya çıkarılmıştır. Revize edilen formun üretiminin ardından performansın belirlenmesi için kalıplar denenmiştir. Yapılan üretim denemelerinde kalıp performansının 3 kat artırıldığı ortaya konmuştur. Ayrıca, kullanılamaz hale gelen kalıplar incelendiğinde revizyon ile birlikte kalıpta meydana gelen baskın hasar mekanizmasının değiştiği saptanmıştır. Kalıpların aşınmadan dolayı kullanılamaz hale geldiği, çatlak veya kırılma gibi bir hasar oluşmadığı belirlenmiştir.



SURFACE FINISHING OF CEMENTED TUNGSTEN CARBIDE USING ABRASIVE FLOW MACHINING

Ömer EYERCİOĞLU

Kürşad GÖV

Engin TEK

M. Burak TOPARLI



The 4th International Conference of Materials and Engineering Technology (TICMET'22)

SURFACE FINISHING OF CEMENTED TUNGSTEN CARBIDE USING ABRASIVE FLOW MACHINING

Omer Eyercioglu¹, Kursad Gov², Engin Tek¹, M. Burak Toparl³

¹ Gaziantep University, Engineering Faculty, Mechanical Engineering Department, Gaziantep, TURKEY.

² Gaziantep University, Aeronautics and Aerospace Faculty, Aeronautics and Aerospace Engineering Department, Gaziantep, TURKEY.

³ Norm Civata R&D Center, Izmir, TURKEY

Abstract

In this article, the abrasive flow machining (AFM) method is used for the surface finishing of tungsten carbide-cobalt (WC-Co) material. A total of six groups of abrasive flow media with different abrasive particle sizes and concentration ratios were used. Aluminum oxide was used as an abrasive and a polymer-based carrier was used for the abrasive media. Tungsten carbide specimens were cut by electrical discharge machining and AFM processes were applied at various cycle numbers. Surface roughness and material remove rate were measured before and after processing with abrasive machining, and the variation of surface quality and material remove rate was investigated. The surface roughness values were decreased to (R_a)=0.5 μ m levels in about 20 cycles.

Keywords: Abrasive flow machining, tungsten carbide, surface finishing, abrasives, surface roughness.

1. Introduction

Despite the new technologies developed in recent years, traditional finishing processes, finishing complex shapes in hard, high strength, heat resistant alloys, die steels and fasteners have not yet reached the desired speeds and quality. Abrasive flow machining (AFM) is an uncommon new technique that has the potential to provide high precision and economical means to finish inaccessible areas and complex internal and external passages. This method has been applied in aviation, aircraft, medical, and other precision manufacturing fields, and successful results have been obtained[1].

The AFM technique has been carried out to enhance the floor integrity of the machined workpiece by the use of numerous machining methods along with milling, turning, grinding, and in particular electric discharge machining (EDM). AFM is used to do away with deburring, polishing, radius, and recast (white) layer [2],[3]. The Abrasive flow machining method enables the surface to be polished as the paste under pressure moves over the workpiece surfaces. Thanks to this method, it has been demonstrated by the studies that the surface roughness values that cannot be obtained with the classical polishing methods or that take a very long time are reached[4].

The main parameters in the abrasive fluid processing method; fluid parameters are classified as process parameters and workpiece parameters[4]. Process parameters; the pressure applied, the number of cycles, and the flow rate and volume of the abrasive paste used. Workpiece parameters; material properties of the workpiece, its geometry, and mechanical processing (turning, milling, electro-erosion, etc.) method. The fluid parameters are viscosity, temperature, abrasive grain size, abrasive ratio, and abrasive type. The most important parameters affecting the surface roughness are considered abrasive parameters [5].

The material to be used in this work is tungsten carbide with 15% Carbon. The composite of tungsten carbide and cobalt (WC-Co) has special importance in the production of cutting tools, dies, and other special tools and components due to its very high hardness and excellent resistance to shock and wear. It is possible to process this material with some conventional methods; however, the high precision required for machining complex shapes cannot be achieved[5],[7]. Therefore, AFM was applied for surface finishing after EDM cutting.

In another study by Jain et al., a theoretical model was determined in which acceptable results could be obtained, close to the experimental results [8]. In a different study, they determined the parameters that depend on the paste viscosity. Accordingly, paste viscosity; It is directly proportional to the abrasive grain size and inversely proportional to the abrasive ratio and temperature. It has been observed that high viscosity provides higher material removal rate and lower surface roughness value [9]. Flenther and Fioravanti used polyborosiloxane as the polymeric carrier for the abrasive paste. In this study, it has been proven that the abrasive ratio is more effective than the abrasive size and polymetric carrier properties. In different studies using polyborosiloxane, abrasives such as aluminum oxide (Al_2O_3), silicon carbide (SiC), and garnet were used. [10] A study by Gov and Eyercioglu examined the effects of abrasive types on abrasive flow machining surfaces [2]. In a study in which the forces acting on the surfaces during the AFM process were measured, the effects of the abrasive paste parameters on the surface roughness were tested[11].

In this study, AFM application was applied to coarse-grained tungsten carbide alloy with a 15% Carbon ratio using two different sizes of 180 mesh size and 400 mesh size Al_2O_3 abrasive. An abrasive is produced by mixing the polymer and Al_2O_3 abrasive at 50%, 60%, and 70% by mass for each mesh size of this abrasive. As a result of this application, the surface roughness and Material Remove Rate (MRR) values of the material were compared.

2. Materials and Methods

The samples were produced from Tungsten carbide material. The samples were cut with EDM from the same stock material as 20x10x5 mm and a total of 36 samples were prepared. Surface measurements and weight measurements were made from all samples before AFM and are given in Table 1. All technical specifications of the sample material are given in Table 2.

Table 1. Surface roughness values and weights of samples before AFM.

Specimen No	R_a (μ m)	Weight	Specimen No	R_a (μ m)	Weight	Specimen No	R_a (μ m)	Weight
s1	3,9	13,8883	s13	3,8	12,6032	s25	4,1	12,9724
s2	3,8	13,0023	s14	4,2	12,9795	s26	4,2	13,1516
s3	3,6	13,6090	s15	4,0	13,9230	s27	3,9	12,2252
s4	4,1	13,0377	s16	4,1	13,2264	s28	4,0	14,2198
s5	3,7	12,9573	s17	3,7	12,9687	s29	3,8	13,0917
s6	4,2	13,7179	s18	3,8	13,7182	s30	4,2	13,6462
s7	4,0	13,0721	s19	3,9	13,2783	s31	4,1	13,2332
s8	4,1	13,1673	s20	3,8	13,9637	s32	3,8	13,0771
s9	3,9	12,6757	s21	4,2	12,9919	s33	3,8	13,3118
s10	3,8	14,1594	s22	4,2	13,4144	s34	3,9	13,0329
s11	3,8	12,5368	s23	4,1	13,0420	s35	4,0	12,9458
s12	3,9	13,0551	s24	4,0	13,7214	s36	4,1	13,3831

Table 2. Workpiece Material Properties.

Properties	Unit	Value
Density	g/cm ³	14
Hardness	HV 30	1100
Elastic Modulus	kN/mm ²	550
WC	%	84,55
Co	%	15
TiC+TaNbC	%	0,45

2.2 Abrasive Flow Machine

In this study, a two-way AFM processing bench was used. The bench consists of four parts the main body, hydraulic unit, control unit, and cooling unit (Figure 1.). The samples are placed in the pre-prepared dies. These dies are connected to the flow path of the abrasive fluid of the machine and are compressed by means of four pistons (Figure 2). The AFM process consists of two main pistons pushing the abrasive fluid through the die with forwarding and backward movement. The full forward and backward movement of these pistons is called a cycle. In this experimental study, one cycle takes 1.5 minutes.

**Fig. 1.** Abrasive flow machine.**Fig. 2.** Dies.

2.3 Abrasive media

In this experimental study, a mixture of Al₂O₃ abrasive 180 mesh size and 400 mesh size, hydraulic oil, and the polymeric carrier was prepared. In order for the mixture to be homogeneous, 5 cycles were made with a die in AFM. The properties of the abrasive fluid are given in Table 3.

Table 3. Abrasive Properties.

	Al ₂ O ₃
Mesh size	180, 400
Hardness (Mohs)	9
Density (g/cm ³)	3.7
Apparent density (g/L)	1800
Viscosity (Pa s, 25 °C)	60
Concentration (% wt)	50, 60, 70

2.4 Experimental Procedure

Experiments were made on six groups of samples. Six specimens in each experimental group were attached to the abrasive fluid machine. 1, 5, 10, 20, 60, and 100 cycles were applied to these samples for each abrasive. A total of six surface measurements were made from each sample, perpendicular to the flow direction and flow direction of the samples. These measurements were taken using a Mitutoyo SJ 401 surface measuring machine with a cutting length of 0.8 mm (ASTM D7127). Samples were weighed before and after the experiment using a SHIMADZU AUX220 balance to calculate the MRR.

3. Results and Discussion

3.1 Surface roughness

The surface roughness values of the WC-Co material, on which the AFM process was applied, were made and the measurements were taken. In Figure 3, the concentration ratios of 50%, 60%, and 70% of the abrasive and the surface roughness values of the abrasive flow direction are given for 180 mesh. It is seen that the surface roughness values show a similar trend here. It is seen that the Ra value of the 60% concentration ratio abrasive drops below 0.50 μm in 20 cycles and has the lowest surface roughness value.

The surface roughness values taken from the flow direction of 400 mesh, which is another abrasive, are given in figure 4. The surface roughness of the process applied with 50%, 60%, and 70% concentration ratios in 20 cycles of 70% concentration ratio was measured as R_a = 0.7 μm.

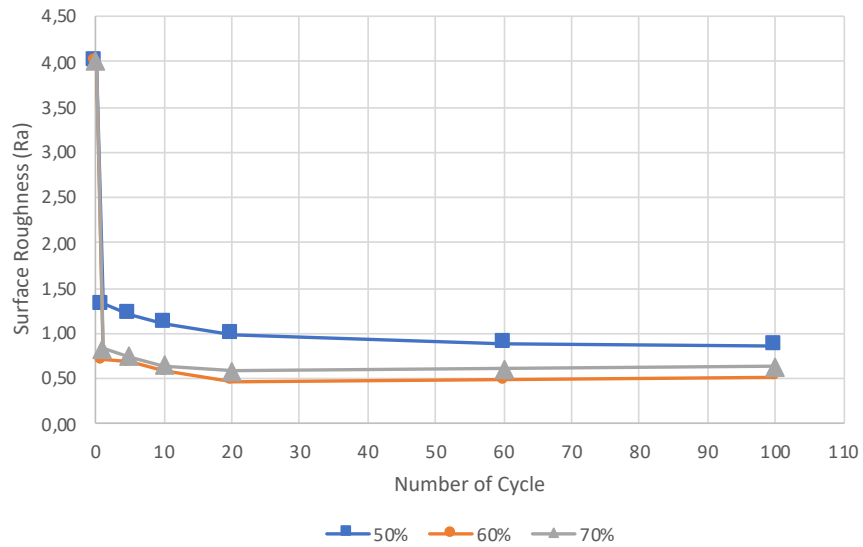


Fig. 3. 400 Mesh median flow direction surface roughness.

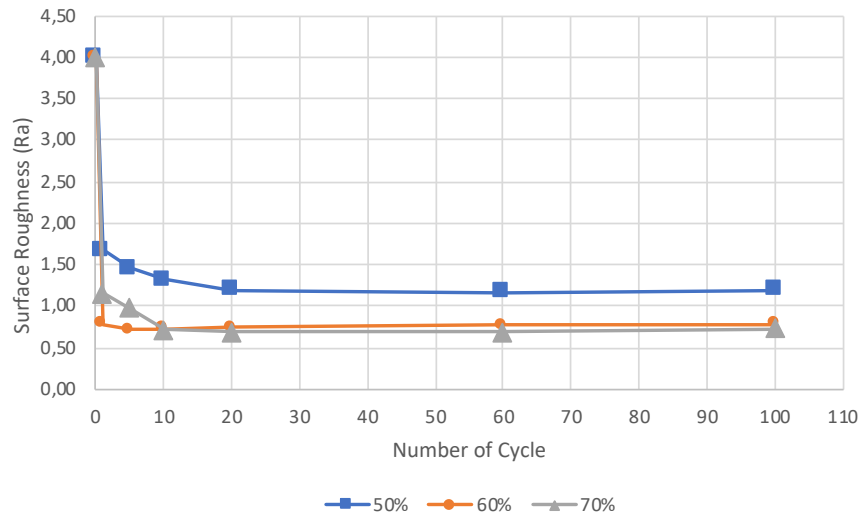


Fig. 4. 400 Mesh median flow direction surface roughness.

In Figure 5 and Figure 6, the graphs of the measured values with 3 repetitions perpendicular to the median flow direction are given. In Figure 5, the surface roughness value was measured as 0.53 in 20 cycles at a 60% concentration of 180 mesh size abrasive. Measurements perpendicular to the median flow direction and the median flow direction showed similar trends. Similarly, the surface roughness of 70% concentration ratio in 400 mesh size in 20 cycles was measured as approximately $R_a = 0.8$.

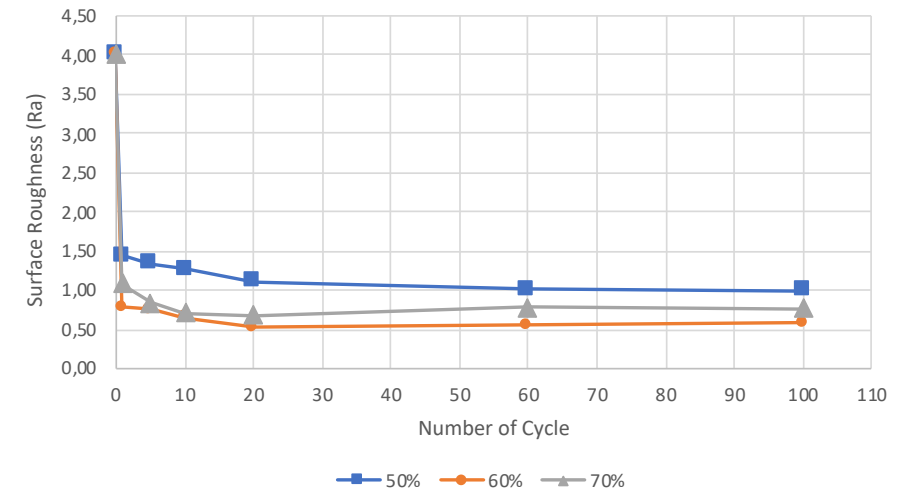


Fig. 5. 180 Mesh perpendicular to the median flow direction surface roughness.

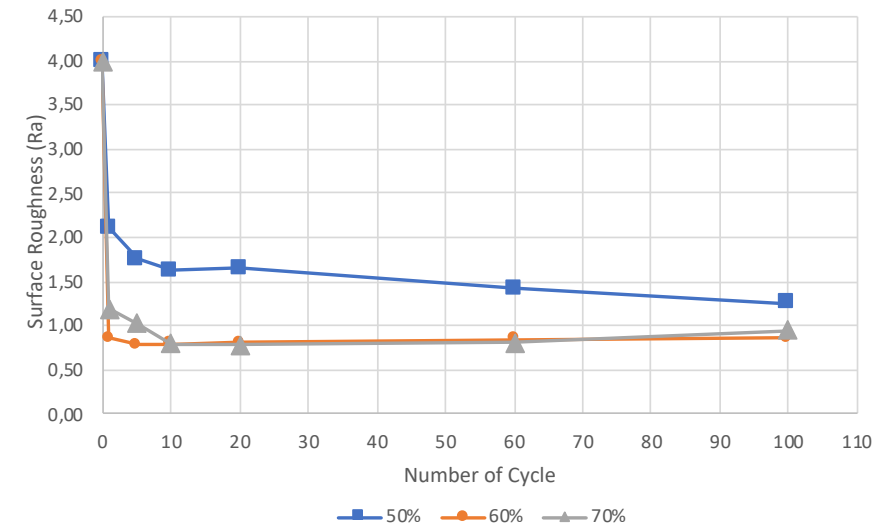


Fig. 6. 400 Mesh perpendicular to the median flow direction surface roughness.

3.2 Material remove rate (MRR)

The material removal rate is given in figure 7 and figure 8. A nonlinear increase in MRR was observed. The MRR acceleration did not increase as the number of cycles increased. This can be explained by the high surface roughness values of the specimen before AFM. A smoother surface is formed in the next cycle as the median flow particles flatten the crests on the material. Thus, it was seen that the number of cycles and MRR did not increase at the same rate.

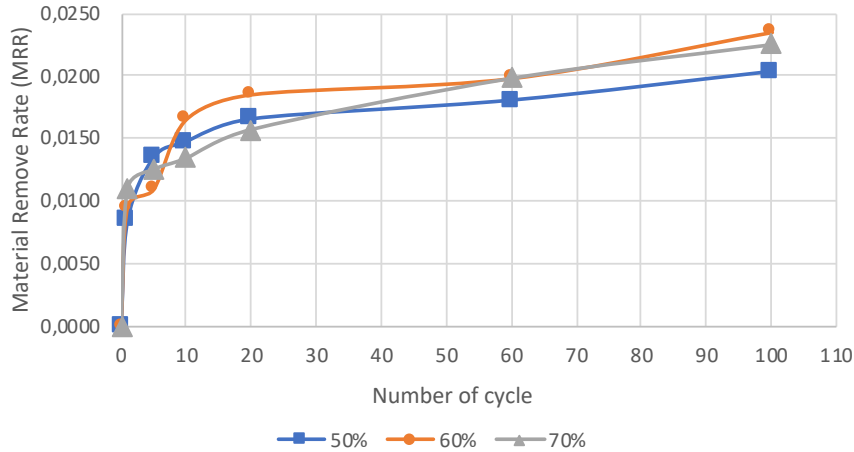


Fig. 7. 180 Mesh size MRR.

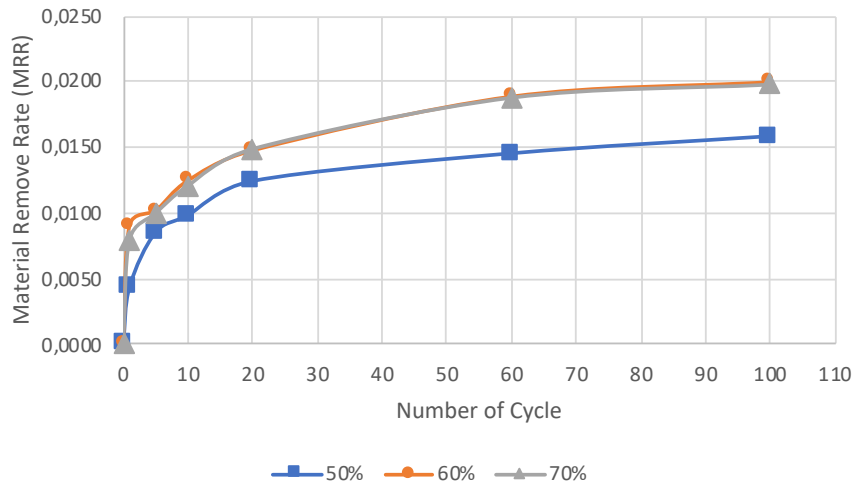


Fig. 8. 400 Mesh size MRR.

4. Conclusions

In this study, the effects of processing Tungsten carbide material with abrasive fluid on the surface quality were investigated experimentally. The following conclusions can be drawn from this study.

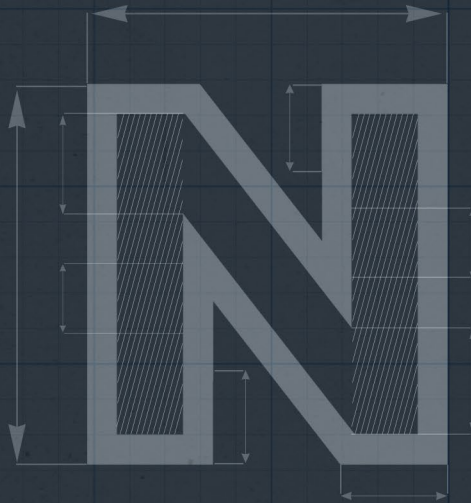
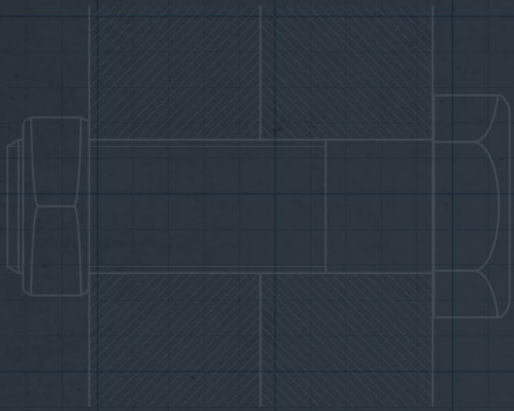
- The abrasive flow machining (AFM) method can be used as a fast and effective method for polishing WC-Co material.
- The average surface roughness of the samples decreased from 4 to 0.50 in approximately 20 cycles.
- In the AFM process, AlO_2 180 mesh gave you better results than 400 mesh size.
- In the median concentration ratio, the 60% concentration ratio is the most effective compared to other ratios.
- 180 mesh with larger grain in MRR values gives you a higher material removal rate. The MRR did not increase at the same rate depending on the number of cycles.

Acknowledgments

The authors would like to acknowledge the contributions of the TUBITAK TEYDEB (1505-PROJECT 5200068) and Norm Civata Company.

References

1. Venkatesh, G., Singh, T., Sharma, A.K., and Drivedi, A. Finishing of micro-channels using abrasive flow machining. *Lecture Notes in Mechanical Engineering*, (2014), 15, 243-252.
2. Gov, K., and Eyercioglu, O. Effects of abrasive types on the surface integrity of abrasive-flow-machined surfaces. *Proceedings of the Institution of Mechanical Engineers, Part B: Journal of Engineering Manufacture*, (2018), 232 (6), 1044-1053.
3. Eyercioglu, O., Aksoy, A., and Aladag, M. Bağlantı Elemanları Şekillendirme Kalıplarının Aşındırıcı Akışkan Yöntemiyle Parlatılması. (2019), (November).
4. Rhoades, L. Abrasive flow machining: a case study. *Journal of Materials Processing Tech.*, (1991), 28 (1-2), 107-116.
5. Jain, V.K., and Adsul, S.G. Experimental investigations into abrasive flow machining (AFM). *International Journal of Machine Tools and Manufacture*, (2000), 40 (7), 1003-1021.
6. Mahdaviinejad, R.A., and Mahdaviinejad, A. ED machining of WC-Co. *Journal of Materials Processing Technology*, (2005), 162-163 (SPEC. ISS.), 637-643.
7. Exnert, B.H.E., and Gurland, J. A REVIEW OF PARAMETERS INFLUENCING SOME MECHANICAL Exner and Gurland : Parameters Influencing Some. *Powder Metallurgy*, (1970), 13 (25), 13-31.
8. Jain, R.K., and Jain, V.K. Finite element simulation of abrasive flow machining. *Proceedings of the Institution of Mechanical Engineers, Part B: Journal of Engineering Manufacture*, (2003), 217 (12), 1723-1736.
9. Jain, V.K., Ranganatha, C., and Muralidhar, K. Evaluation of rheological properties of medium for AFM process. *Machining Science and Technology*, (2001), 5 (2), 151-170.
10. Fletcher, A.J., and Fioravanti, A. Polishing and honing processes : An investigation of the thermal properties of mixtures of polyborosiloxane and silicon carbide abrasive. *Proceedings of the Institution of Mechanical Engineers, Part C: Journal of Mechanical Engineering Science*, (1996), 210 (3), 255-265.
11. Gorana, V.K., Jain, V.K., and Lal, G.K. Experimental investigation into cutting forces and active grain density during abrasive flow machining. *International Journal of Machine Tools and Manufacture*, (2004), 44 (2-3), 201-211.



HYBRID FAILURE CRITERIA APPLICATION FOR COLD FORGING DIES

M. Burak TOPARLI

Baybars SARICA

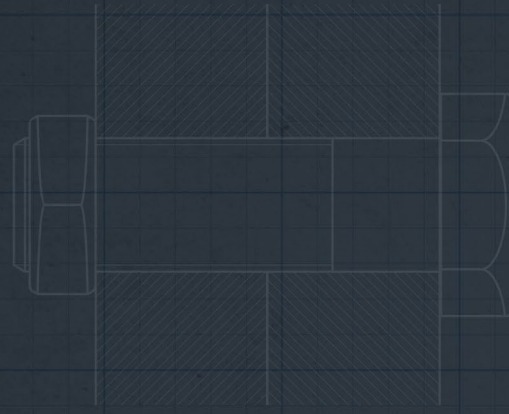


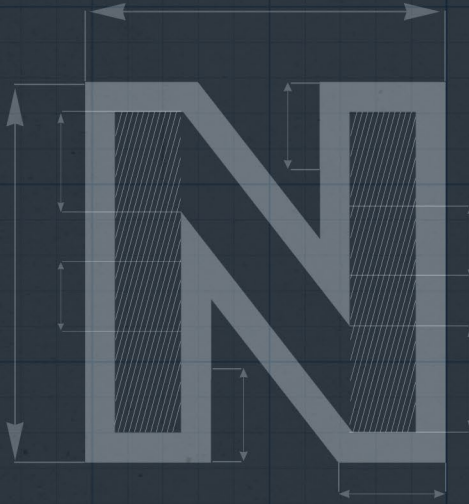
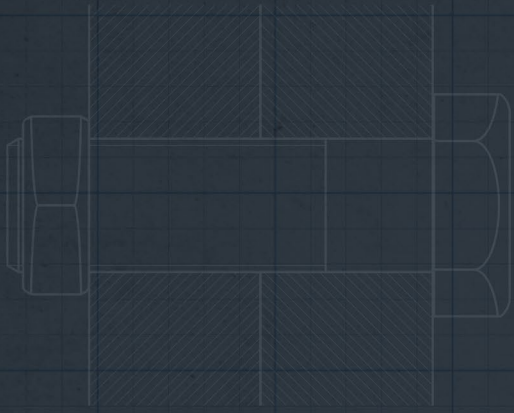
The 4th International Conference of Materials and Engineering Technology (TICMET'22)

HYBRID FAILURE CRITERIA APPLICATION FOR COLD FORGING DIES

M. Burak TOPARLI - Baybars SARICA

Low energy consumption and high efficiency production have become more crucial in recent years since the COVID pandemic increases environmental awareness, commodity and energy costs. In this study, a new failure criteria approach was presented for cold forging dies for the sake of improvement in die performance leading to increase in efficiency in production, i.e. OEE (Overall Equipment Effectiveness) and decrease in cost. Particular interest was directed to die inserts and stress rings which are assembled with pre-stressing. Since, the mechanical behaviour of the materials preferred for die inserts (WC-Co metal ceramic composite) and stress rings (tool steels) deviates under tension and compression, application of different failure criteria was required. In this study, particular interest was directed to WC-Co hard materials and various failure criteria available in the literature. A standard DIN 6921 M12 hexagonal bolt with flange was chosen in this scope. After finite element modelling of the cold forging process, die analysis was carried out and different failure criteria were applied for die insert and stress ring. As a result, die design was modified and new dies were produced. At the production floor, new dies were employed and performance was monitored. About 80% performance increase was achieved with the new design leading to significant increase in OEE and decrease in cost of both dies and overall production.





FOR MORE SUSTAINABLE COLD FORGING PROCESS: USE OF SAND BLASTING INSTEAD OF PICKLING AND RINSING

Baybars SARICA
M. Burak TOPARLI
Doğuş ZEREN
Umut İNCE

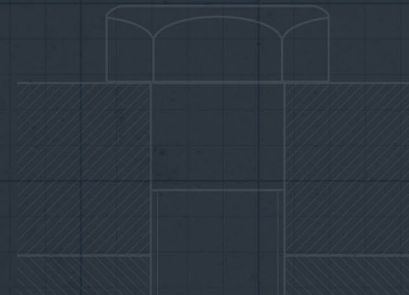
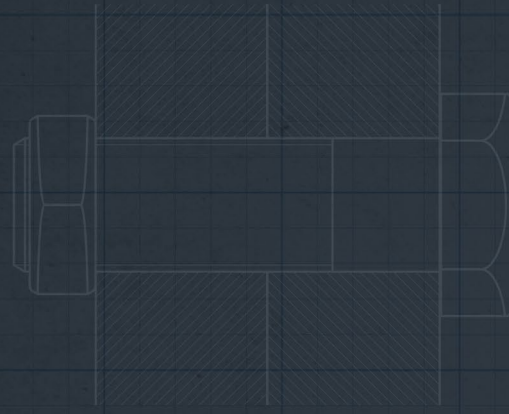


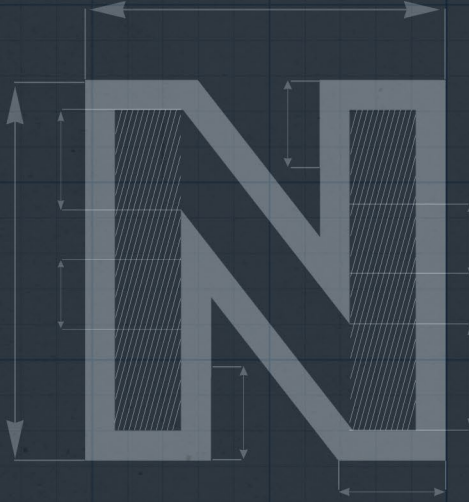
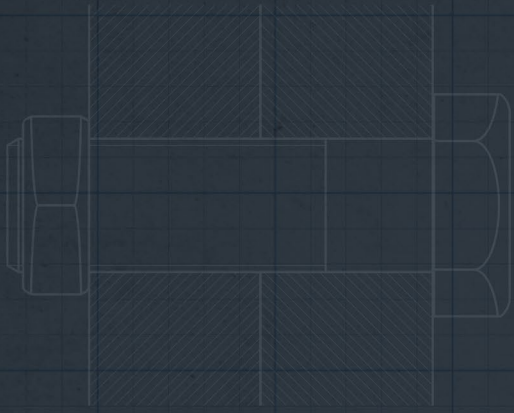
21. Uluslararası Metalurji ve Malzeme Kongresi (IMMC 2022)

FOR MORE SUSTAINABLE COLD FORGING PROCESS: USE OF SAND BLASTING INSTEAD OF PICKLING AND RINSING

Baybars SARICA - M. Burak TOPARLI - Doğuş ZEREN - Umut İNCE

Due to increasing environmental awareness and energy costs, alternative production methods have gained importance for the sake of sustainable manufacturing. Pickling and rinsing are commonly used in cold forging, as initial stages of traditional metal wire surface cleaning and preparation operations. However, hazardous waste disposal and recycling issues, significant energy and water consumption and human health risks are some of the main problems of these traditional methods. Sand blasting can be considered as an alternative and more sustainable method for surface preparation. In this study, use of sand blasting instead of pickling and rinsing was examined. Process parameters namely blasting time and blasting rate were investigated for 8.0 mm-thick metal wires. Surface roughness and hardness measurements were carried out to characterize the effect of process parameters. Polymer-based coating was applied to sand blasted-surfaces and surface roughness measurements were repeated. Extrusion tests were conducted for final performance evaluations. In addition, a comparison was made between sand blasting and pickling and rinsing with respect to sustainable manufacturing. It was revealed that sand blasting offered less water and chemical agents usage compared to pickling and rinsing. Moreover, production efficiency was higher for sand blasting process.





INDUSTRIAL WIRELESS TRACKING TOOLS OF COLD FORGING DIES FOR INDUSTRY 4.0 SYSTEMS: RFID & QR CODE APPLICATIONS

Fatih KOCATÜRK
Sezgin YURTDAS
Cenk KILIÇASLAN
Umut İNCE
Emre ERBİL



Forming Technology Network Bulk (ForTech Bulk 2022)

INDUSTRIAL WIRELESS TRACKING TOOLS OF COLD FORGING DIES FOR INDUSTRY 4.0 SYSTEMS: RFID & QR CODE APPLICATIONS

Fatih Kocatürk^{1,a,*}, Sezgin Yurtdaş^{1,b}, Cenk Kılıçaslan^{1,c}, Umut İnce^{1,d} and Emre Erbil¹

¹R&D Center, Norm Cıvata San. ve Tic. A.Ş., AOSB, Çiğli, İzmir, Turkey

^afatih.kocaturk@normfasteners.com, ^bsezgin.yurtdas@normfasteners.com, ^ccenk.kilicaslan@normfasteners.com,

^dumut.ince@normfasteners.com, ^eerbil.emre@gmail.com

Abstract

In this study, tools to track service life of forging dies used in the production of fasteners were investigated and their performance was determined with production trials. First, the use of RFID technology for die tracking was presented and it was seen that this technology was not suitable for tracking operations of dies in terms of both cost and production efficiency in mass production conditions. An alternative tracking tool, QR code technology, was also presented. The dot peen marking method was found to be suitable for printing QR codes on dies, and it was possible to track the die-service life more cost-effectively and efficiently in the production trials. Since there is no need for assembly and disassembly operations as for RFID tags, using QR codes provided a serious advantage in labor and warehouse management speed. Following the determination of the die tracking tool, the cold forging die tracking system was developed by designing the relevant user interfaces on SAP ERP system and constructing the necessary database connections. By using the developed system, die service life will be tracked automatically and factors such as machine, raw material and product type that affect die life will be analyzed in detail.

Keywords: Die tracking tools, RFID, QR code, cold forging, metal forming.

1. Introduction

Fasteners can be produced by methods such as cold forging, warm forging, hot forging and machining. Cold forging method is preferred by many companies due to its advantages such as surface quality of the final product, mechanical properties, production with tighter tolerance ranges and energy saving. Fastener production by cold forging is carried out by horizontal presses having two or more stations. In the first station, the cylindrical raw material is cut into a certain length and transferred to the next stations with transfer fingers, gradually obtaining the final product form. Each station has two die blocks, stationary and punch. Die blocks used in cold forging stations are formed by assembling multiple dies, ejector pin or punch. Die types used in die blocks can be classified as intermediate dies that can be used more than once in a product project and special dies used to obtain critical forms of the bolt. Special dies generally used only one in the project of product, no more than one of the same die. Special dies generally consist of front heading dies or reduction/extrusion dies. Since dimensions and designs of special dies are complex, production costs are high and supply processes are longer. For this reason, determining the parameters that affect the service-life of special dies and then improving these parameters will significantly reduce total use of dies in production. In addition, the correct correlation of the service-life of special dies with project type and cold forging press ensures more effective management of stocks and reduces unnecessary inventory costs.

QR code and RFID technologies can be utilized to track cold forging dies. There are many reviews and studies that provide basic information on RFID tool tracking. Basic information about RFID can be found in studies [1–5]. Performing tracking process with radio signals without visual reading is the main advantage of RFID applications. Wu et al. (2006)[6] examined the disadvantages of RFID applications and the issues that need attention in their study. Considering the production line applications, they stated that the biggest disadvantage is the costs of the preparation processes that must be done carefully before the assembly of the chips. In addition, the cost of the equipment used to transfer the data arranged with barcodes to RFID chips was mentioned. Tajima (2007)[7] examined the RFID application in terms of industrial application and listed the possible risks as follows: Failure to recover the return of investment of RFID, technical risks, simplicity of using barcodes versus RFID chips and security problems. According to the researches, the cost spent on RFID investments can be recovered in 2 years at the earliest. As a technical risk, it was observed that the rate of not reading in the field tests performed at the reading points varied between 20% and 50%.

Large companies use RFID to increase the efficiency of their operations and gain competitive advantage. Through the use of RFID, it is possible to automate some operations of tool management including search and selection of tools, data entry operations, machine set-ups, evaluation of the wear level of a tool and life cycle management [8]. The literature on the application of RFID technology in the management of manufacturing and supply chain were reviewed in the reference [9]. The level of tool inventories can be reduced significantly with a good planning system exploiting at best the sharing of tools among machines as stated from [10] and this improvement results also in tool utilization maximization. In [10], a tool management system architecture with RFID support was proposed and it has been observed that the proposed tool management system has improved data collection and tool management automation. The potential benefits resulting from the application of RFID identification tags on machine tools were investigated in the study of [11]. As a results of a case study carried out on machine tools, a direct comparison between data before and after the application of RFID tags could be made. A higher accuracy than the manual process with significant potential in terms of reduced time for information sharing and less occurrence of human errors can be guaranteed by RFID-based automatic processes.

Although RFID technology is a good alternative for tool management applications, problems such as low reliability of reading and high assembly cost of RFID tag arise during the tracking of metal parts. This situation has forced the metal industry to find an alternative tracking tool, and in recent years, DataMatrix 2D barcode (QR Code) encoded on the metal surface with dot peen marking method was used to track metal parts. Tracking is carried out by recording the unique ID of the product and transferring information into the QR code printed on the tool. Readability of QR Code constructed with dot peen marking method was analyzed by [12]. Data including traceability information is printed on metal product surface by stamping with carbide needle. Readability analysis were conducted on three types of materials and also different marking parameters as code size and stamping depth (impact force). A correlation was found between material hardness, impact force of dot peen and size of QR code which impacts code readability.

In this study, RFID and QR code technologies to track cold forging dies were investigated. Firstly, RFID tracking tool was analysed and it was observed that RFID technology was not convenient for tracking steel dies. Then, QR code tracking tool was examined and different QR code printing methods such as laser marking and dot peen marking were investigated. Dot peen marking method for QR code printing was preferred since both the printing machine is more affordable and the codes printed on steel dies were not damaged even under cold forging conditions. Following the determination of the die tracking tool, the cold forging die tracking system was developed by designing the relevant user interfaces on SAP ERP system and constructing the necessary database connections. By using the developed system, die service life will be tracked automatically and factors such as machine, raw material and product type that affect die life will be analyzed in detail.

Tracking Methods for Cold Forging Dies

Cold Forging Die Traceability with RFID Technology

RFID technology consists of an RFID tag and RFID reader connected to a computer system. The tag is the part that collects instant data and then transmits the collected data through radio frequency. Tags usually consist of two parts, a small chip and an antenna. An antenna is used to receive and transmit information, while a chip is used to store and process information. A unique code belonging to the product is stored in the chip embedded in the tag and the product is tracked through this code. This information is read by an RFID reader when a tag is within the coverage area of the reader. The information stored in RFID tag is detected by the reader and the relevant transaction updates are performed on the computer system.

Tag selection was the first process of selecting the appropriate RFID hardware to track steel cold forging dies. The following criteria were taken into consideration to determine the appropriate RFID tag: Temperature resistance, loss of function in oil/liquid contact, reading distance and ease of assembly. Two different (dot and dash type) small sized Xerafy XS series RFID tags [13] were selected in accordance with these features. The tags were positioned parallel to the surface. The reading/writing temperature range of the selected tags is given as -40 and 150 °C. Tests were carried out in mass production to determine the temperature values occurring on the die surfaces during cold forging. First, the tag was placed on a stationary die used in mass production, as shown in Fig. 1. Then, the steady-state temperature occurred on the die was measured with a thermal camera. The measurement pattern, which starts from the center and continues in the radial direction until the outer diameter, was shown in Fig. 2(a). Temperature changes along the measurement pattern were given in Fig. 2(b) and maximum temperature was observed on the surface as 71 °C. Towards the outer diameter, the surface temperature drops to around 60 °C. These temperature values were within the working range of the tags.



Fig. 1. RFID tag assembly steps: (a) Opening the assembly slot, (b) placing the tag, and (c) sealing with a liquid gasket.

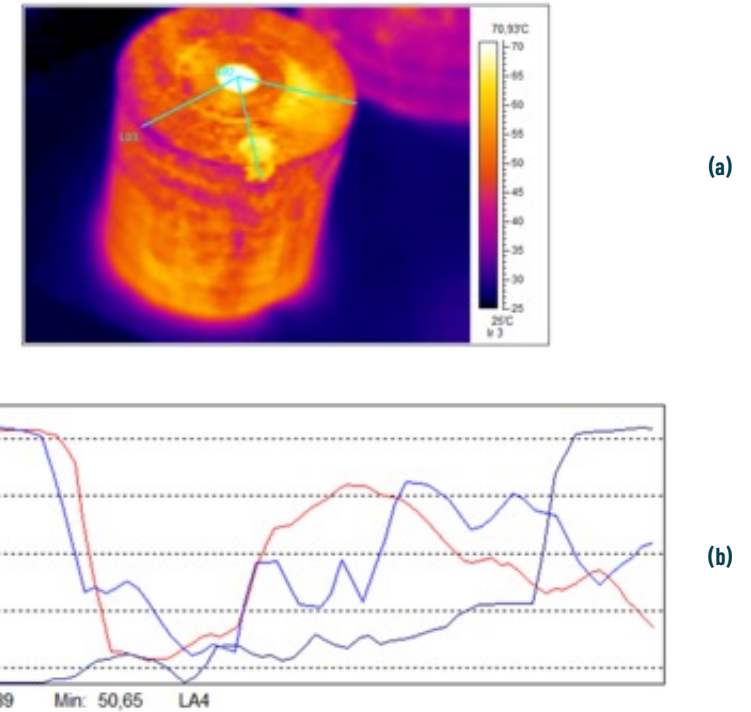


Fig. 2. Temperatures observed on the die surface used in mass production: (a) Measurement pattern, (b) temperature changes along the measurement pattern.

After RFID tag assembly studies, experimental tests were carried out under mass production conditions in order to track cold forging steel dies by using RFID technology. For production trials, a stud of M12x1.25x47.5 measurements and having high production quantities was chosen. RFID tag was assembled on stationary front die of the second station. One of the problems encountered under mass production was that the liquid gasket connection completely lost its ability to bond and was detached from the surface. Therefore, RFID tags fell into the cold forging machine and disappeared. Another problem encountered was that RFID tags could not be easily removed from the broken/damaged die. Since the liquid gasket could not be easily removed from the die surface, it must be broken down using intensive labor. During the dismantling process carried out in this way, the tags were failed and lost their reading/writing ability. After the production of 25,000 fasteners, 3 tags were lost and 5 tags were broken down during disassembly. As a result, it was revealed that the liquid gasket does not show a stable behavior under cold forging conditions, and so the surface on which the tag will be placed must be specially prepared or the curing process must be done under certain conditions. This case will both increase the assembly cost and negatively affect the mass production process of the dies. Since the assembly of the tags on the dies which entering the die warehouse will take a long time, it will slow down the process and cause productivity losses.

Cold Forging Die Traceability with QR Code Technology

Higher cost of system hardware, low reliability of reading on metal object and degradation under environmental damage can be listed as disadvantages of RFID tag. In order to avoid using stickers or other elements for product labelling, direct product marking such as ink jet printing, laser marking, electrochemical etching and dot peen marking was addressed as an alternative traceability tool. Ink jet printing method is not long lasting due to problems such as ink fade and easy damage. In laser marking system, the material surface is melted with laser printers and the QR code is marked on the



Fig. 3. Portable dot peen marking printer with a stand located in die warehouse.

surface. Although laser marking and electrochemical etching methods are more reliable than ink jet printing, readability decreases in case of oil and dirt accumulation on the product surface. In addition, these systems are both very expensive and harmful to the environment and health resulting from toxic vaporization.

Dot peen marking is the technology where data including traceability information is printed on metal product surface by stamping with carbide needle. This method is more robust on surface damage since data is stamped on product surface. Alphanumeric text data (letters and numbers) and two-dimensional codes can be print by dot peen marking technology. There exist two types of dot peen marking printers, desktop and portable. The material to be written in desktop printers must be placed on the table. The marking head stands on the material and writes the desired text or code on the material. Portable dot peen marking printer located in die warehouse was shown in Fig. 3. These types of devices meet the energy required for printing from the battery they have. They can be used portable as well as fixed to the desktop with special apparatus. After dot peen marker is fixed to the metal surface, marking head creates point holes by deforming the metal surface with a high-speed impact. A close view of the QR code printed with a dot peen marking printer was given in Fig. 4. The dimensions of the code and depth of the points can be changed by adjusting the software settings on the marker device, and so the printing process can be performed successfully even on harder materials. QR code between 4x4 and 10x10 mm sizes can be printed with the selected dot peen marker. If the code to be printed is in small scales, the dot strike intensity must be reduced at a certain rate, otherwise the readability of the code would decrease since the dots would be too close to each other.

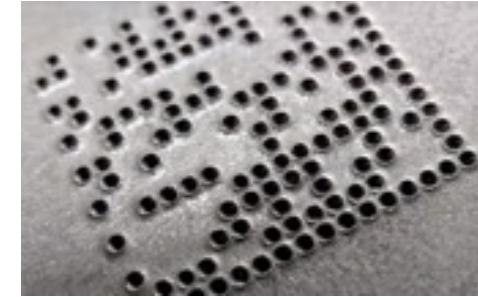


Fig. 4. QR code printed with a dot peen marking printer.

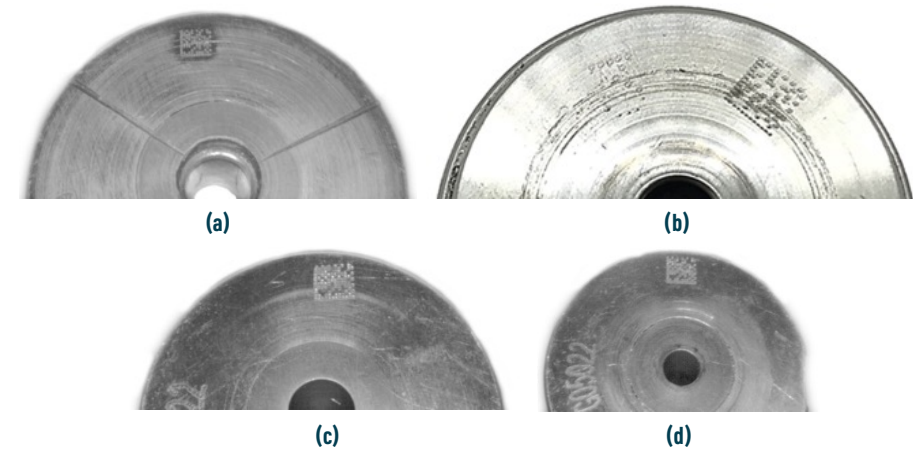


Fig. 5. QR code status on the dies used in mass production: (a) Front die produced 25,000 pieces and (b) 90,000 pieces, (c) extrusion die produced 400,000 pieces and (d) 650,000 pieces.

In order to perform production trials, different die types having high consumption rates were determined. One of the selected die types was the front stationary die which comes into direct contact with the forged material and it is directly exposed to oil and coolant in the machine. The other one is the intermediate die that does not come into direct contact with the forged material. Under these conditions, it was aimed to see the readability of the QR code in production trials. The codes were printed on the outer ring of the dies as far from the inner WC-Co part as possible, since the main deformation zone is the inner WC-Co part of the die under cold forging conditions. QR code printed dies were tracked according to the production numbers in mass production conditions and the status of the codes was examined. The surface conditions after approximately 25,000, 90,000, 400,000 and 650,000 pieces of production were shown in Fig. 5. Compared to front die, the surface condition of the intermediate die was better as it was not exposed to oil. No wear or deterioration was detected in the QR codes of both die types and the reading tests were successful.

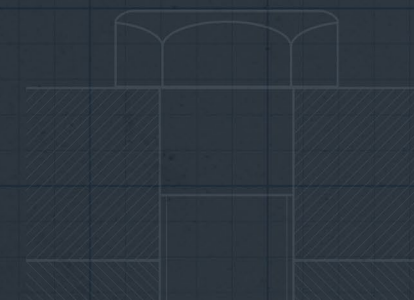
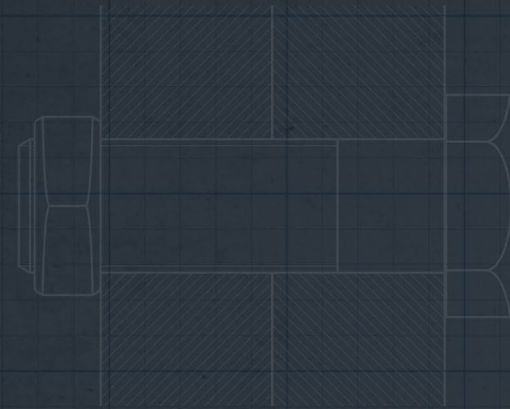
Conclusion

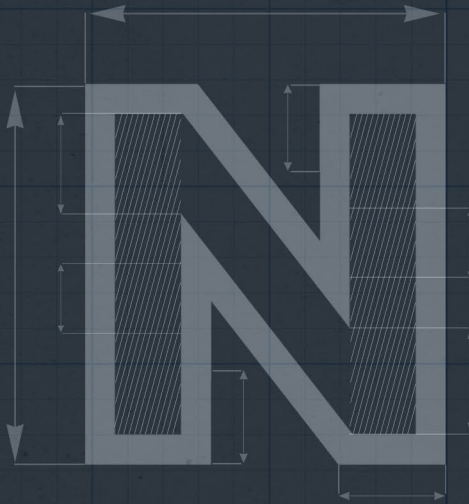
Positive results were obtained in printing, production and reading tests performed with QR code. The main advantages of using QR code compared to RFID technology were as follows:

1. No consumables as RFID tags were used to track the cold forging dies. For this reason, there was no need for any extra consumption and labor cost for the assembly. With a portable dot peen marking printer, the QR code could be printed on the die surface within seconds. Here, the price of a dot peen marker device should be taken as the first investment cost.
2. There was no need to prepare a surface by machining for QR code printing and it was not necessary to use any binder chemicals as used for RFID tags.
3. Reading operations were done as quickly and effectively as RFID tags. Since there was no need for an antenna, there was no need to construct a separate table or mechanism to read the dies.
4. QR codes printed with dot peen marker were not affected by the cold forging production conditions. Since it is possible to print more than one code on the front and back surfaces of the dies, the reading process can be guaranteed directly.
5. Since there is no need for assembly and disassembly operations as for RFID tags, using QR codes provided a serious advantage in labor and warehouse management speed.

References

1. S. Véronneau, J. Roy, RFID benefits, costs, and possibilities: The economical analysis of RFID deployment in a cruise corporation global service supply chain, *Int. J. Prod. Econ.* 122 (2009) 692-702.
2. A. Sarac, N. Absi, S. Dauzère-Pérès, A literature review on the impact of RFID technologies on supply chain management, *Int. J. Prod. Econ.* 128 (2010) 77-95.
3. X. Zhu, S.K. Mukhopadhyay, H. Kurata, A review of RFID technology and its managerial applications in different industries, *J. Eng. Technol. Manag.* 29 (2012) 152-167.
4. S. Fosso Wamba, A. Anand, L. Carter, A literature review of RFID-enabled healthcare applications and issues, *Int. J. Inf. Manage.* 33 (2013) 875-891.
5. E.W.T. Ngai, K.K.L. Moon, F.J. Riggins, C.Y. Yi, RFID research: An academic literature review (1995-2005) and future research directions, *Int. J. Prod. Econ.* 112 (2008) 510-520.
6. N.C. Wu, M.A. Nystrom, T.R. Lin, H.C. Yu, Challenges to global RFID adoption, *Technovation.* 26 (2006) 1317-1323.
7. M. Tajima, Strategic value of RFID in supply chain management, *J. Purch. Supply Manag.* 13 (2007) 261-273.
8. G. Wang, H. Nakajima, Y. Yan, X. Zhang, L. Wang, A methodology of tool lifecycle management and control based on RFID, in: 2009 IEEE Int. Conf. Ind. Eng. Eng. Manag., IEEE, 2009: pp. 1920-1924.
9. M. Liukkonen, RFID technology in manufacturing and supply chain, *Int. J. Comput. Integr. Manuf.* 28 (2015) 861-880.
10. N. Ren, J. Zhang, Y. Zhao, Development of RFID-enabled tool management system, *Appl. Mech. Mater.* 121-126 (2012) 3899-3903.
11. E. Dovere, S. Cavalieri, S. Ierace, An assessment model for the implementation of RFID in tool management, *IF-AC-PapersOnLine.* 48 (2015) 1007-1012.
12. D. Dragičević, S. Tegeltija, G. Ostojić, S. Stankovski, M. Lazarević, Reliability of Dot peen marking in product traceability, *Int. J. Ind. Eng. Manag.* 8 (2017) 71-76.
13. P.L. Xerafy Singapore, XS series-The Smallest RFID Tags for the Most Critical Process, (n.d.). <https://www.xerafy.com/xs-series>.





APPLICATION OF COLD EXPANSION MECHANICAL SURFACE TREATMENT TO COLD FORGING DIES AGAINST LOW CYCLE FATIGUE

M. Burak TOPARLI

Sarper DOĞAN

Sezgin YURTDAS

Tolga AYDIN

Umut İNCE



6th International Conference on Structural Integrity and Durability September 20 – 23, 2022, Dubrovnik

APPLICATION OF COLD EXPANSION MECHANICAL SURFACE TREATMENT TO COLD FORGING DIES AGAINST LOW CYCLE FATIGUE

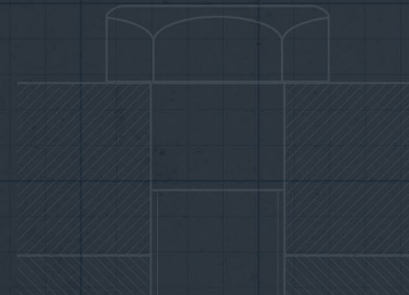
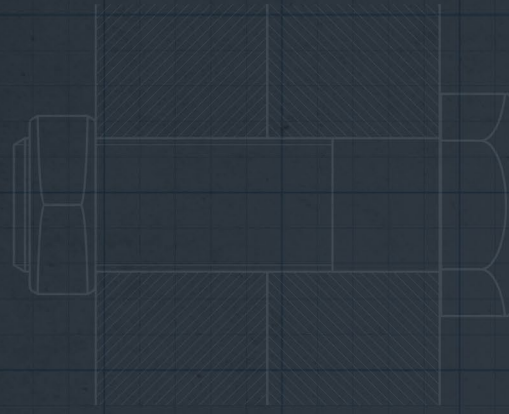
M. Burak Toparli¹, Sarper Doğan¹, Sezgin Yurtdaş¹, Tolga Aydın¹, Umut İnce¹

¹Norm Fasteners R&D Center, AOSB 10007. Sok No:1/1, İzmir, Turkey

Cold expansion is one of the mechanical surface treatments applied in mostly aerospace industry for fatigue life improvement. An oversized mandrel is applied to holes so that non-homogenous plastic deformation-induced hardness increase and compressive residual stress fields are achieved. As proven in the literature, hardness increase and compressive residual stresses act against structural loads leading to increase in performance [1]. In this study, cold expansion was applied to cold forging dies to increase service life. Cold forging dies are exposed to complex loading conditions and one of the main failure mechanisms is low cycle fatigue. In this context, finite element modelling of the cold expansion process was initially conducted for the sake of tool geometry and process parameters optimization. After finalizing tool geometry and die form, tools and dies were produced. After process optimization and trials, cold expansion application was conducted to cold forging dies. At the first trial, due to excess heat generated during cold expansion originating from friction, mandrel and cold forging dies were fractured due to adhesion. Therefore, in order to decrease heat generation, AlCrN based PVD coating was applied to tools to be used as mandrel and MoS₂-based dry lubricant was applied to tools and dies before cold expansion process. At the second trial, cold expansion application was finished without any failure. After dimensional control, surface roughness and hardness measurements, processed dies were used at production floor. To compare, dies without application of cold expansion were also employed. Comparing low cycle fatigue performance, service life obtained for dies without cold expansion was about 6.000. After cold expansion, service life was increased to 16.000. Hardness increase after cold expansion was found to be the main reason for fatigue life improvement. Failed dies were investigated and it was revealed that cracking was observed due to significant radial loads exposed during cold forging. Main failure mechanism was the same for dies with and without application of cold expansion.

References

1. Toparli, M. Burak. Effect of shot peening on ballistic limit of Al6061-T651 aluminium alloy plates. *Experimental Techniques* 2020; 44:37-47.



COMPARATIVE WEAR PERFORMANCE OF TIN COATED AND SHOT PEENED PIERCING PUNCHES USED IN NUT PRODUCTION BY COLD FORGING

Fuat Can AĞARER

Hatice SANDALLI

M. Burak TOPARLI

Umut İNCE

İbrahim Etem SAKLAĞOĞLU



6th International Conference on Structural Integrity and Durability
September 20 – 23, 2022, Dubrovnik

COMPARATIVE WEAR PERFORMANCE OF TiN COATED AND SHOT PEENED PIERCING PUNCHES USED IN NUT PRODUCTION BY COLD FORGING

Fuat Can AĞARER¹, Hatice SANDALLI¹, M. Burak TOPARLI², Umut İNCE², İbrahim Etem SAKLAĞOĞLU³

¹Norm Somun San.ve Tic. A.Ş., A.O.S.B., İzmir, Turkey

²Norm Cıvata San. ve Tic. A.Ş., A.O.S.B., İzmir, Turkey

³Ege University, Faculty of Engineering, İzmir, Turkey

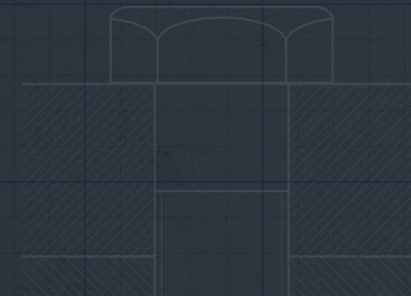
Cold forging is one of the metal forming methods used in production of high-strength machine parts within narrow geometric tolerances. Additionally, since it is suitable for mass production, it is widely preferred in various engineering applications such as fastener production. In cold forging, metals are forged at temperatures below their recrystallization temperatures. Because of that, higher stresses are required to deform the material and this causes extreme tribological conditions such as high contact pressure, temperature and relative velocities [1]. These conditions, may lead to tool wear and fatigue, common types of failure modes in cold forging. Surface quality of tools and their performance can be improved with various coatings and mechanical surface improvement methods. The most common of these coating types is Titanium Nitride (TiN) coating. This type of coating is used in various industrial applications, especially in cold forging dies, since it reduces wear significantly. One of the mechanical surface improvement methods used to increase fatigue performance is shot peening method, increasing hardness and introducing beneficial compressive residual stresses into applied materials.

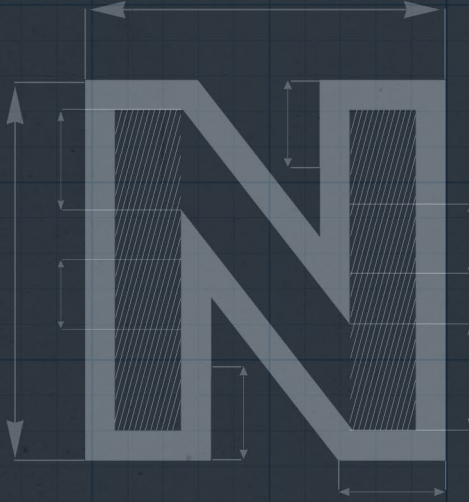
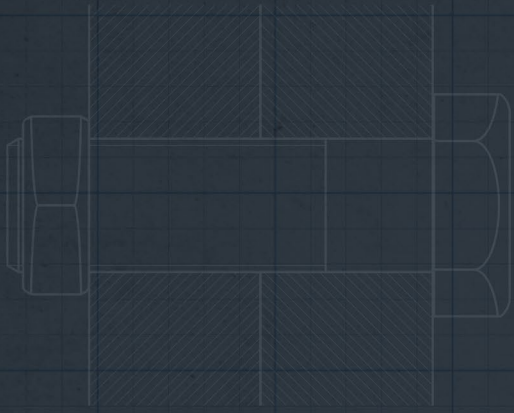
In this study, performance of piercing punches made of DIN 1.3343 high speed steel during the production of a nut with the dimensions of M12x1.75 was investigated in detail. In the first stage of the study, shot peening with different parameter sets was applied to a group of piercing punches without any coating. In addition, TiN coating was applied to base punches. Then, performance of only shot peened and TiN coated punches were monitored under mass production conditions. In the second part of the study, TiN coating was applied to a group of shot peened punches and these punches were tried under mass production conditions. Surface roughness and Vickers hardness values of the investigated punches were measured before production.

Based on trials, it was revealed that piercing punches failed due to two different damage mechanisms. In the first one, surface quality of the produced nuts was lowered from piercing punches so that final products did not meet the required surface expectations. In the second mechanism, after a certain number of production, diameter of the piercing punches became out of tolerances due to wear, and therefore, punches were accepted to be failed. Base piercing punches without any surface treatments failed due to first damage mechanism type with 0,008 micron/ part wear rate. However, shot peened punches failed due to second damage mechanism with 0,005 micron/part wear rate. In addition, TiN coating decreased the wear rate from 0,008 to 0,0017 micron/ part and did not change the main damage mechanism compared to base punches. When the effects of TiN coating on shot peening were examined, wear rate was calculated as 0,00026 micron/part. Therefore, it was found that service life of punches were prolonged significantly. For punches treated with shot peening and TiN coating, it was seen that punches were failed due to first damage mechanism. Based on all trials, it was concluded that TiN coating on shot peened punches had the highest performance increase compared to base, TiN coated and shot peened punches. In addition, depending on applied surface treatments, main damage mechanism was found to be changed.

References

1. Groche P, Müller C, Jahn A. Effects of the Tool Lubrication in Cold Forging. Tribology Letters 2014; 53(2):599-605.





NORM ONE WAY PATENTLİ ÜRÜNÜNDE AĞIRLIK AZALTIMI İÇİN MEKANİK DAYANIM VE TORKLAMA ÇALIŞMALARININ GERÇEKLEŞTİRİLMESİ

Doğuş ZEREN
Fatih KOCATÜRK
M. Burak TOPARLI



International Conference on Design, Research and Development December 14 - 17, 2022

NORM ONE WAY PATENTLİ ÜRÜNÜNDE AĞIRLIK AZALTIMI İÇİN MEKANİK DAYANIM VE TORKLAMA ÇALIŞMALARININ GERÇEKLEŞTİRİLMESİ

Doğuş Zeren¹, Fatih Kocatürk¹, M. Burak Toparlı¹

¹ Norm Fasteners R&D Center, Orcid ID: 0000-0002-7878-5886, dogus.zeren@normfasteners.com

¹ Norm Fasteners R&D Center, Orcid ID: 0000-0001-7387-9907, fatih.kocaturk@normfasteners.com

¹ Norm Fasteners R&D Center, Orcid ID: 0000-0002-5203-5171, burak.toparli@normfasteners.com

* Sorumlu Yazar: dogus.zeren@normfasteners.com; Tel.: +90232 376 76 10-2362

Özet

Günümüzde güvenlik ve kalıcı bağlantı ihtiyacının ön planda olduğu durumlar için özel geliştirilmiş bağlantı elemanları mevcuttur. Bunlardan ilk akla gelen "shear bolt" olarak bilinen sadece sıkılmaya izin veren bağlantı elemanıdır. Bu bağlantı elemanında kafa altında özel olarak talaşlı imalat ile inceltilmiş bir bölge yer almakta ve bu sayede cıvata belli bir tork değerine ulaştığında kafa kısmında kırılma meydana gelmektedir. Böylece altı köşe formda olan ve sadece sıkım esnasında kullanılan kısım ortadan kalktığı için çözilemez bir bağlantı elde edilmektedir. Shear bolt kullanımı ile ortaya çıkan dezavantajların başında sadece sıkım esnasında kullanılan ciddi bir malzeme miktarının olması ve maliyeti artırması gelmektedir. Ayrıca, kırılma yüzeyinde meydana gelen kaplamasız alan ve olası korozyon problemleri ve talaşlı imalatından gelen ekstra bir maliyet söz konusudur. Seri imalat koşullarında kırılan kafa kısmının bertaraf da ekstra maliyet olarak ortaya çıkmaktadır. Bu problemlerin önüne geçmek amacıyla patenti Norm Cıvata 'ya ait olan Norm One Way (NOW®) ürünü geliştirilmiştir. Özel kafa ve soket geometrisi sayesinde yalnızca tek yönde sıkım yapılmakta, söküm yapılamamaktadır. Bu çalışmada soket derinliği artışının cıvatanın kafa dayanımına olan etkisi, deneysel, analitik ve sonlu elemanlar yöntemleri kullanılarak incelenmiştir. Sonuç olarak daha güvenli, montaj sırasında sıyırma ihtimalini ortadan kaldıracak ve aynı zamanda maksimum ağırlık azaltımı sağlayacak kafa formunu sahip NOW® ürünü elde edilmiştir.

Anahtar Kelimeler: Soğuk dövme, cıvata, bağlantı elemanlar, ağırlık azaltma

Abstract

Today, there are specially developed fasteners for situations where the need for security and permanent connection is at the forefront. The first thing that comes to mind is the "shear bolt", a fastener that only allows tightening. In this fastener, there is a specially thinned area under the head with machining, and thus, when the bolt reaches a certain torque value, a break occurs in the head part. Thus, a permanent connection is obtained since the hexagon part used only during tightening is eliminated. One of the disadvantages that arise with the use of shear bolts is that there is a significant amount of material used only during tightening and it increases the cost. In addition, uncoated area on the fracture surface makes possible corrosion problems and an extra cost from machining is another disadvantage. The disposal of the broken head part during mass production also appears as an extra cost. In order to prevent these problems, the Norm One Way (NOW®) product, whose patent belongs to Norm Cıvata, has been developed. Thanks to the special head and socket geometry, tightening is done only in one direction and disassembly is not possible. In this study, the effect of increasing the socket depth on the head strength of the bolt was investigated using experimental, analytical and finite element methods. As a result, NOW® product was obtained which is safer, has a head form that will eliminate the possibility of stripping during assembly and at the same time provide maximum weight reduction.

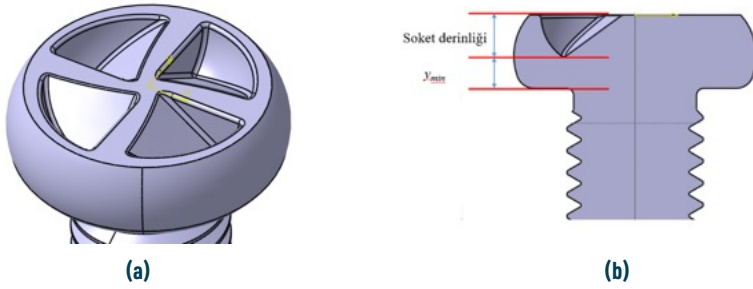
Keywords: Cold forging, bolt, fasteners, weight reduction

1. Giriş

Günümüzde otomotiv endüstrisinde CO₂ emisyonlarının azaltılmasına yönelik sınırlamalar getirilmesiyle beraber otomotiv endüstrisinde ağırlık azaltma önemli bir konu haline gelmiştir. Otomotivdeki en önemli parçalardan biri olan bağlantı elemanlarında da ağırlık azaltma konusundaki çalışmalar bu kapsamda oldukça önem kazanmaktadır. Bağlantı elemanlarındaki ağırlık azaltma çalışmaları da genellikle kafa kısmında yoğunlaşmaktadır. Bağlantı elemanlarında tasarım çalışmaları yapılırken, mekanik performanstan ödün vermeden maksimum ağırlık azaltmayı yakalayabilmek için kritik soket derinliğini belirlemek çok önemli bir parametredir. Ayrıca soket derinliğini belirlerken torklama esnasında sıyırma problemi gerçekleşmemesi açısından bitle cıvata arasında yeterli bir temas alanı olması gerekmektedir. Patenti Norm Cıvata'ya ait olan Norm One Way (NOW®) ürününün soket derinliği artışıyla birlikte cıvatanın kafa kısmında tam dayanım gösterip göstermediğini anlayabilmek için öncelikle Ar-Ge Merkezimizde geliştirilen ve maksimum soket derinliğini hesaplamak için kullanılan analitik model kullanılarak kritik soket derinliği hesaplanmıştır [Kocatürk&Toparlı, 2020]. Standart M8 DIN933 cıvatalara minimum kırılma torku uygulanarak oluşan kontakt alanı hesaplanmıştır ve M8 NOW® ürünü ile bu temas alanının yakalayacak uygun soket derinliği tasarımları yapılmıştır. Analitik model yardımıyla elde edilen kritik soket derinliklerini doğrulamak amacıyla NOW® ürünlerine sayısal benzetim yöntemleri kullanılarak çekme testleri gerçekleştirilmiştir. Çekme testi simülasyonları farklı soket derinliklerinde gerçekleştirilerek kafa altındaki yüksek gerilme değerlerinin dış bölgesine geçiş yaptığı kritik soket derinlikleri bulunmuştur. Sayısal benzetim çalışmaları sonucunda analitik model kullanılarak elde edilen kritik soket derinliklerine benzer sonuçlar elde edilmiştir.



Şekil 1. M8x1,25 DIN 933 cıvata için torklama testi sonrası temas alanlarının belirlenmesi.

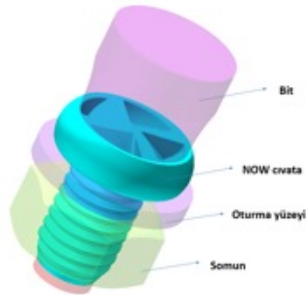


Şekil 2. M8 NOW® ürününün üç boyutlu modeli; (a) izometrik görünüm, (b) kesit görüntüsü.

2. Metot ve Yöntemler

2.1. Temas Alanı Çalışmaları

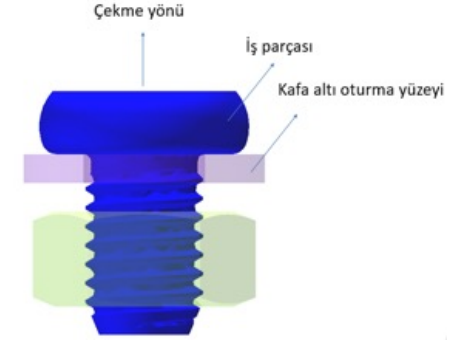
Hedef temas alanını belirlemek amacıyla standart bir M8x1,25 DIN 933 (anahtar ağız, SW=13) cıvata numuneleri kullanılarak deneysel torklama testleri yapılmıştır. Testlerde M8x1,25 için gerekli olan minimum kırılma torku değerine kadar sıkma işlemi gerçekleştirilmiştir. Standart altı köşe sıkıcıyla torklama sonrası temas alanlarını belirlemek için cıvataların kafa kısmı basınçlı kağıt ile sarılmıştır. Torklama sonrası bit ile cıvata kafasındaki temas alanları Şekil 1'de görüldüğü üzere kırmızı renge dönmektedir. Deneysel torklama testleri sonrasında basınçlı kâğıttan stereo mikroskop altında görüntüler alınmış ve cıvataların temas alanları ImageJ görüntü işleme yazılımıyla ölçülmüştür.



Şekil 3. M8 NOW® torklama simülasyonu modeli.

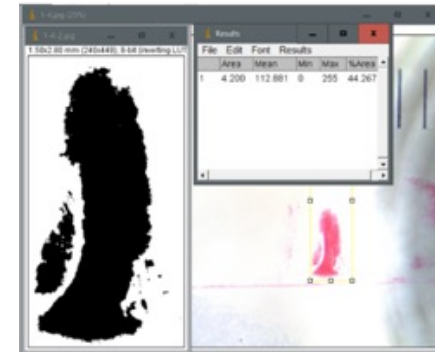
2.2. Analitik Formülasyon

Çalışmada incelenen M8 NOW® ürününün üç boyutlu modeli Şekil 2'de gösterilmiştir. Şekilde kritik olan ölçüler soket derinliği ve maksimum soket derinliği ile cıvatanın kafa altı arasındaki yemin değeridir.



Şekil 4. Çekme testi simülasyonu modeli.

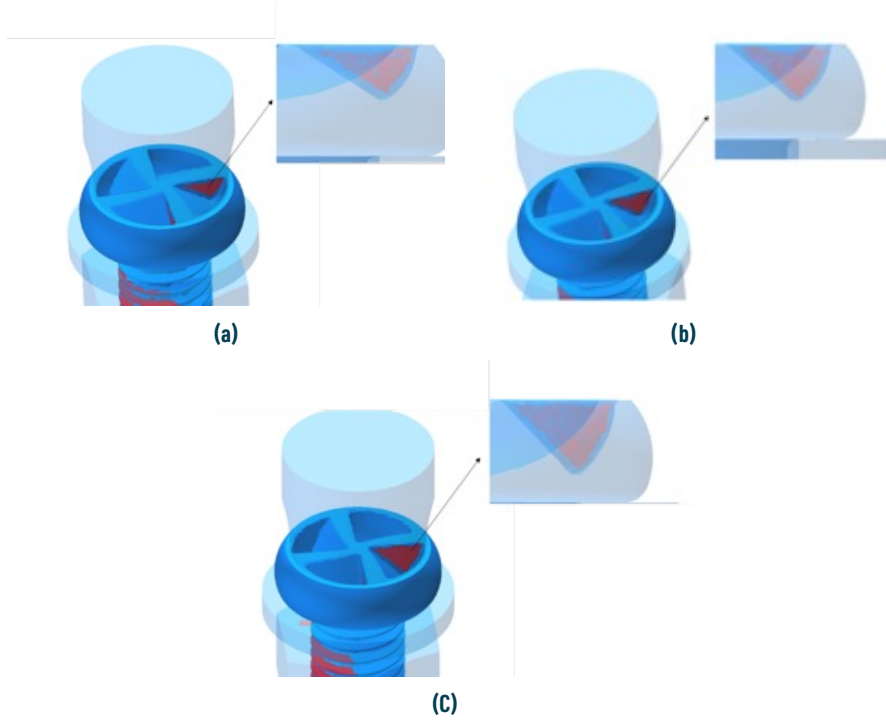
Cıvatanın kafa bölgesinde tam dayanıma sahip olduğu maksimum soket derinliğini hesaplayabilmek için Norm Cıvata Ar-ge Merkezi tarafından geliştirilen analitik model kullanılmıştır [Kocatürk&Toparlı, 2020]. Bu model ile cıvata kafasında tam dayanımı sağlayan soket ucu ile kafa altı arasındaki minimum yükseklik, y_{min} , hesaplanabilmektedir. Cıvatanın kafa yüksekliğinden yemin değeri çıkarıldığında maksimum soket derinliği elde edilebilmektedir.



Şekil 5. M8 DIN 933 cıvataların ImageJ görüntü işleme yazılımıyla kontak alanlarının belirlenmesinin sonuçları.

2.3. Numerik Analizler

Numerik analizlerde torklama modeli Simufact.Forming sonlu elemanlar yazılımında gerçekleştirilmiştir. Simülasyonlarda bit (sıkıcı), oturma yüzeyi ve somun rijit olarak modellenmiştir. Cıvata ise elastik-plastik olarak modellenmiştir.

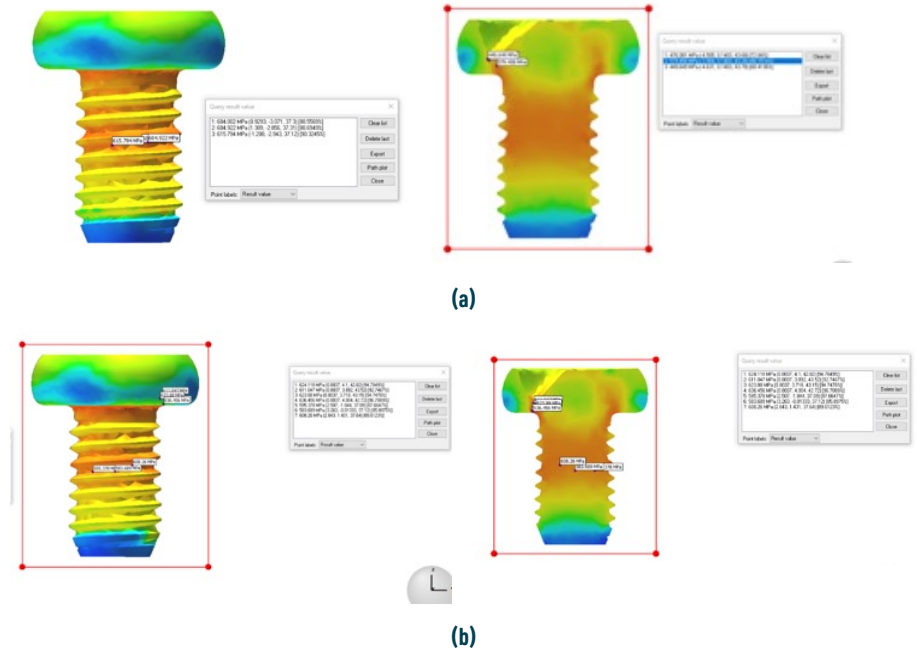


Şekil 6. (a) 1,95, (b) 2,45, (c) 2,95 mm soket derinlikleri için gerçekleştirilmiş torklama analizleri.

Simülasyon ortamında farklı soket derinliklerindeki ürünlere çekme testi yapılarak kritik soket derinliği ve kafadaki tam dayanım ilişkisi belirlenerek tam dayanımı sağlayacak maksimum soket derinliği değeri belirlenmiştir. NOW® ürünü elastik-plastik olarak tanımlanmıştır. Kafa altındaki oturma yüzeyi sayesinde cıvata çekme yönünde deformasyona maruz bırakılmıştır. Cıvatanın kalitesi 8.8 olduğu için kafa altındaki gerilmelerin 640 MPa akma değerine ulaşmış dış dibindeki gerilmeleri geçtiği derinlik, kritik soket derinliği belirlenmiştir.

3. Bulgular ve Sonuçlar

DeneySEL torklama testleri sonrasında basınçlı kâğıttan stereo mikroskop altında görüntüler alınmış ve cıvataların temas alanları ImageJ görüntü işleme yazılımıyla ölçülmüştür (Şekil 5). 3 farklı cıvata dan alınan ölçümler sonucunda ortalama temas alanı elde edilmiştir.



Şekil 7. Farklı soket derinlikleri için çekme simülasyonu sonuçları (a) 2,7 mm soket derinliği, (b) 2,95 mm soket derinliği.

Sırasıyla 1,95 mm, 2,45 mm ve 2,95 mm nominal soket derinliklerindeki NOW® kafa formları için torklama analizleri gerçekleştirilmiştir ve bu soket derinliklerine göre sırasıyla 11,45 mm², 15,35 mm² ve 17,75 mm² temas alanları elde edilmiştir. Sonuçlara göre 1,95 mm soket derinliği ile hedef temas alanı sağlanamamış olup 2,45 mm ve 2,95 mm soket derinliğinde hedeflenen temas alanına ulaşılmıştır.

Çekme testi analizlerine 2,70 mm soket derinliği ile başlanmıştır. Sırasıyla 2,75, 2,80, 2,85, 2,90, 2,95 mm soket derinliklerine göre çekme testi analizleri gerçekleştirilmiştir. Şekil 9'daki çekme testi sonuçlarına göre 2,95 mm soket derinliği ile birlikte soket altındaki gerilmeler dış dibinden önce 640 MPa değerine ulaşmıştır. Bu durumda hasar mekanizması olarak kafadan kopma olabileceği için bu istenen bir durum değildir. Dişli bağlantı elemanlarında kırılmaların dış dibinden olması beklenmektedir. Bu sebeple kritik soket derinliği değeri sonlu elemanlar yöntemine göre 2,90 mm olarak belirlenmiştir.

Table 1. Analitik model ve çekme testi simülasyonları ile elde edilen kritik soket derinlikleri.

Kafa Yüksekliği [mm]	y_{min} Analitik [mm]	y_{min} Sonlu Elemanlar [mm]	Maks. Soket Derinliği Analitik [mm]	Maks. Soket Derinliği Sonlu Elemanlar [mm]
4,2	1,76	1,30	2,44	2,90



Şekil 8. NOW® ürünü (a) görseli (b) çekme testi sonrası dış dibinden kırılma

Norm Cıvata Ar-Ge Merkezi tarafından geliştirilen analitik model kullanılarak yapılan çalışmada maksimum soket derinliği 2.44 mm olarak hesaplanmıştır. Farklı yöntemler kullanılarak elde edilen kritik soket derinlikleri Tablo 1'de özetlenmiştir. Elde edilen sonuçlar değerlendirildiğinde maksimum soket derinliği 2.44 mm olarak belirlenmiştir. Soğuk şekillendirme istasyon ve kalıp tasarımları elde edilen bu değere göre oluşturulmuştur. Üretimler sonucunda ürün şekillendirmesi ile alakalı bir problemle karşılaşılmemiştir. Ürünler üzerinde yapılan torklama testleri sonucunda sıyırma gözlenmemiş ve mekanik çekme testi sonucunda da kırılma dış dibinden olduğu gözlenmiştir. Bu sayede, yapılan çalışmalar doğrulanmış ve nihai ürün formu doğrulanmıştır.

4. Sonuçlar

Bu çalışma kapsamında güvenlik ve kalıcı bağlantı ihtiyacı olan uygulamalarda kullanılabilecek patenti Norm Cıvata 'ya ait NOW® ürünü ele alınmıştır. Yapılan torklama testleri ve görüntü işleme ile hedef temas alanı belirlenmiştir. Bu sayede montaj sırasında olası sıyırma probleminin önüne geçilmesi için gerekli kontak alanı ortaya çıkarılmıştır. Ayrıca, özellikle otomotiv sektörünün beklentisini karşılamak amacıyla maksimum ağırlık azaltışı da elde etmek için Norm Cıvata tarafından geliştirilen analitik model ve Simufact.Forming sonlu elemanlar yöntemi kullanılarak maksimum soket derinliği elde edilmiştir. Yapılan çalışmalar üretilen nihai ürünler üzerinde testler yapılarak doğrulanmıştır. Sonuç olarak, daha güvenli, montaj sırasında sıyırma ihtimalini ortadan kaldıracak ve aynı zamanda maksimum ağırlık azaltışı sağlayacak kafa formu için çalışmalar yürütülmüş ve bu forma sahip NOW® ürünü elde edilmiştir.

Referanslar

Kocatürk F, Toparlı M.B, Tanrikulu B.,İnce U.,Kılıçaslan C., "A new analytical model to estimate maximum internal socket depth of non-reduced strength bolts", Procedia Structural Integrity, Volume 28, 2020, Pages 1276-1285, ISSN 2452-3216, <https://doi.org/10.1016/j.prostr.2020.11.109>.



NORM FASTENERS

www.normfasteners.com